Chapter 2: Mathematical Preliminaries

Radon Transform and Central Slice Theorem

General Inverse Problem and Image Reconstruction

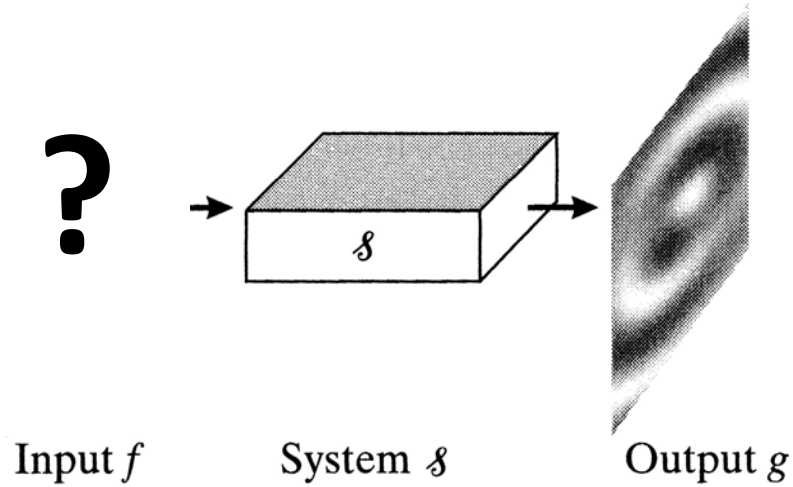

***The inverse problem*:**

- **Given a set of measured output signal**
- **Given the statistical description of the data**
- **Given a known system response function**

what should be the input signal that gave rise to the output data?

Projection Data from Early X-ray CT Systems

Data measured by translating the detector is a typical projection data.

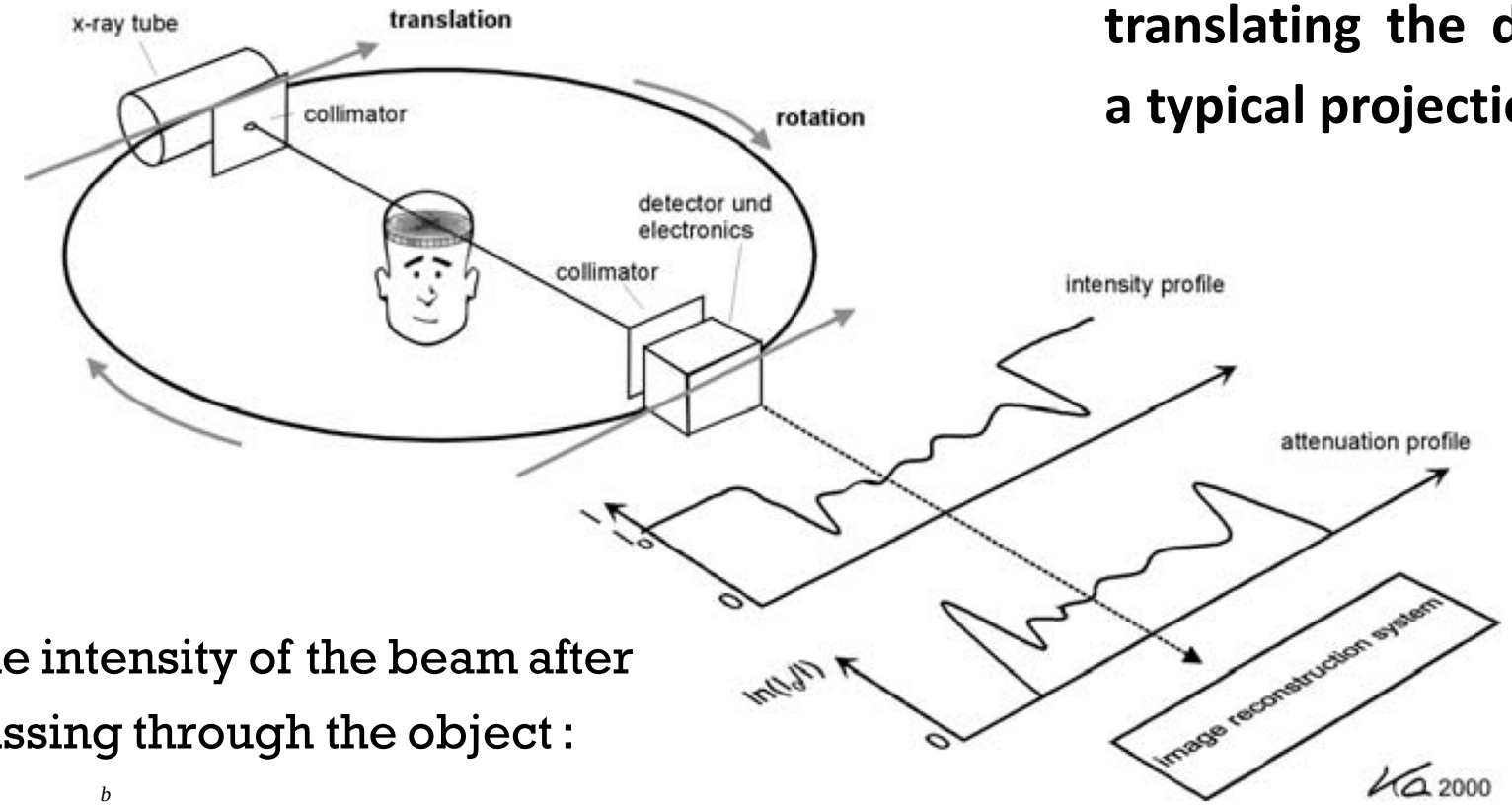

The intensity of the beam after passing through the object :

$$I = I_0 e^{-\int_a^b \mu(t)\cdot dt} \Leftrightarrow \ln(I_0 / I) = \int_a^b \mu(t)\cdot dt$$

From Computed Tomography, Kalender, 2000.

Line Impulse Signal (1)

$$\delta_L(x,y) = \delta(x\cos\theta + y\sin\theta - l)$$

$$where\ \delta(x) = \begin{cases} > 0, & x\cos\theta + y\sin\theta = l \\ 0, & otherwise \end{cases}$$

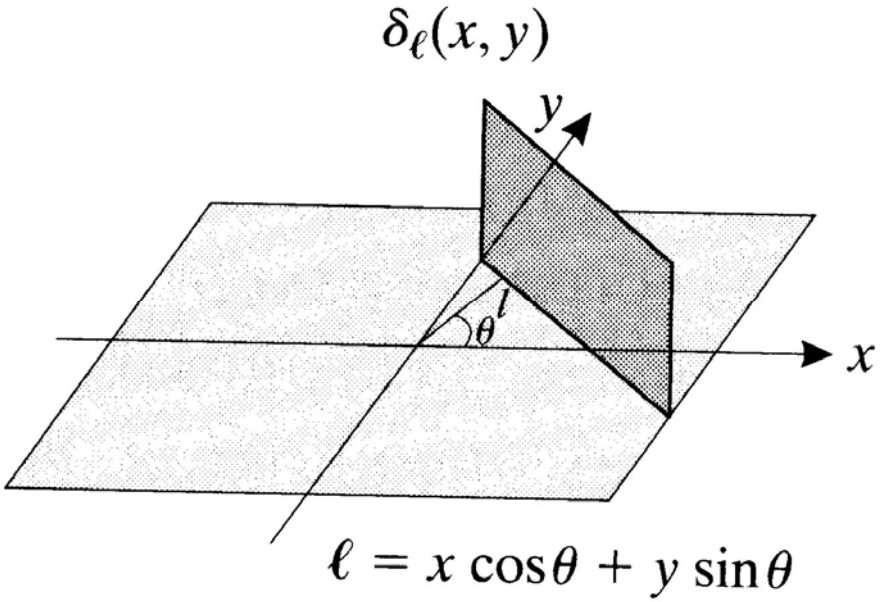

Line Impulse Signal (2)

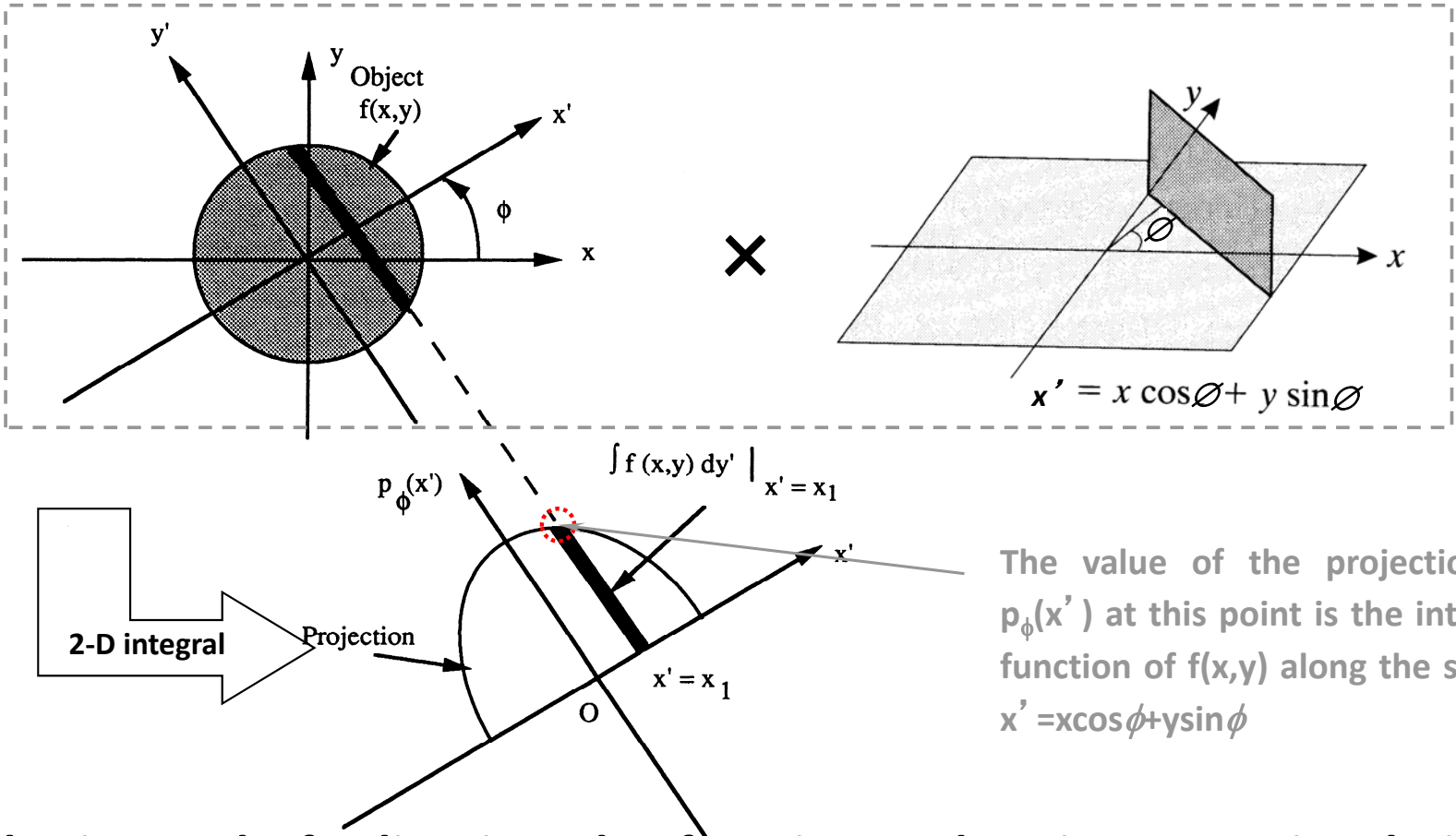

The value of the projection function $p_\phi(x')$ at this point is the integral of the function of f(x,y) along the straight line: $x' = x\cos\phi + y\sin\phi$

The integral of a line impulse function and a given 2-D signal gives the *projection* data from a given view …

$$p(\phi, x') = \int_{-\infty}^{\infty}\int_{-\infty}^{\infty} f(x,y)\delta(x\cos\phi + y\sin\phi - x')dxdy$$

Radon Transform (1)

The Radon transform of a 2-D function is defined as

$$p(\phi, x') \equiv \mathcal{R}[\, f(x,y)]$$
$$= \int_{-\infty}^{\infty}\int_{-\infty}^{\infty} f(x,y)\delta(x\cos\phi + y\sin\phi - x')dxdy$$
$$= \int_{-\infty}^{\infty} f(x'\cos\phi - y'\sin\phi, x'\sin\phi + y'\cos\phi)dy'$$

where

$$\begin{bmatrix} x' \\ y' \end{bmatrix} = \begin{bmatrix} \cos\phi & \sin\phi \\ -\sin\phi & \cos\phi \end{bmatrix} \begin{bmatrix} x \\ y \end{bmatrix}$$

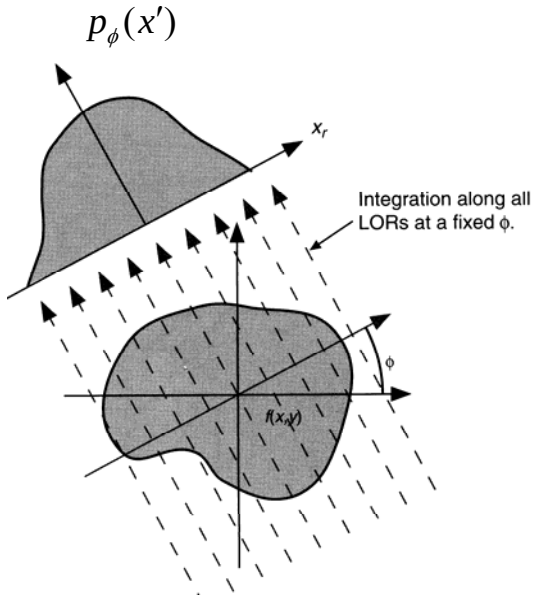

Radon Transform and Sinogram

Radon transform maps a 2-D function f(x,y) into a sinogram.

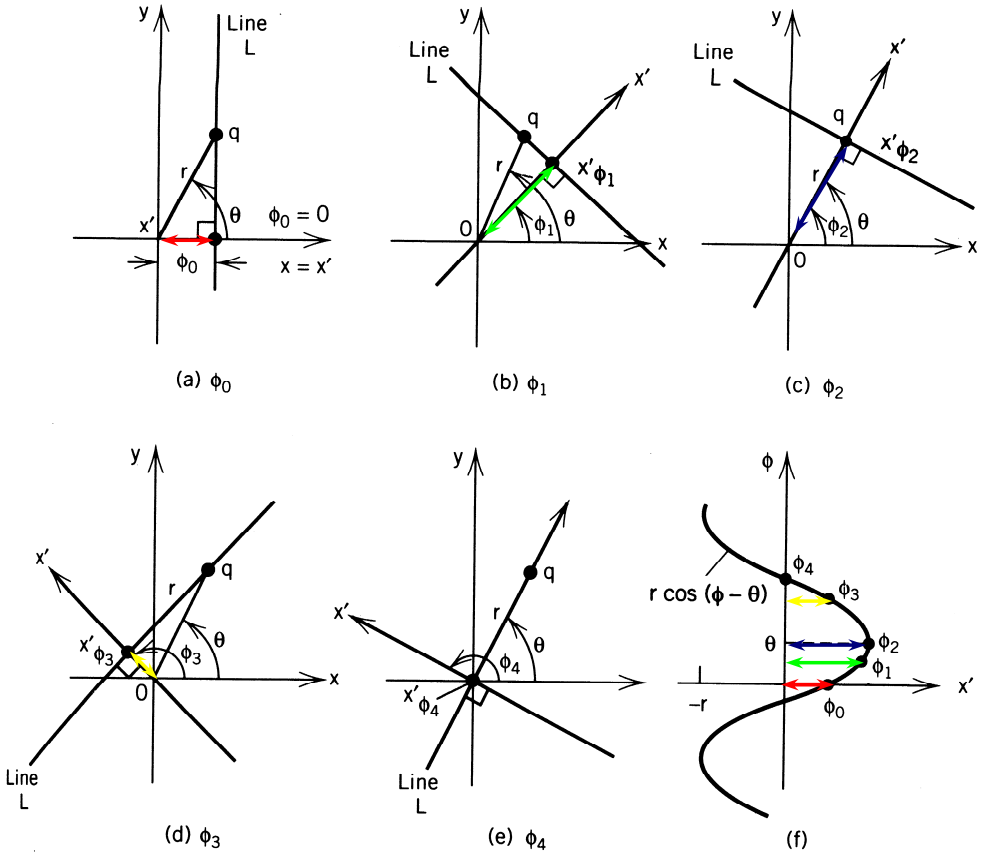

Figure 3-2 Sinogram of a point q at a various angles ϕ_i for a given θ: (a) $\phi_0 = 0$, (b) $\phi_1 = 45°$, (c) $\phi_2 = 60°$, (d) $\phi_3 = 135°$, and (e) $\phi_4 = 150°$. At $i = 0$ or $\phi_i = 0$, the rotated coordinates x' coincide with the reference x-axis and give $x' = r\cos(\phi - \theta) = r\cos\theta$.

$$\mathcal{P}(\phi, x') = \mathcal{R}\left[f(x, y) \right]$$

Any point represented by polar coordinates (r,θ) will simply follow the equation x' =rcos(ϕ-θ) in the sinogrsm space.

Radon Transform and Sinogram

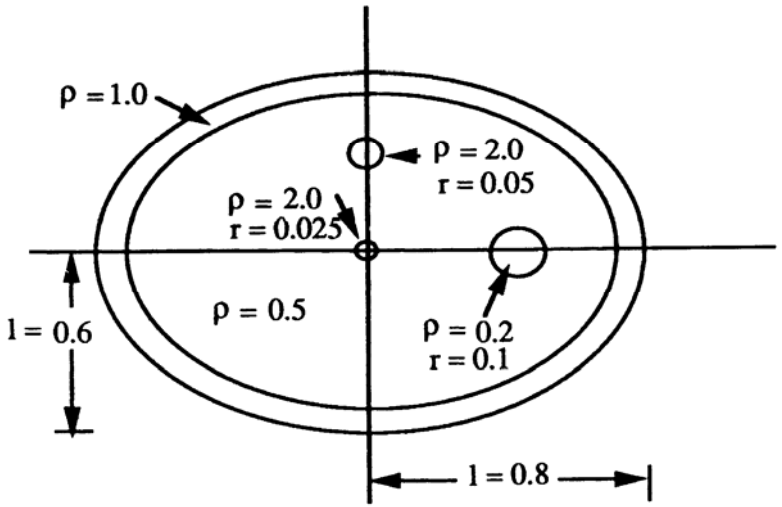

(a)

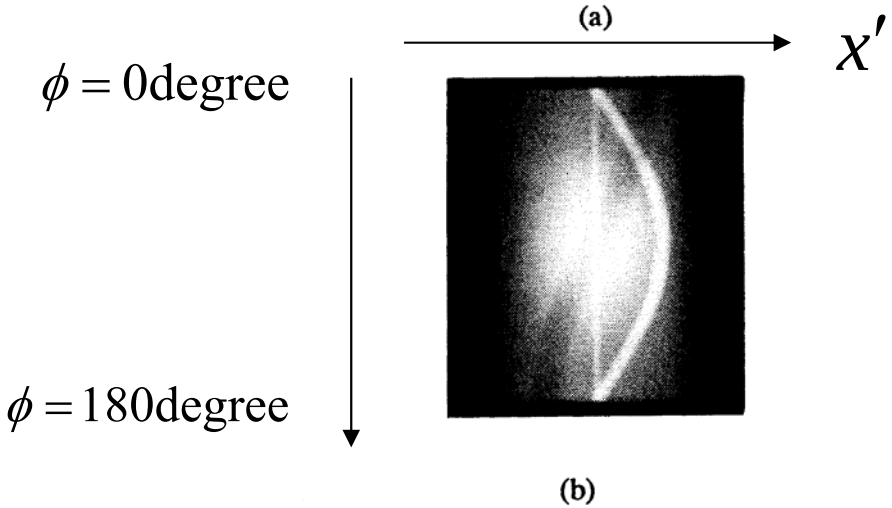

(b)

Figure 3-3 (a) Phantom with several distinct objects at various positions; (b) correspondi sinogram.

Sinogram is a 2-D function representing the original function f(x,y) into the projection data space.

Sinogram is the basic data format for reconstruction

Central Slice Theorem

$$F\{p(\phi, x')\} = F(r,\phi)$$

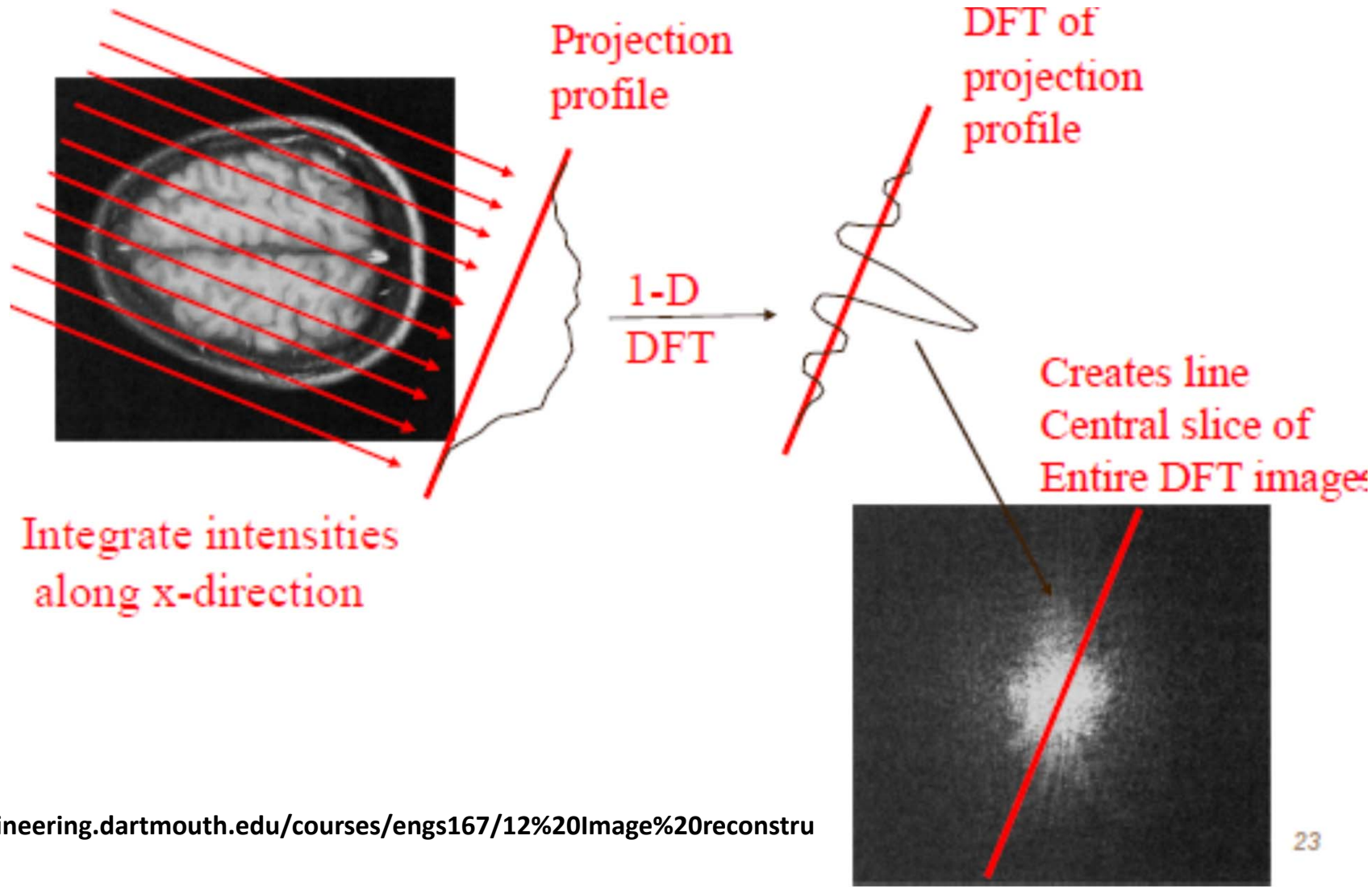

http://engineering.dartmouth.edu/courses/engs167/12%20Image%20reconstruction.pdf

23

Central Section Or Projection Slice Theorem

$$F\{p(\phi, x')\} = F(r,\phi)$$

So in words, the Fourier transform of a projection at angle ϕ gives us a line in the polar Fourier space at the same angle ϕ.

Central slice theorem is the key to understand reconstructions from projection data

Central Slice Theorem

Let's consider the 2D FFT of an arbitrarily given function

$$F(u,v) = \int\int f(x,y)\, e^{-i\,2\pi\,(ux + vy)}\, dx\, dy$$

$$\mathcal{F}[f(x-t)] = \mathcal{F}[f(x)] \cdot e^{-2\pi j \cdot \omega \cdot t}$$

$$\mathcal{F}[\delta(x)] = 1$$

$$\mathcal{F}[\delta(x-t)] = e^{-2\pi j \cdot \omega \cdot t}$$

In polar coordinates within the spatial-frequency domain,

$$u = \rho \cos\beta \qquad\qquad v = \rho \sin\beta$$

$$F(\rho,\beta) = \int\int f(x,y)\, \exp\left[-i\,2\pi\,\rho\,(x\cos\beta + y\sin\beta)\right] dx\, dy$$

If $x\cos\beta + y\sin\beta$ = constant, $\exp\left[-i\,2\pi\,\rho\,(x\cos\beta + y\sin\beta)\right]$ is a linear phase shift. This is the Fourier transform of a shifted delta function. Let's write the complex exponential as the FT of a δ function.

$$F(\rho,\beta) = \int_y \int_x f(x,y)\, \mathcal{F}[\delta(x\cos\beta + y\sin\beta - x')]\, dx\, dy$$

$$F(\rho,\beta) = \int_y \int_x f(x,y) \int [\delta(x\cos\beta + y\sin\beta - x')]\, e^{-i\,2\pi\,\rho x'}\, dx'\, dx\, dy$$

Central Slice Theorem

$$F(\rho,\phi) = \int\int f(x,y) \int [\delta(x\cos\phi + y\sin\phi - x')]\, e^{-i\,2\pi\rho x'}\, dx'\, dx\, dy$$

Recall how we wrote the projection as a double integral of f(x,y) where a delta function performs the line integral,

$$p(\phi, x') = \int\int f(x,y)\, \delta(x\cos\phi + y\sin\phi - x')\, dx\, dy$$

We take the Fourier Transform of $p(\phi, x')$:

$$F\{p(\phi, x')\} = \int_{x'} \left[\int_y \int_x f(x,y)\, \delta(x\cos\phi + y\sin\phi - x')\, dx\, dy \right] e^{-i\,2\pi\rho x'}\, dx'$$

which is exactly what we wrote for $F(\rho, \beta)$ above!

Thus, $F\{p_\phi(x')\} = F(\rho, \phi)$

Review of 2-D Analytical Reconstruction Methods
Projection Data

Projection data p(ϕ, x’)

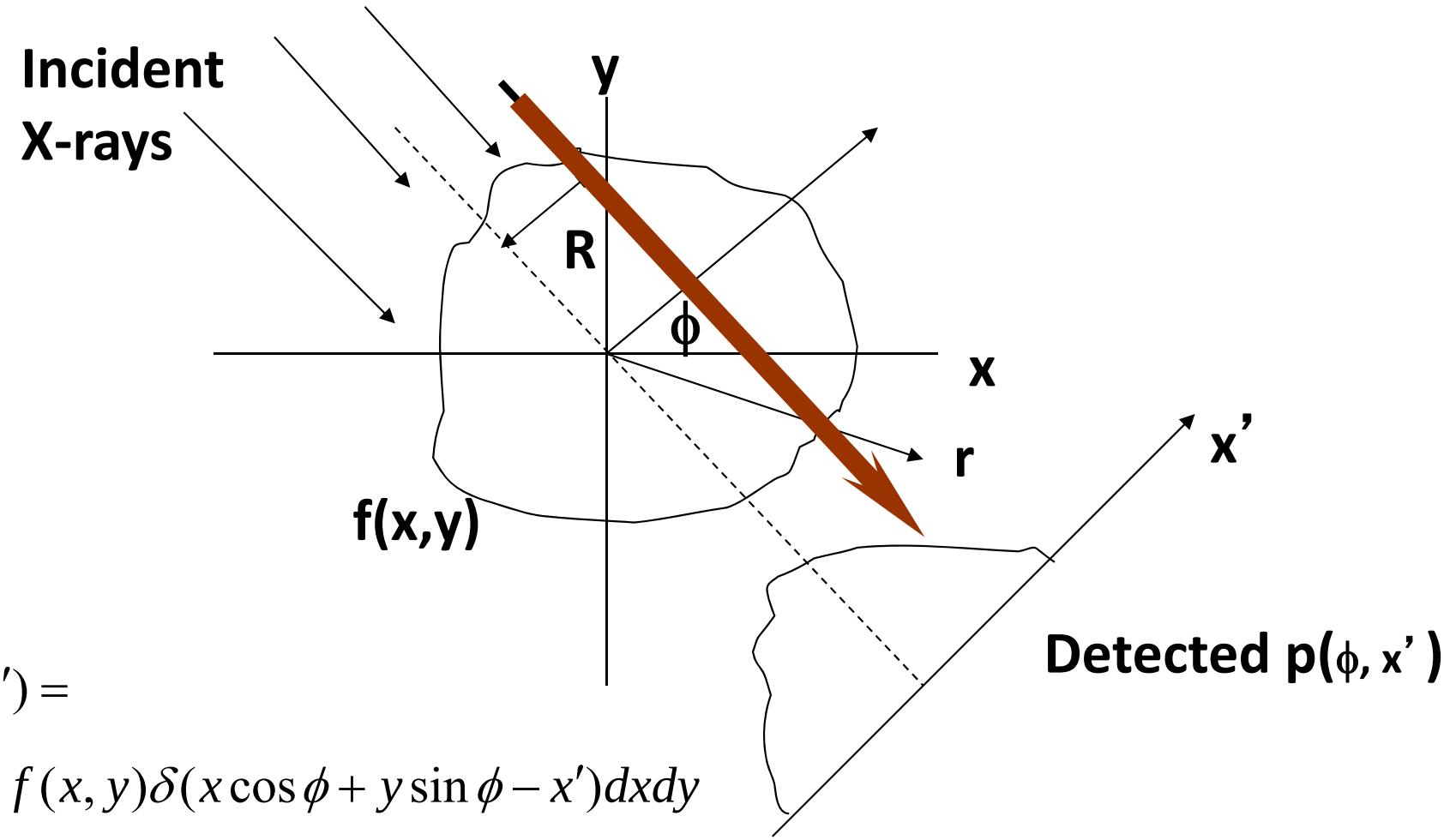

$$p(\phi, x') = \int_{-\infty}^{\infty}\int_{-\infty}^{\infty} f(x,y)\delta(x\cos\phi + y\sin\phi - x')dxdy$$

Simple Backprojection

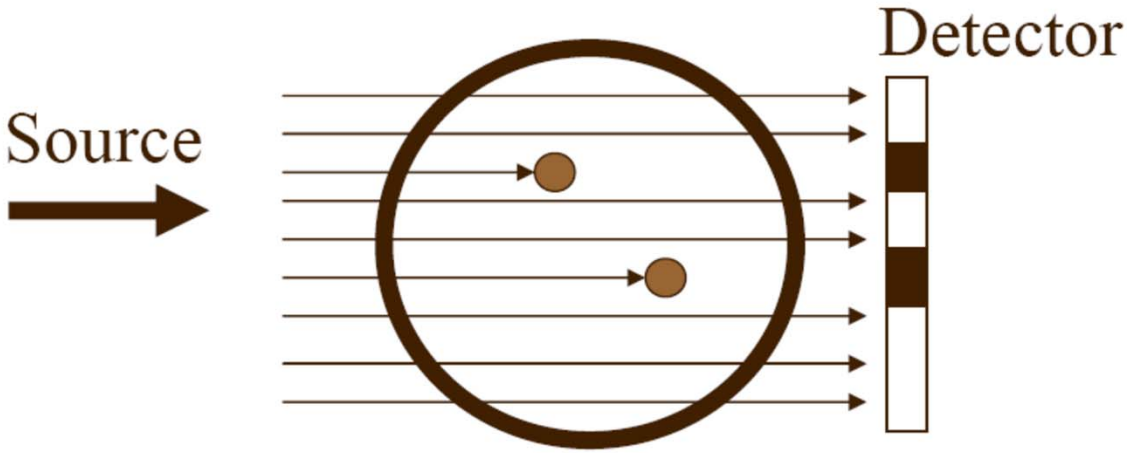

inverse = 1 back projection

Simple Backprojection

Crude Idea 1: Take each projection and smear it back along the lines of integration it was calculated over.

Result from a back projection from a single view angle:

$$b_\phi(x,y) = \int_{x'} p_\phi(x') \, \delta(x\cos\phi + y\sin\phi - x') \, dx'$$

Adding up all the back projections from all the angles gives,

$$f_{\text{back-projected}}(x,y) = \int b_\phi(x,y) \, d\phi$$

$$f_b(x,y) = \int_0^\pi d\phi \int_{-\infty}^{\infty} p_\phi(x') \, \delta(x\cos\phi + y\sin\phi - x') \, dx'$$

Simple Back-projection and the 1/r Blurring

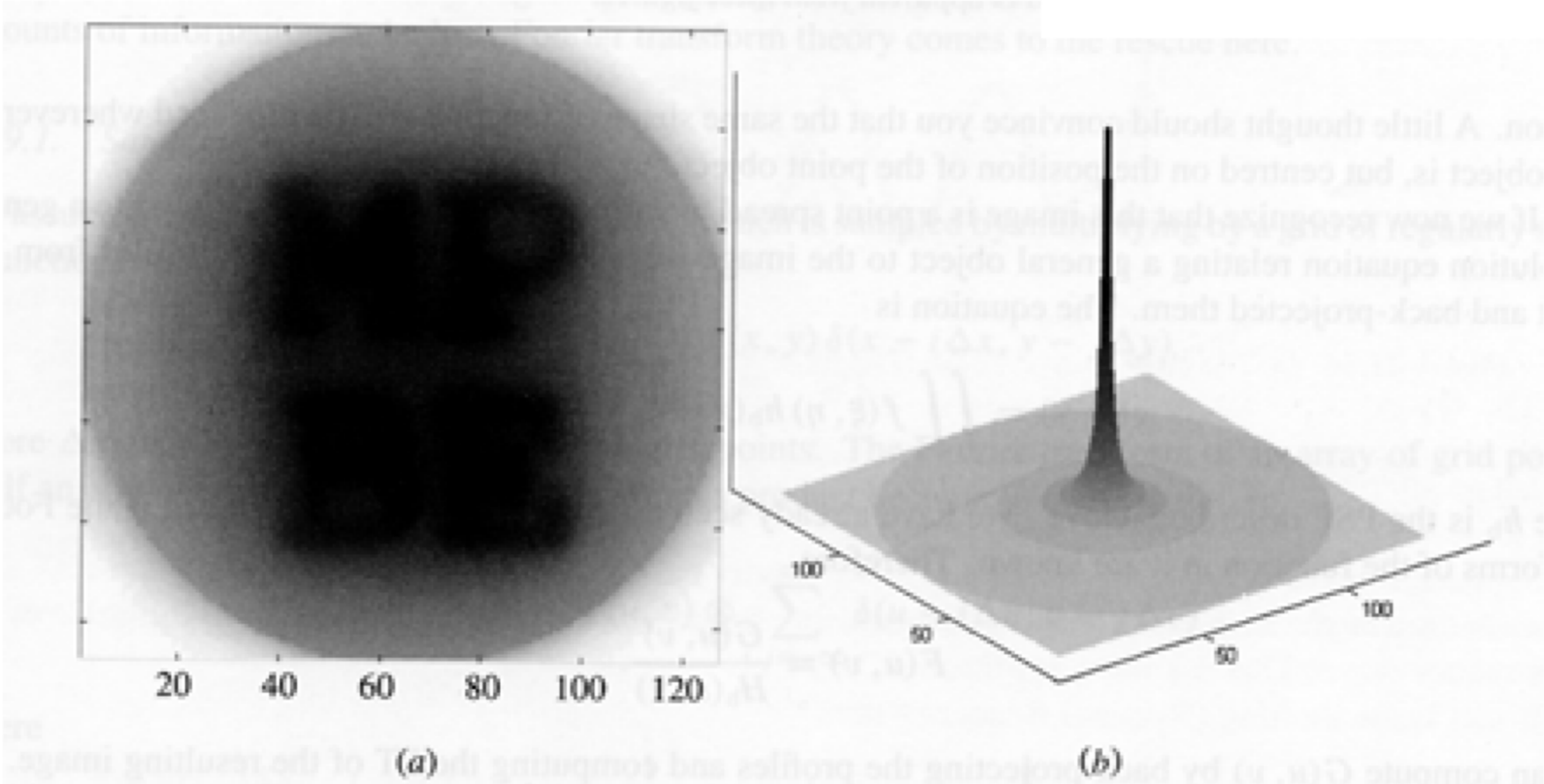

Figure 11.14. *(a) Image produced by back-projecting the sinogram given in figure 11.12(b); (b) the response to a point object in the middle of the field of view.*

From Medical Physics and Biomedical Engineering, Brown, IoP Publishing

Impulse Response Function of Simple Backprojection Operator

$h_b(r) = 1/r$

$f_b(x,y) = f(x,y) * 1/r$

$F_b(\rho,\phi) = F(\rho, \phi) / \rho$ since $F\{1/r\} = 1/\rho$

Back projected image is blurred by convolution with 1/r

Simple Back-projection and the 1/r Blurring

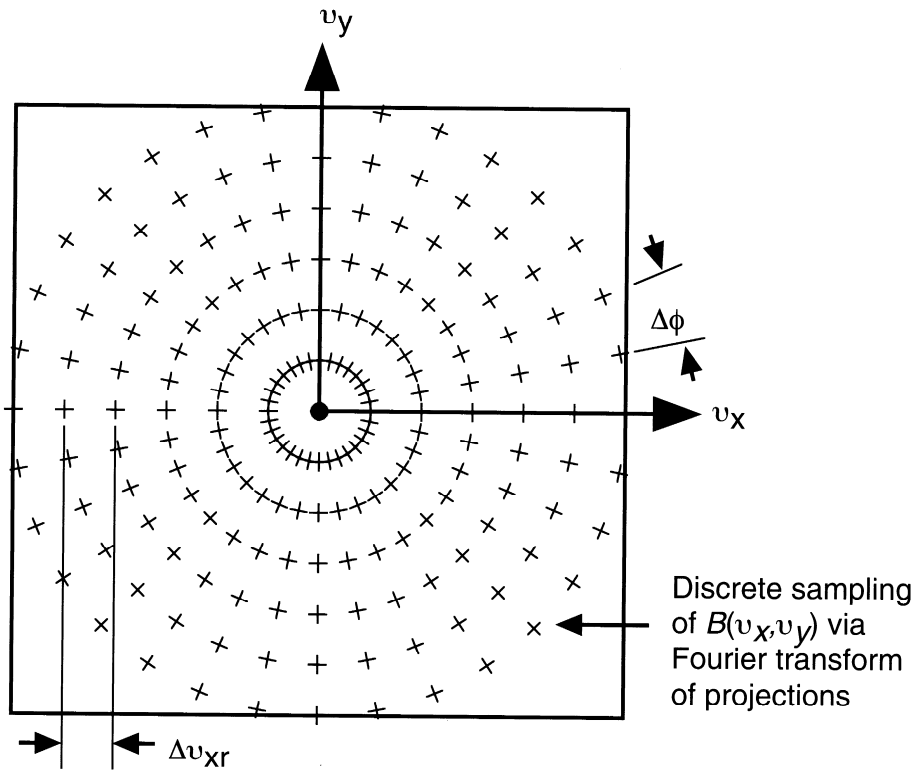

FIGURE 18 The discrete sampling pattern of $F(\upsilon_x,\upsilon_y)$ contained in $B(\upsilon_x,\upsilon_y)$, resulting from the use of discretely sampled projections.

The nature of the 1/r blurring:
Radon transform produced equally spaced radial sampling in Fourier domain.

Simple Backprojection

Crude Idea 1: Take each projection and smear it back along the lines of integration it was calculated over.

Result from a back projection from a single view angle:

$$b_\phi(x,y) = \int_{x'} p_\phi(x') \, \delta(x\cos\phi + y\sin\phi - x') \, dx'$$

Adding up all the back projections from all the angles gives,

$$f_{\text{back-projected}}(x,y) = \int b_\phi(x,y) \, d\phi$$

$$f_b(x,y) = \int_0^\pi d\phi \int_{-\infty}^{\infty} p_\phi(x') \, \delta(x\cos\phi + y\sin\phi - x') \, dx'$$

Inverse Radon Transform

Suppose the sample projection data preserves all information contained in the original function f(x,y), can we recover the exact function f(x,y) with an *Inverse Radon Transform*?

$$\mathscr{R}^{-1}\{\mathscr{R}[f(x,y)]\} = \hat{f}(x,y)$$

Filtered Back-projection

Mathematically, we can define a *filtered back-projection* FBP operation to remove the 1/r blurring.

$$\hat{f}(x,y) = \frac{1}{\pi}\int_0^{\pi} d\phi \int_{-\infty}^{\infty} dx'\, p_\phi(x')h(x\cos\phi + y\sin\phi - x')$$

where

$$h(x) = \mathcal{F}_1^{-1}[|\omega|]$$
$$= \mathcal{F}_1^{-1}[H(\omega)]$$

Can this be realized ??

Due to the diverging nature of the |w| function, the corresponding filter kernel does not exist in spatial domain!

Inverse Radon Transform

The estimate of the original image f(x,y) can be obtained as

$$\hat{f}(x,y) = \hat{f}(r,\theta) = \beta \mathscr{H}\{p_\phi(x')\}$$

The simple back projection operator

$$= \beta \mathscr{H}\{\mathscr{R}[f(x,y)]\}$$

$$= \mathscr{R}^{-1}\{\mathscr{R}[f(x,y)]\}$$

where

$$\mathscr{H}\{p_\phi(x')\} = \mathscr{F}_1^{-1}[|\omega|] * p_\phi(x')$$

The inverse Radon transform can be represented as a filtering process followed by a back-projection operation.

Inverse Radon Transform

The estimate of the original image f(x,y) can be obtained as

$$\hat{f}(r,\theta) = \int_0^{\pi}\int_{-\infty}^{\infty} |\omega| P_\phi(\omega) \exp[i\omega(x\cos\phi + y\sin\phi)]\, d\omega\, d\phi$$

$$= \int_0^{\pi} p_\phi^*(x')\, d\phi$$

where

$$p_\phi^*(x') = \int_{-\infty}^{\infty} |\omega| P_\phi(\omega) \exp(i\omega x')\, d\omega$$

$$= \mathcal{F}_1^{-1}\left[|\omega| P_\phi(\omega)\right]$$

$$= \mathcal{F}_1^{-1}[|\omega|] * p_\phi(x')$$

and

The Central Slice Theorem

$$P_\phi(\omega) = F(\omega\cos\phi, \omega\sin\phi)$$

$$= F(\omega_{x'}, \omega_{y'})\big|_\phi \quad \text{or} \quad F(\omega_x, \omega_y)\big|_\phi$$

$$= F(\omega, \phi)$$

Filtered Back-projection

The Ram-Lak filter

$$H_{\mathrm{RL}}(\omega) = \begin{cases} |\omega|, & (|\omega| \le 2\pi B) \\ 0, & (\text{otherwise}) \end{cases}$$

Ram-Lak filter

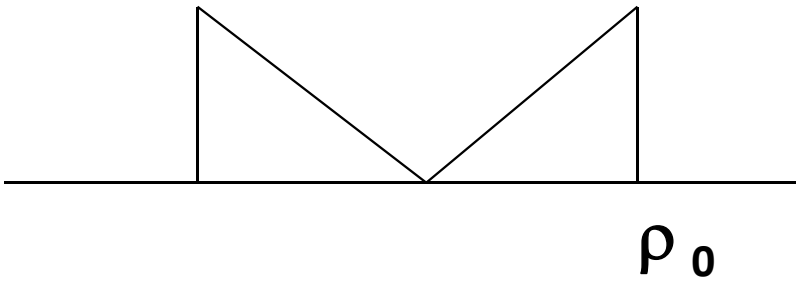

Ideal filter

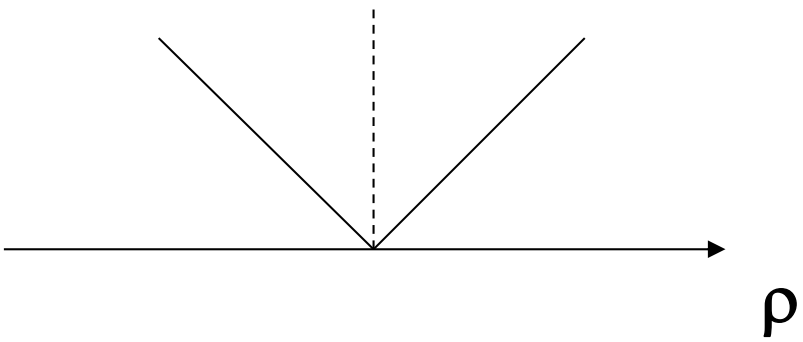

Filtered Back-projection

The Ram-Lak filter in spatial domain

$$h_{\mathrm{RL}}(x) = \frac{1}{2\pi}\int_{-\infty}^{\infty} H_{\mathrm{RL}}(\omega)\exp(ix\omega)\,d\omega$$

$$= \frac{1}{2\pi}\int_{-2\pi B}^{2\pi B} |\omega|\exp(ix\omega)\,d\omega$$

$$= 2B^2\,\mathrm{sinc}(2\pi Bx) - B^2\,\mathrm{sinc}^2(\pi Bx)$$

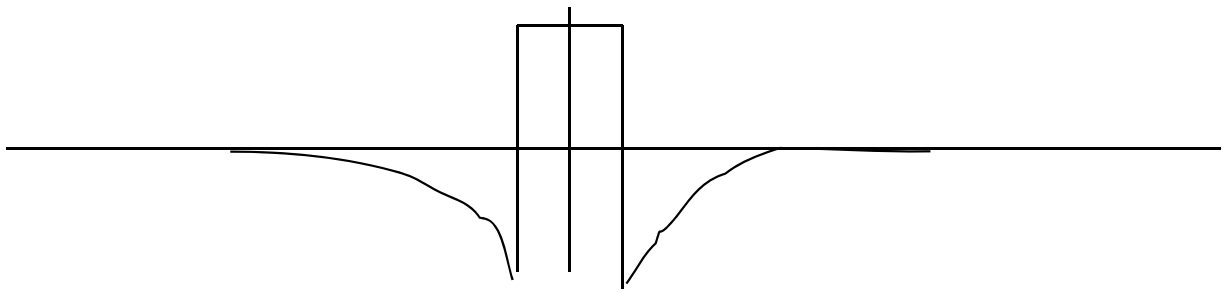

$$\hat{f}(x,y) = \frac{1}{\pi}\int_0^{\pi} d\phi \int_{-\infty}^{\infty} dx'\, p_\phi(x')h(x\cos\phi + y\sin\phi - x')$$

Simple and Filtered Back-projection

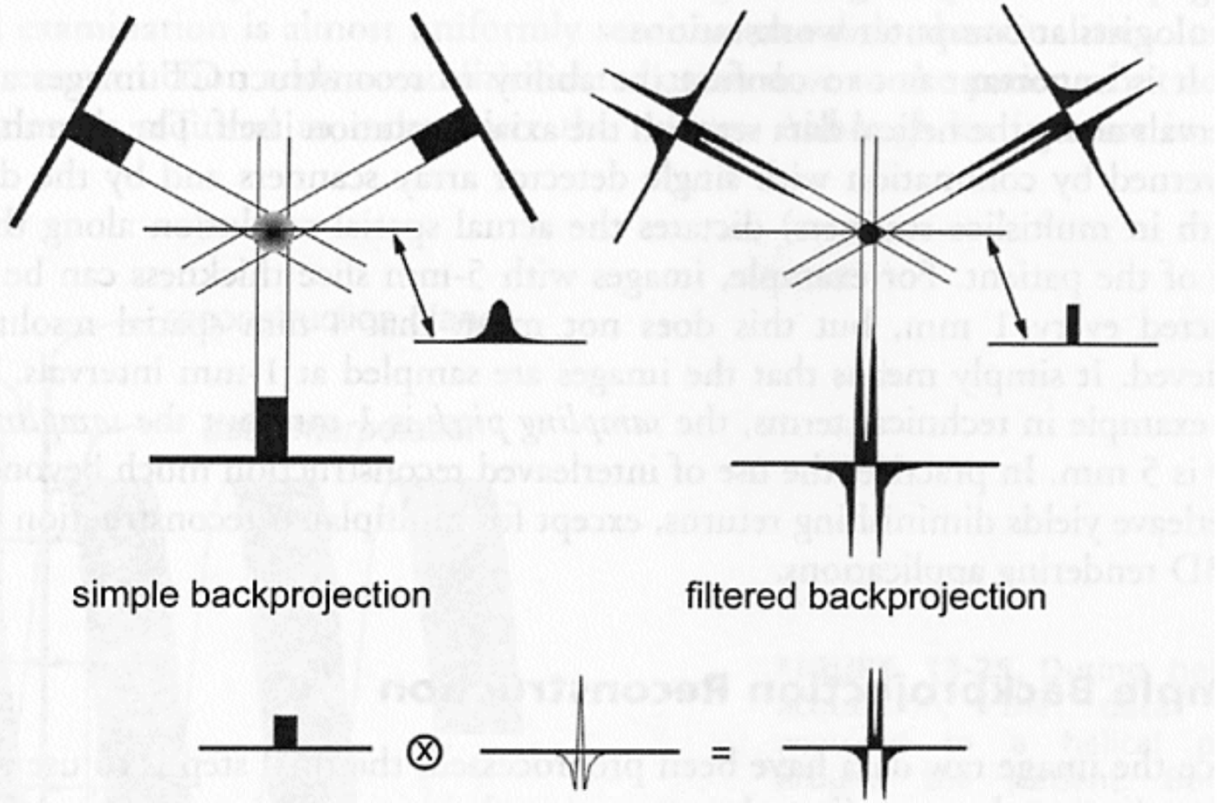

FIGURE 13-28. Simple backprojection is shown on the left; only three views are illustrated, but many views are actually used in computed tomography. A profile through the circular object, derived from simple backprojection, shows a characteristic 1/r blurring. With filtered backprojection, the raw projection data are convolved with a convolution kernel and the resulting projection data are used in the backprojection process. When this approach is used, the profile through the circular object demonstrates the crisp edges of the cylinder, which accurately reflects the object being scanned.

Chapters 12 & 13, The Essential Physics of Medical Imaging, Bushberg

Filtered Back-projection

Therefore the optimum estimator (the optimum reconstruction) of the original image function f(x,y) is

$$\hat{f}(x,y) = \frac{1}{\pi}\int_0^{\pi} d\phi \int_{-\infty}^{\infty} dx'\, \dot{p}_\phi^*(x') h(x\cos\phi + y\sin\phi - x')$$

where the filtered projection data is given by

$$\mathcal{F}_1^{-1}\left[H_{\text{opt}}(\omega,\phi)\right] * \dot{p}_\phi(x') = \dot{p}_\phi^*(x').$$

Image Quality

A Revisit to Key Image Quality Measures

Contrast

- **What is contrast of an image?**
  How to quantify contrast?
  How an imaging system affect contrast?

Covered in lecture

Subject (or Object) Contrast

- **Difference in some aspects of the signal prior to it being recorded**
- **Consequence of fundamental differences in the object, e.g., in x-ray intensity based on attenuation**
- **C = (A-B)/A**

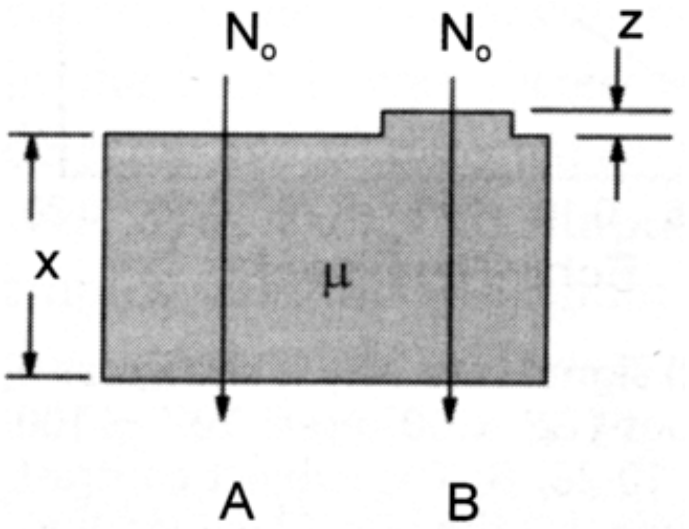

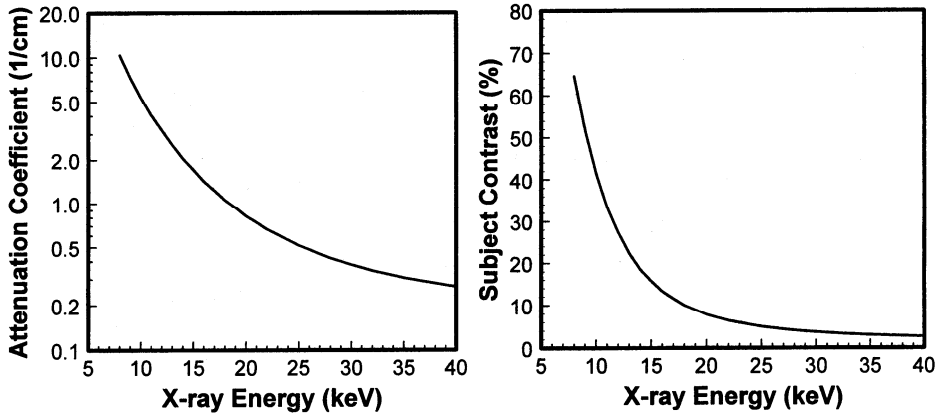

Covered in lecture

Modulation

- **The modulation m_f is an effective way to quantify the contrast of a periodic signal**

$$m_f = \frac{f_{\max} - f_{\min}}{f_{\max} + f_{\min}}.$$

- **In general, m_f is refer to as *the contrast of a periodic signal f(x,y) relative to its average value*.**

- **So within two signals, f(x,y) and g(x,y), with the same average value, f(x,y) is said to have *more contrast* if $m_f > m_g$.**

Covered in lecture

Modulation

- **Suppose an input signal function**

$$f(x, y) = A + B \sin(2\pi u_0 x) ,$$

where A>B and both are non-negative constants.

$$m_f = \frac{f_{\max} - f_{\min}}{f_{\max} + f_{\min}} . \quad \Rightarrow \quad m_f = \frac{B}{A} .$$

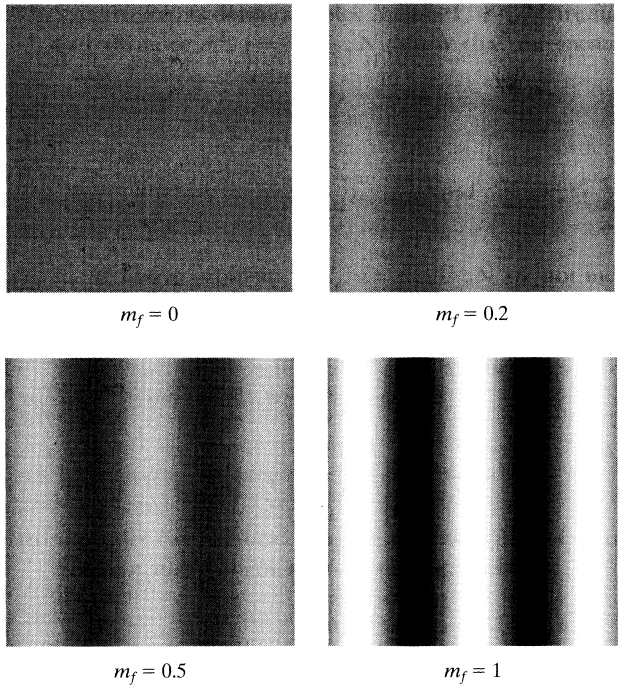

Greater m_f, more contrast

Covered in lecture

Modulation

- **Now let this signal to pass through an LSI imaging system. Suppose an input signal function. Since**

$$f(x,y) = A + B\sin(2\pi u_0 x) = A + \frac{B}{2j}\left[e^{j2\pi u_0 x} - e^{-j2\pi u_0 x}\right],$$

- **Suppose the system impulse response function h(x,y) is circularly symmetric,**

$$g(x,y) = AH(0,0) + B\,|H(u_0,0)|\sin(2\pi u_0 x)\,.$$

- **So the modulation of the output signal is**

$$m_g = \frac{B|H(u_0,0)|}{AH(0,0)} = m_f\frac{|H(u,0)|}{H(0,0)}\,.$$

Covered in lecture

Modulation

- **Now let this signal to pass through an LSI imaging system. Suppose an input signal function. Since**

$$f(x,y) = A + B\sin(2\pi u_0 x) = A + \frac{B}{2j}\left[e^{j2\pi u_0 x} - e^{-j2\pi u_0 x}\right],$$

- **Suppose the system impulse response function h(x,y) is circularly symmetric,**

$$g(x,y) = AH(0,0) + B\,|H(u_0,0)|\sin(2\pi u_0 x)\,.$$

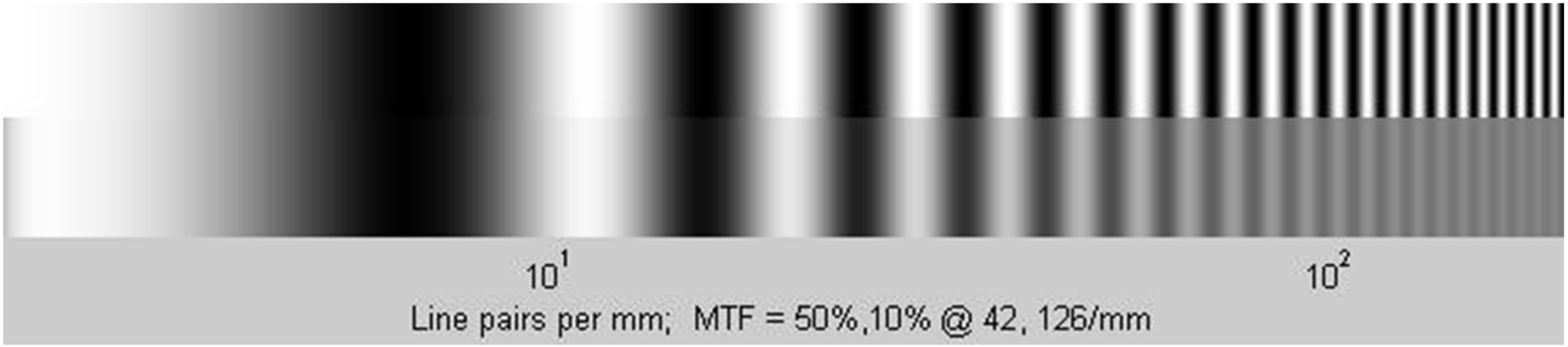

Covered in lecture

Modulation

- **Now let this signal to pass through an LSI imaging system. Suppose an input signal function. Since**

$$f(x,y) = A + B\sin(2\pi u_0 x) = A + \frac{B}{2j}\left[e^{j2\pi u_0 x} - e^{-j2\pi u_0 x}\right],$$

- **Suppose the system impulse response function h(x,y) is circularly symmetric,**

$$g(x,y) = AH(0,0) + B\,|H(u_0,0)|\sin(2\pi u_0 x)\,.$$

- **So the modulation of the output signal is**

$$m_g = \frac{B|H(u_0,0)|}{AH(0,0)} = m_f\frac{|H(u,0)|}{H(0,0)}\,.$$

Covered in lecture

Modulation

- **The effect of an LSI having circular symmetric impulse response function on an input sinusoidal signal is to *scale the input signal by a factor equal to the magnitude spectrum at the same frequency u_0*.**

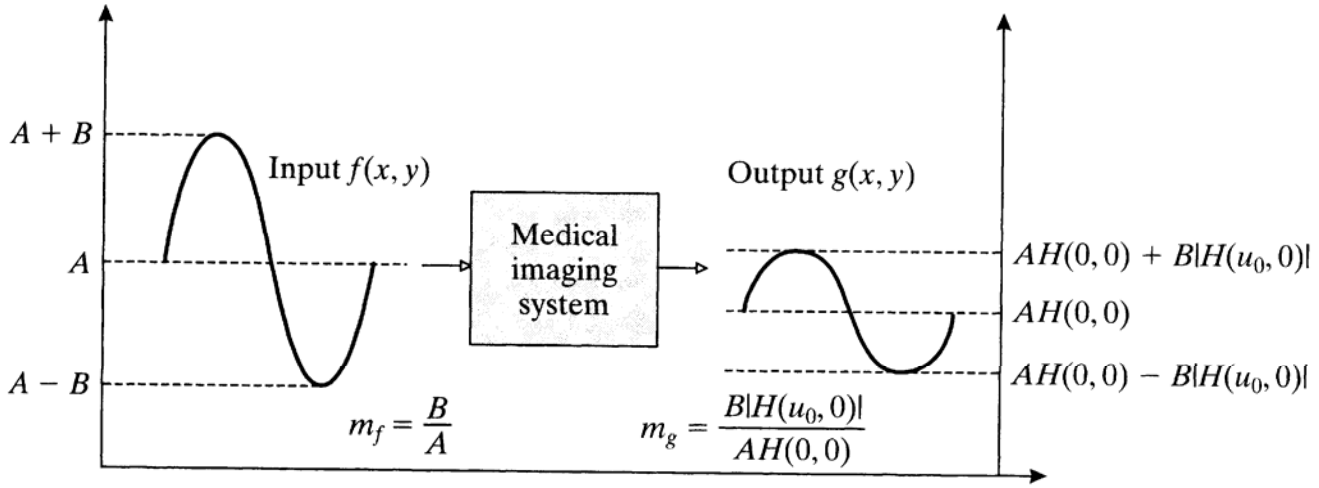

- **It is often true that H(0,0) ≅1, and H(U_0,0) <1. So that the output signal has less contrast, $m_g < m_f$.**

Covered in lecture

Modulation Transfer Function (MTF)

- **In order to fully quantify the response of an LSI for an arbitrary signal, f(x,y), we would need to know the response of the system to sinusoidal signals at different frequencies.**

- **Modulation Transfer Function (MTF).**

$$\mathrm{MTF}(u) = \frac{m_g}{m_f} = \frac{|H(u,0)|}{H(0,0)} .$$

- **MFT is, in effect, the "frequency response function" of an given imaging system. It is normally evaluated for positive frequencies only.**

- **Most imaging systems lead to decreased contrast, so that**

$$0 \leq \mathrm{MTF}(u) \leq \mathrm{MTF}(0) = 1, \qquad \text{for every } u ,$$

Covered in lecture

Modulation Transfer Function (MTF)

- **In case of non-isotropic impulse response function (h(x,y) is not circularly symmetric), the MTF can be defined as**

$$\mathrm{MTF}(u,v) = \frac{m_g}{m_f} = \frac{|H(u,v)|}{H(0,0)},$$

- **A typical MTF of an imaging system**

$$|H(u,v)| = \sqrt{H_R^2(u,v) + H_I^2(u,v)}$$

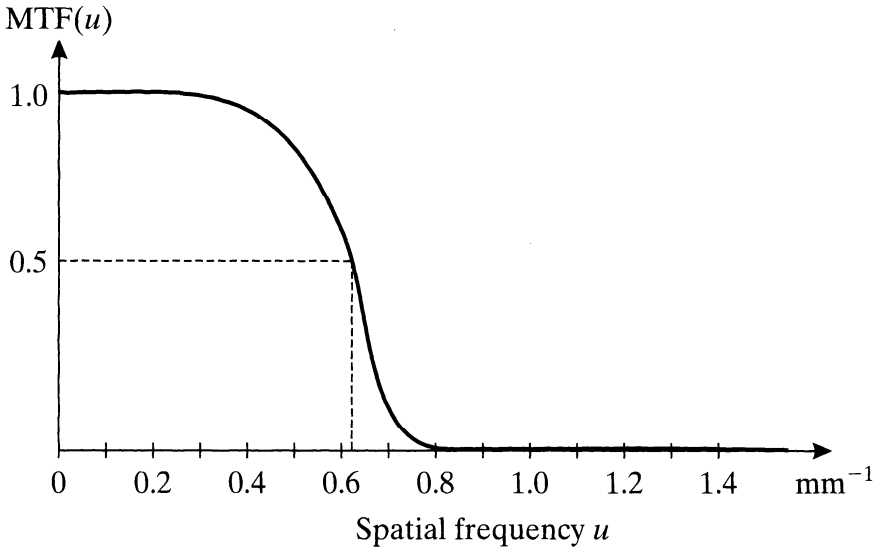

Figure 3.3
A typical MTF of a medical imaging system.

Modulation transfer Function -- Revisited

- **Modulation Transfer Function (MTF).**

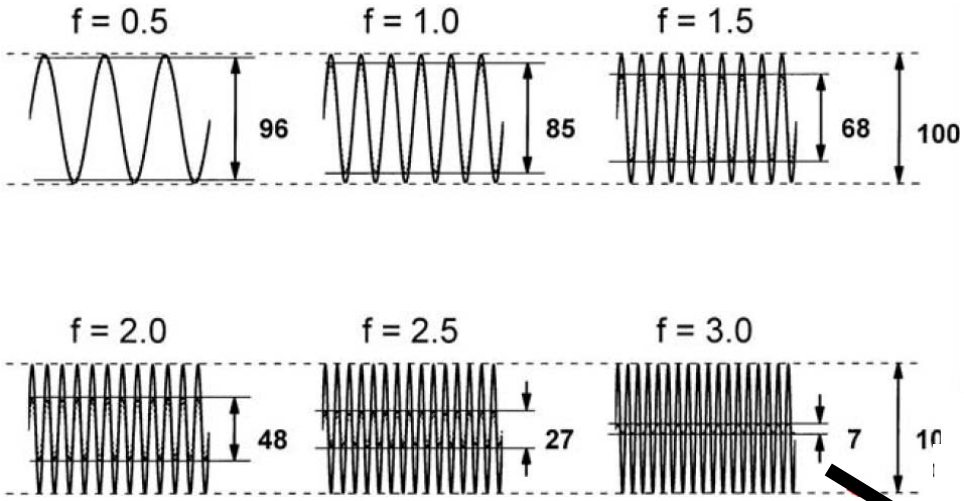

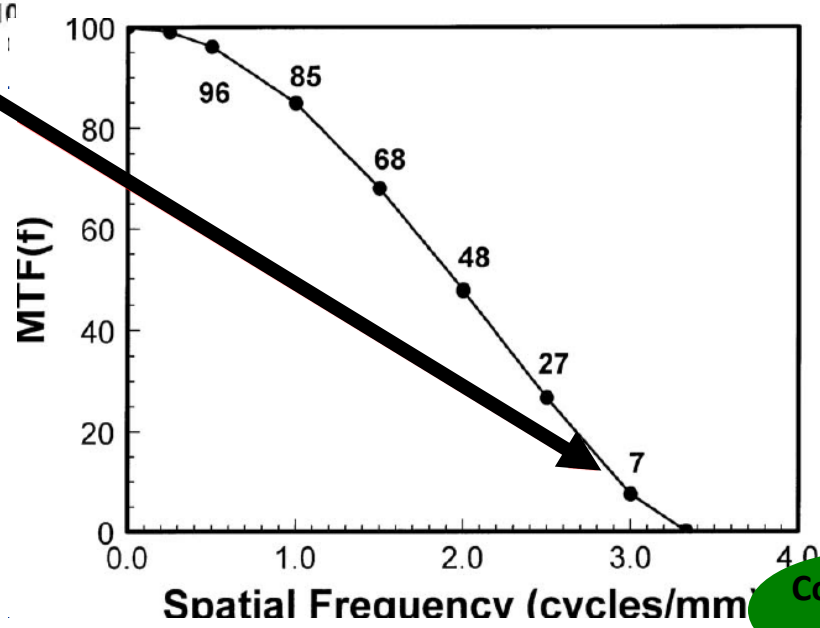

Covered in lecture

A Revisit to Key Image Quality Measures

Spatial Resolution

- **How to quantify spatial resolution?**
- **How to measure spatial resolution?**
- **The relationship between spatial resolution and modulation transfer function (MTF)?**

Spatial Resolution

- ***Resolution*: the ability of an given imaging system to *accurately depict two distinct events in space, time or frequency* respectively.**
- **Resolution can also be thought as the *degree of blurring, smearing*.**

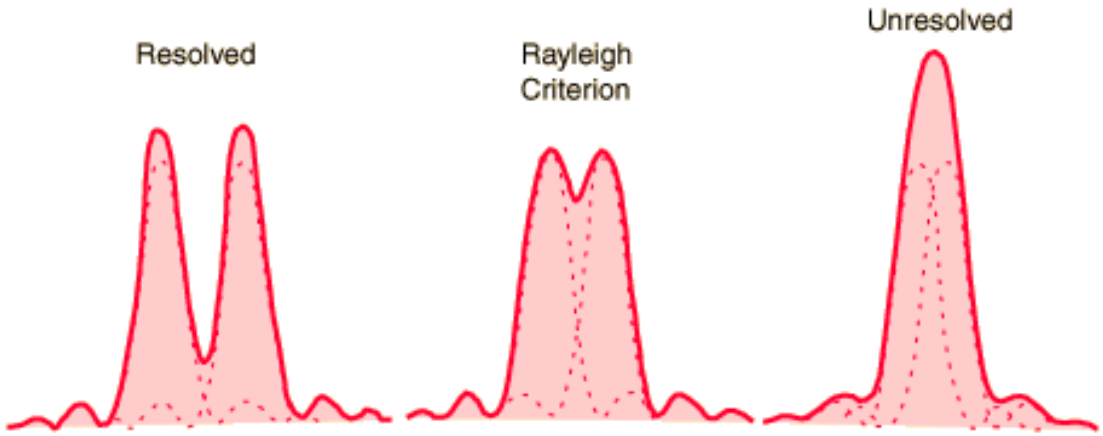

- **Spatial resolution *is fully described by the point-spread function* or *impulse response function, h(x,y)*.**

Full-width at Half Maximum (FWHM) of The Point Spread Function (PSF)

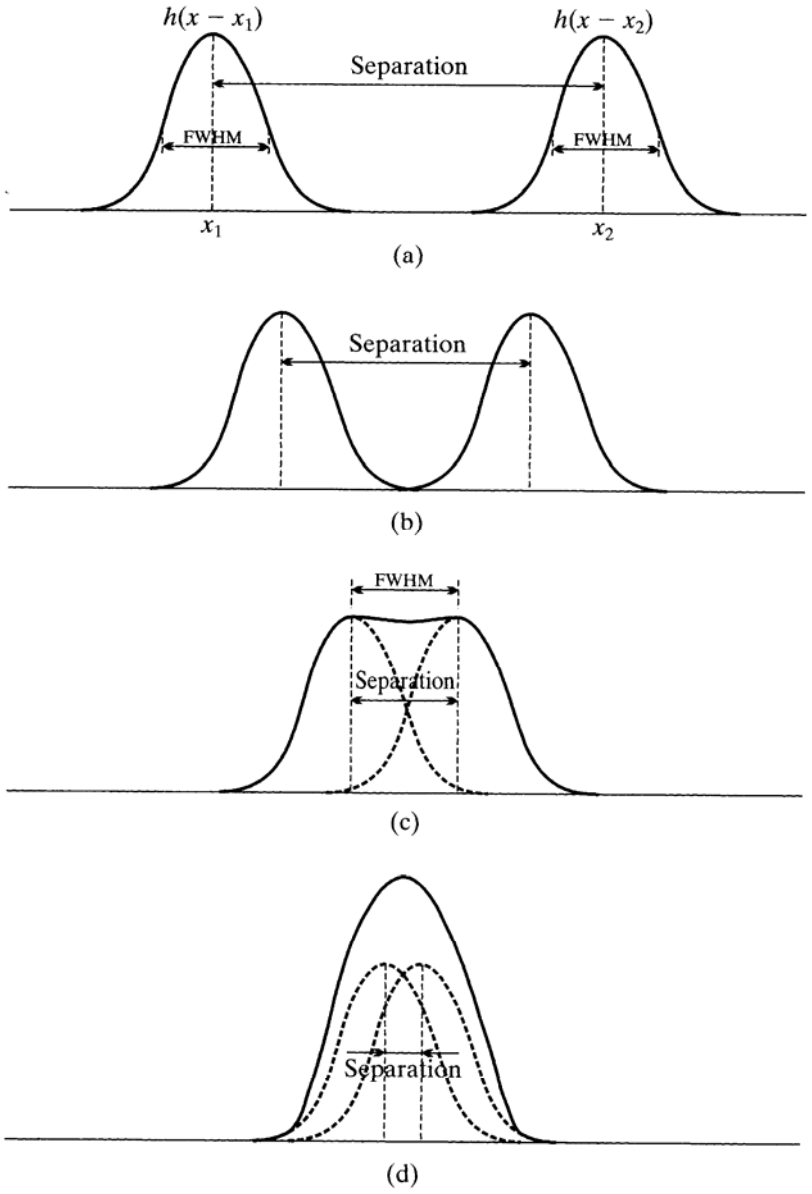

Figure 3.6
An example of the effect of system resolution on the ability to differentiate two points. The FWHM equals the minimum distance that the two points must be separated in order to be distinguishable.

Other Ways to Measure the Spatial Resolution
Line Response Function

- **The resolution of an imaging system can also be estimated with the *line-spread function***
- **Given a line impulse**

$$line\ impulse\ f(x,y) = \delta_\ell(x,y) = \delta(x\cos\theta + y\sin\theta - \ell)$$

- **Assuming the impulse response function of the imaging system h(x,y) is isotropic, *line response function* is**

$$\begin{aligned} g(x,y) &= \int_{-\infty}^{\infty}\int_{-\infty}^{\infty} h(\xi,\eta) f(x-\xi, y-\eta)\, d\xi\, d\eta, \\ &= \int_{-\infty}^{\infty}\left[\int_{-\infty}^{\infty} h(\xi,\eta)\delta(x-\xi)\, d\xi\right] d\eta, \\ &= \int_{-\infty}^{\infty} h(x,\eta)\, d\eta, \end{aligned}$$

Line Response Function

- **The 1-D Fourier transform of the line spread function is**

$$
\begin{aligned}
L(u) &= \mathcal{F}_{1D}[l](u)\,, \\
&= \int_{-\infty}^{\infty} l(x) e^{-j2\pi ux}\, dx\,, \\
&= \int_{-\infty}^{\infty}\int_{-\infty}^{\infty} h(x,\eta) e^{-j2\pi ux}\, dx\, d\eta\,, \\
&= H(u,0).
\end{aligned}
$$

- **So the values of the Fourier transform of the LSF crossing an horizontal line passing through the origin is sufficient for describing the LSF**

LSF and MTF

- **Modulation Transfer Function (MTF).**

$$\mathrm{MTF}(u) = \frac{m_g}{m_f} = \frac{|H(u,0)|}{H(0,0)} = \frac{|L(u)|}{L(0)}, \qquad \text{for every } u.$$

- **For a "reasonable" imaging system, the L(0)=1, so that**

$$\mathrm{MTF}(u) = L(u)$$

- **MTF is an effective way to compare two imaging systems in terms of spatial resolution and contrast.**

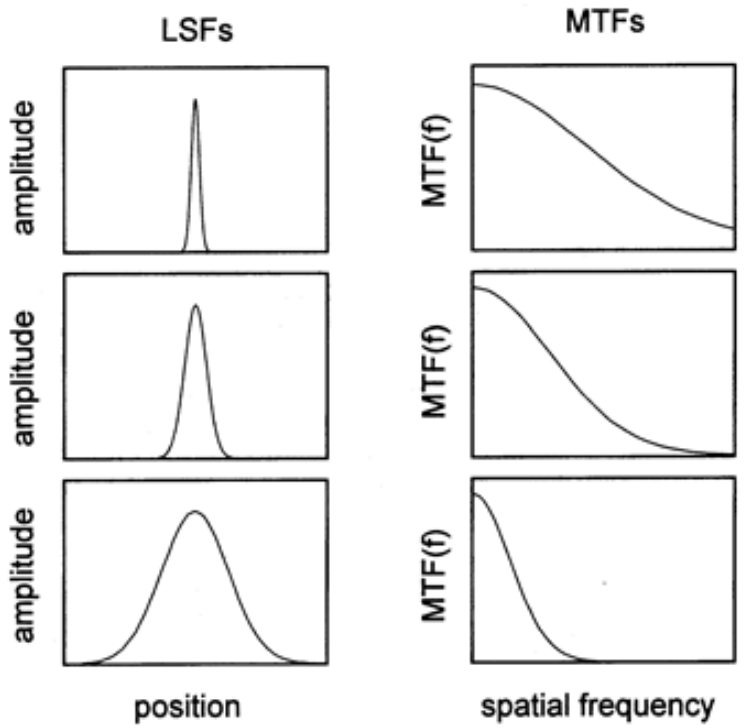

LSF and MTF

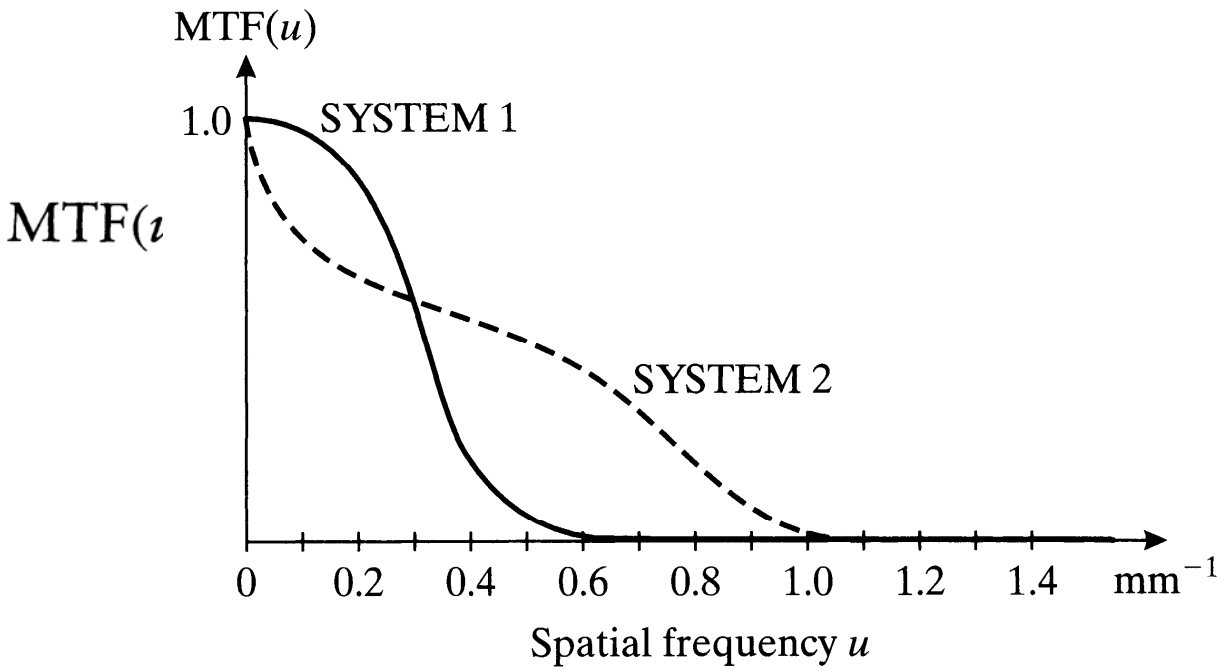

- **System 1 has better low frequency contrast and it is better for imaging coarse features.**
- **System has a better high frequency contrast. It is better for resolving fine details.**
- **The resolution of a system is related to the higher frequency components and the cut-off frequency of the MFT.**

Image Noise

- **The random fluctuation is referred to as the image *noise*. That has dramatic effects on the subsequent analysis, for example, for signal detection and quantification tasks …**

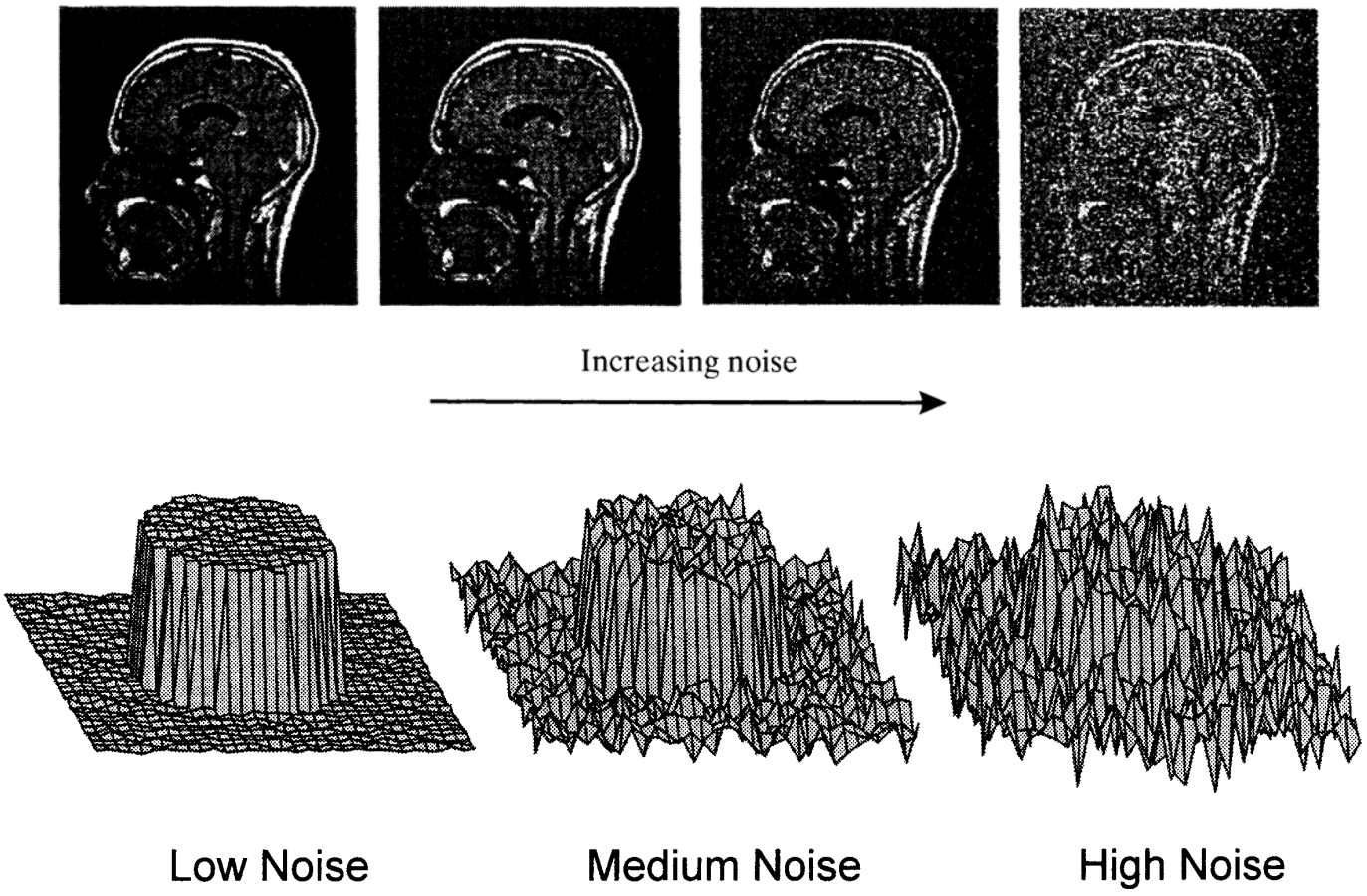

X-ray Imaging

Generations of X-ray CT Systems

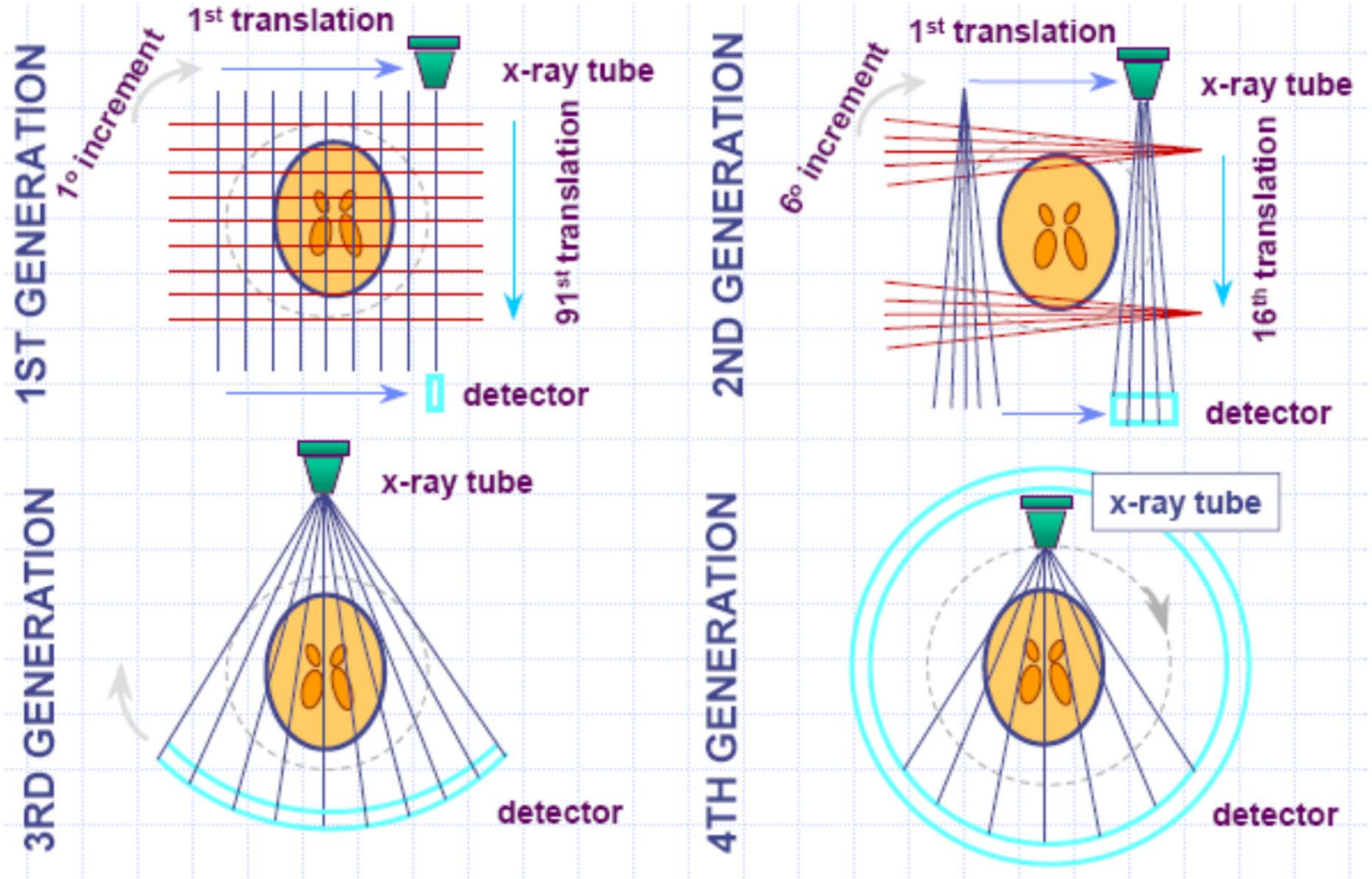

Generations of X-ray CT Systems

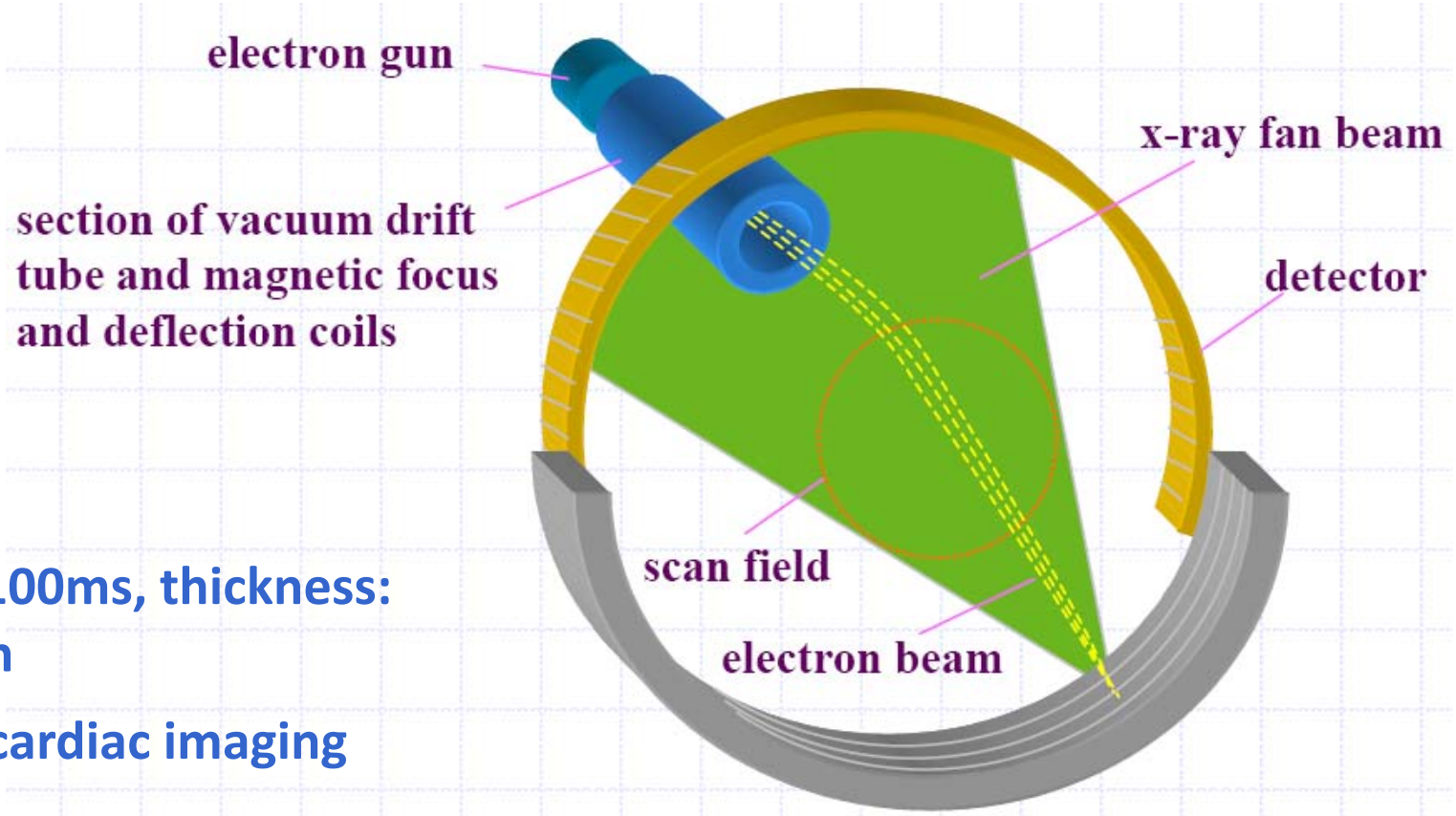

Speed: 50ms, 100ms, thickness: 1.5, 3, 6, 10mm

ECG triggered cardiac imaging

Electron Beam scanner was built between 1980 and 1984 for cardiac applications.

Helical Scanning

In helical scanning, the patient is translated at a constant speed while the gantry rotates.

Helical pitch:

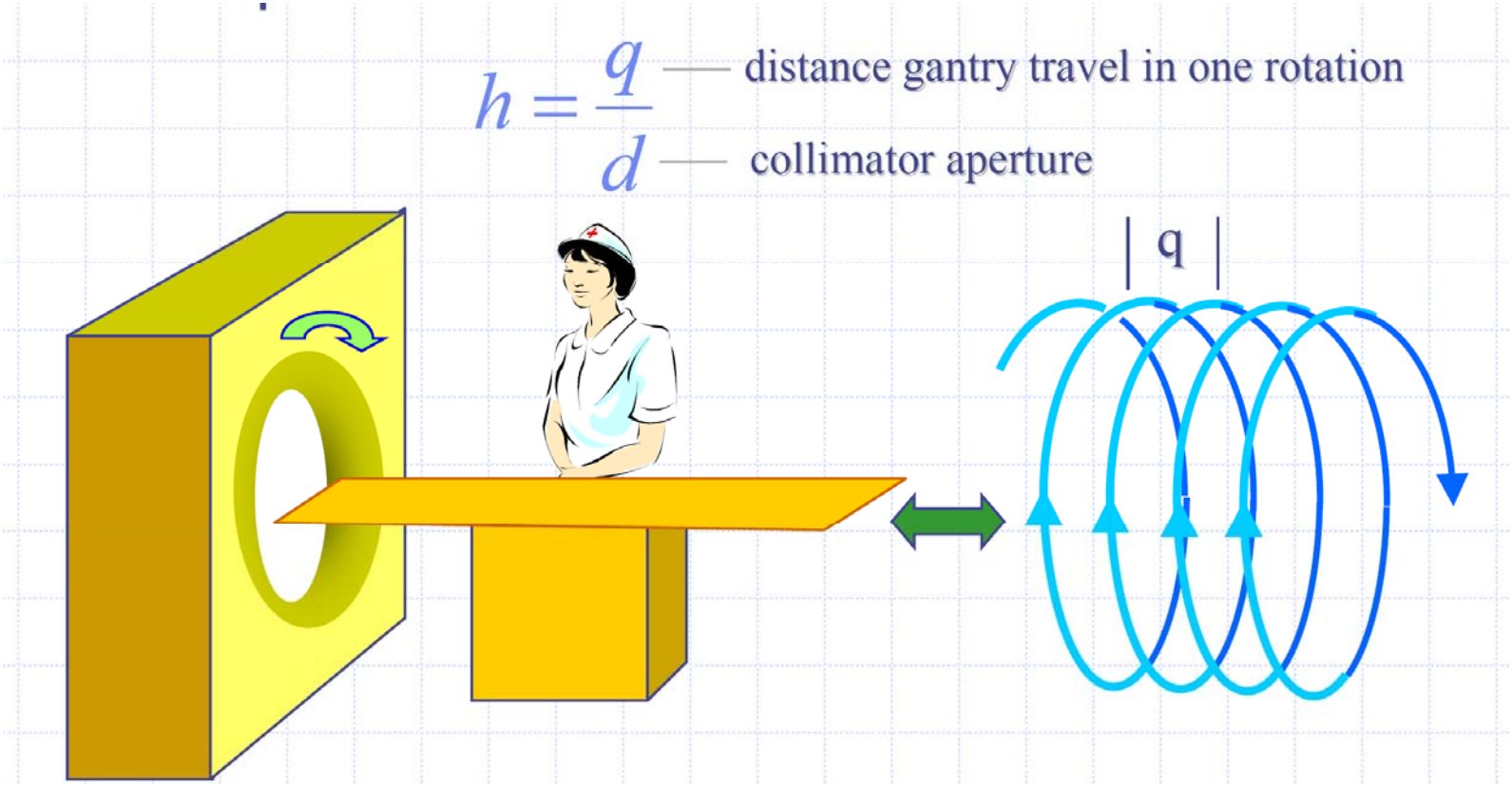

Generations of X-ray CT Systems

- **Multi-slice CT contains multiple detector rows.**
- **For each gantry rotation, multiple slices of projections are acquired.**
- **Similar to the single slice configuration, the scan can be taken in either the step-and-shoot mode or helical mode.**
- **Unlike the single slice, the slice thickness is defined by detector aperture.**

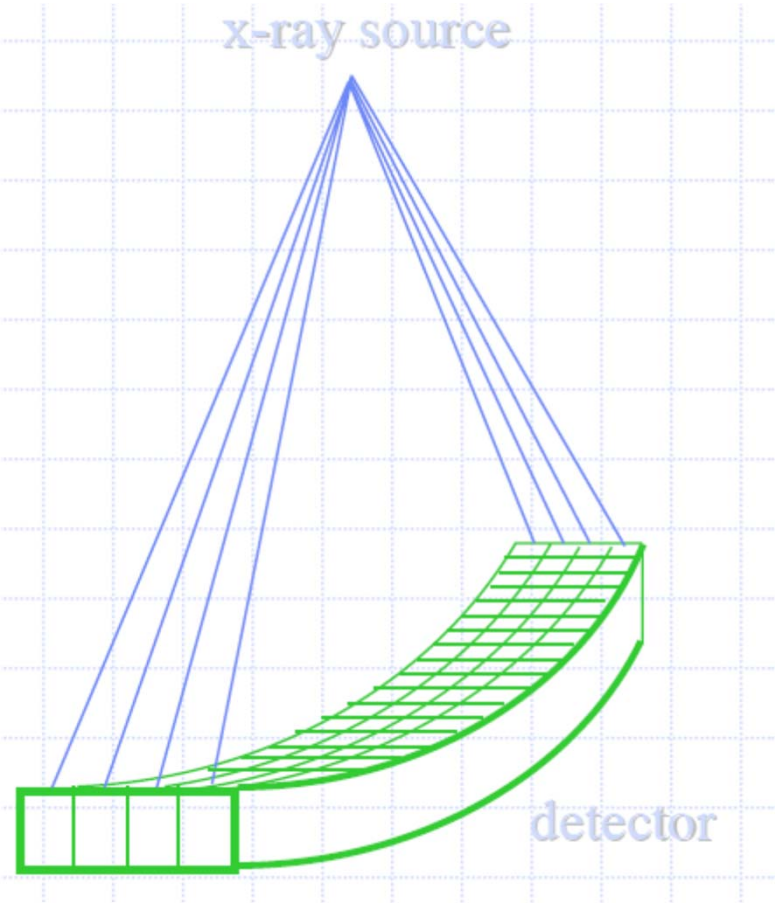

Multi-slice Helical

- When acquiring data in a helical mode, the N (4 or higher) detector rows form N interweaving helixes.
- Because multiple detector rows are used in the data acquisition, the acquisition speed is typically higher.
- Similar to the single slice helical, the projection data are inherently inco

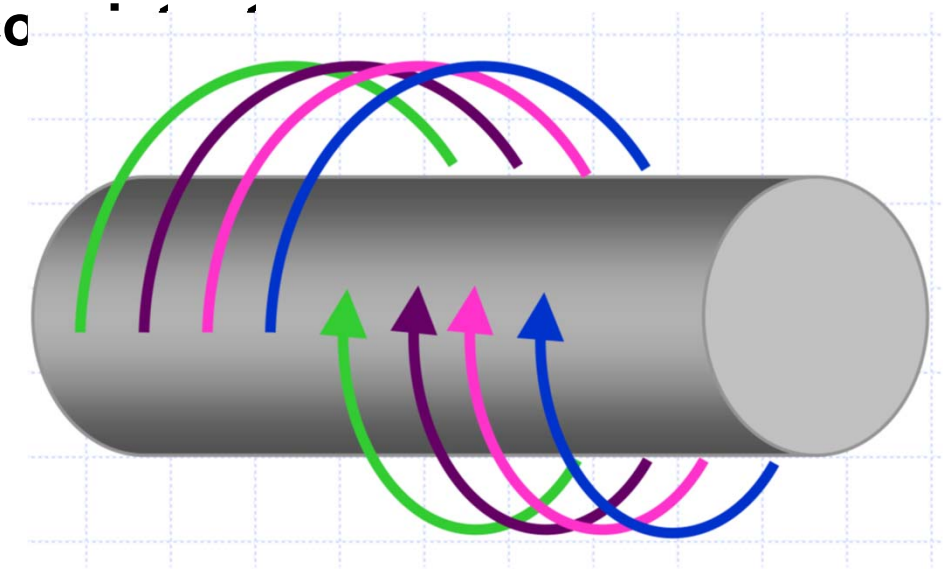

Multi-slice Helical Scanning

- **Large coverage and faster scan speed**
- **Better contrast utilization**
- **Less patient motion artifacts**
- **Near-isotropic spatial resolution**

Inside an X-ray CT System

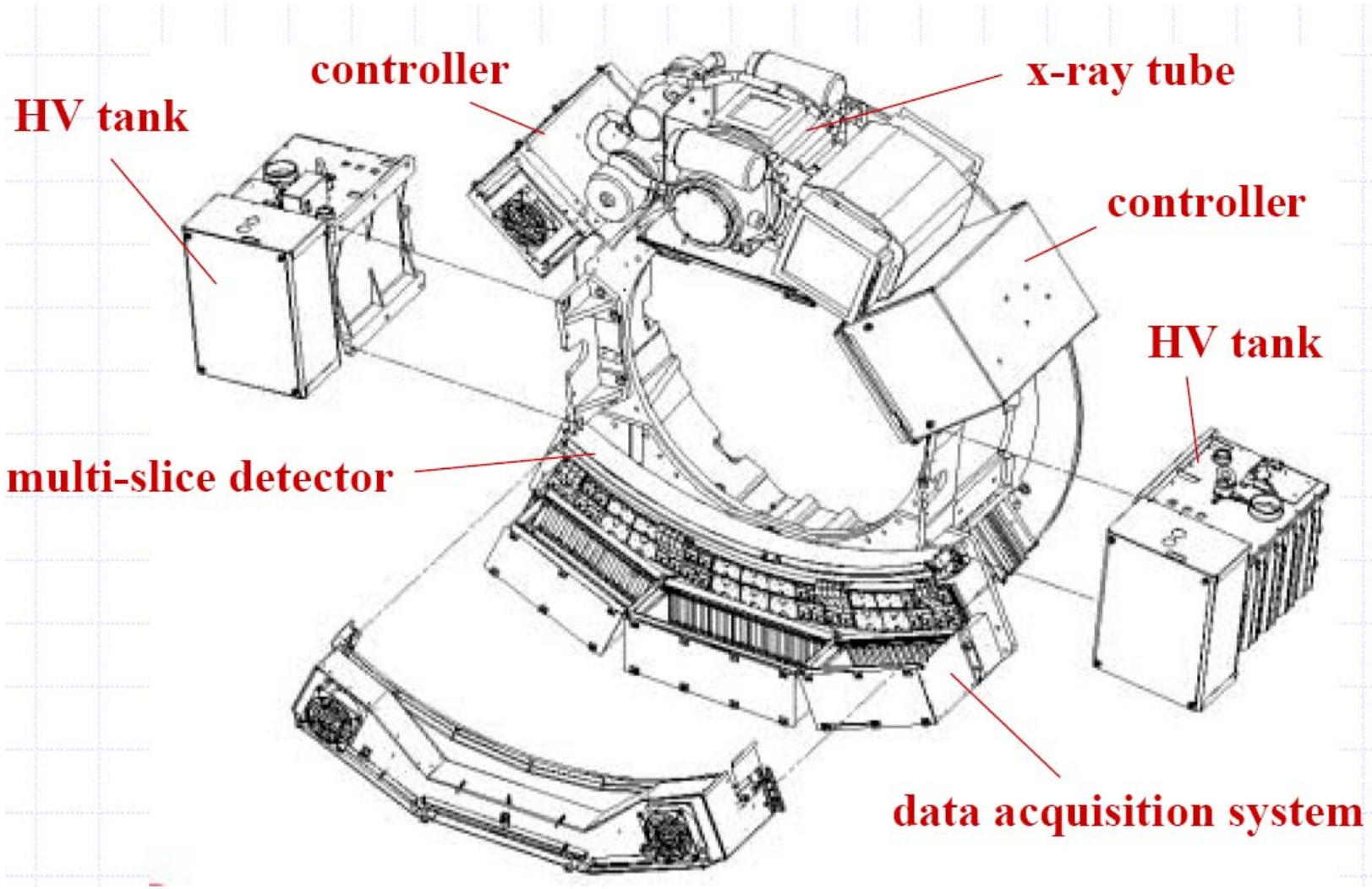

Inside an X-ray CT System

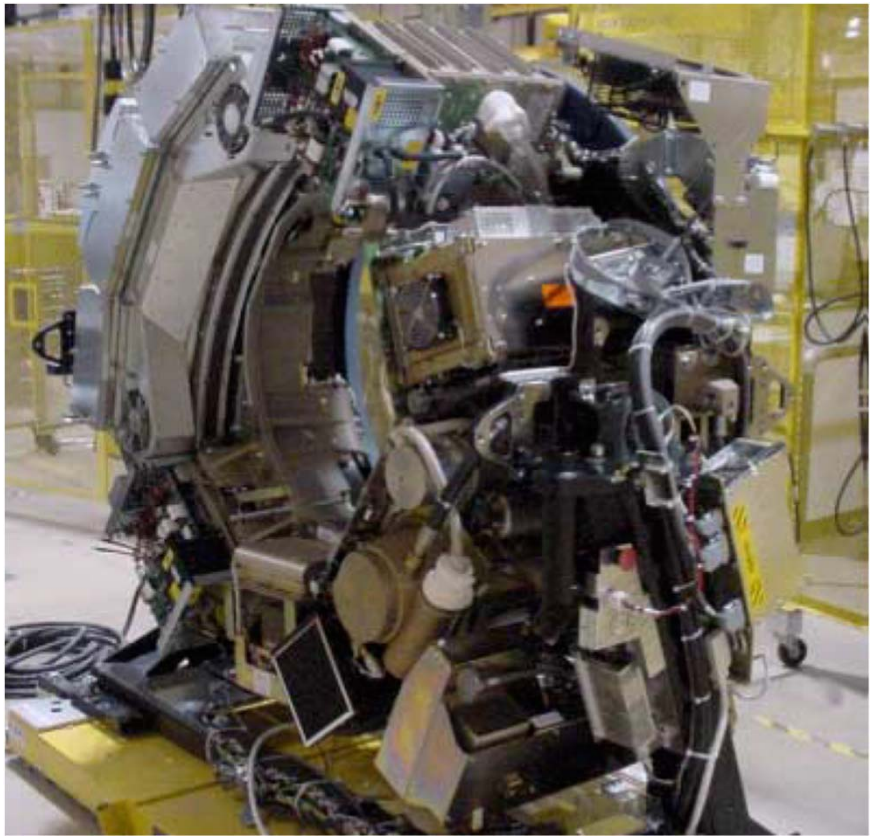

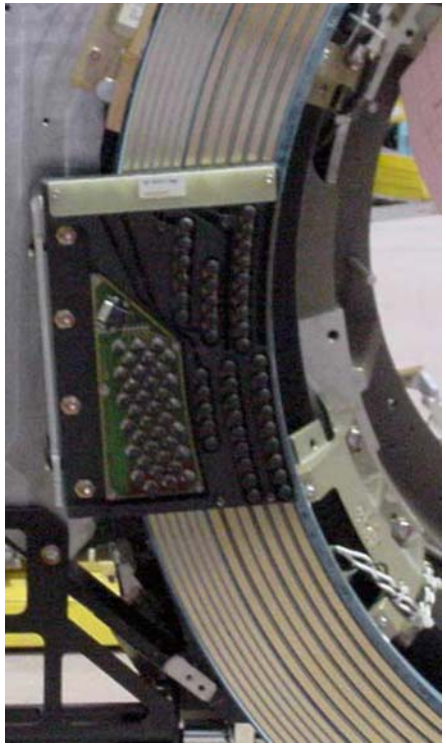

Over 18 millions of samples (400 MBAUD) need to be passed through the slip-ring each second for 8-slice scanner.

For 16-slice, data rate exceeds 800 MBAUD.

X-ray Physics Basics

X-ray Generation – Bremmstrahlung

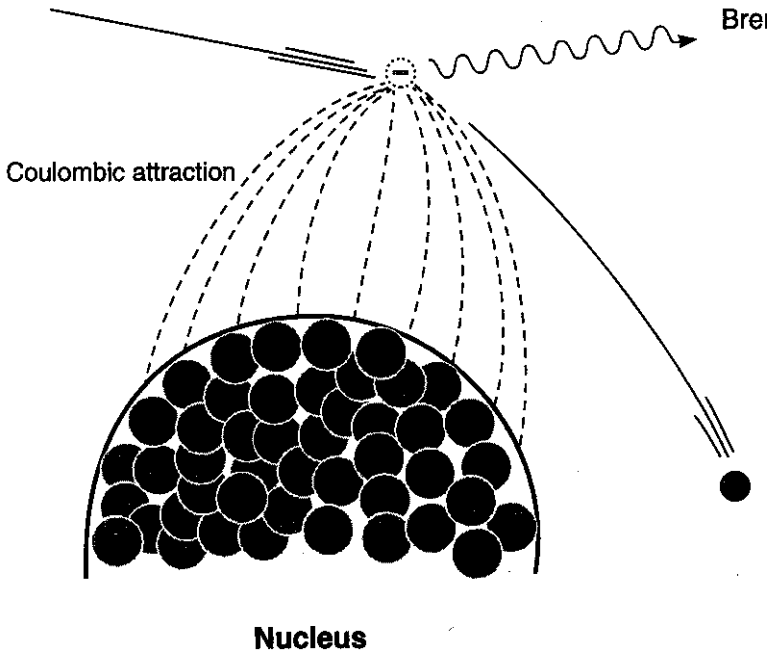

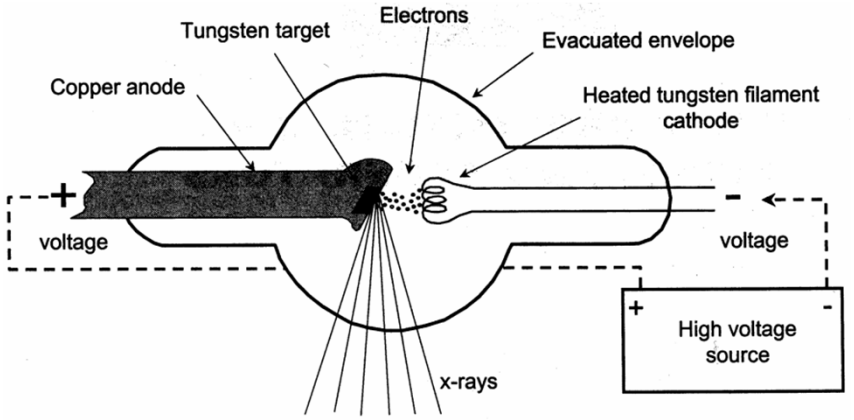

- **X-rays are produced by the conversion of e^- KE into EM radiation - Bremsstrahlung (G: "braking radiation").**
- **A large potential difference is applied across the two electrodes in an evacuated envelope**
- **Neg. charged electrode (*cathode*): source of e^-**
- **Pos. charged electrode (*anode*): target of e^-**

X-ray Generation – Characteristic X-rays

- e^- of the target atom have a binding energy (BE) that depends on atomic Z (rem: $BE_K \propto Z^2$) and the shell ($BE_K > BE_L > BE_M > \ldots$)
- When e^-(KE) incident on the target exceeds the target atom e^-(BE), it's energetically possible for a collisional interaction to eject the bound electron and ionize the atom.
- What would happen then?

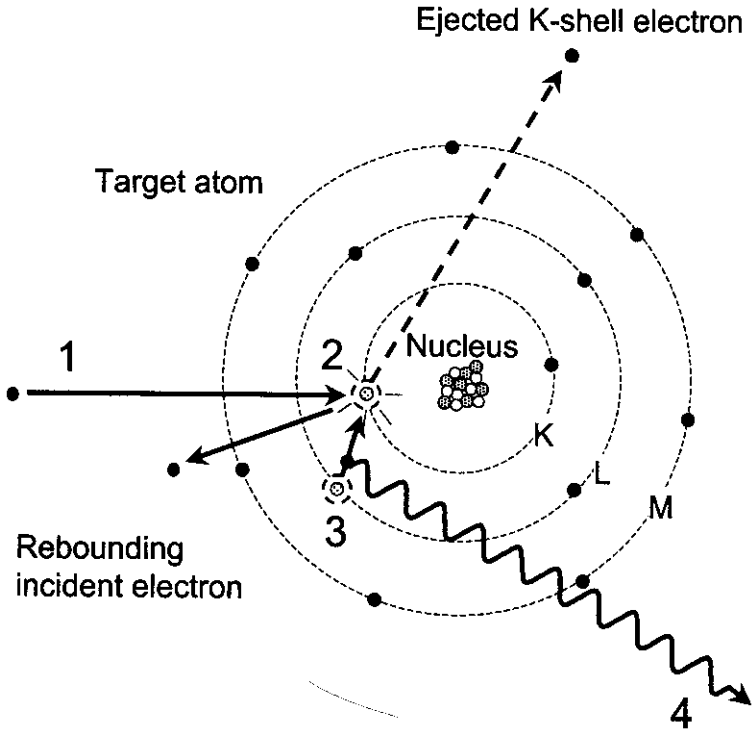

X-ray Spectra from an X-ray Tube

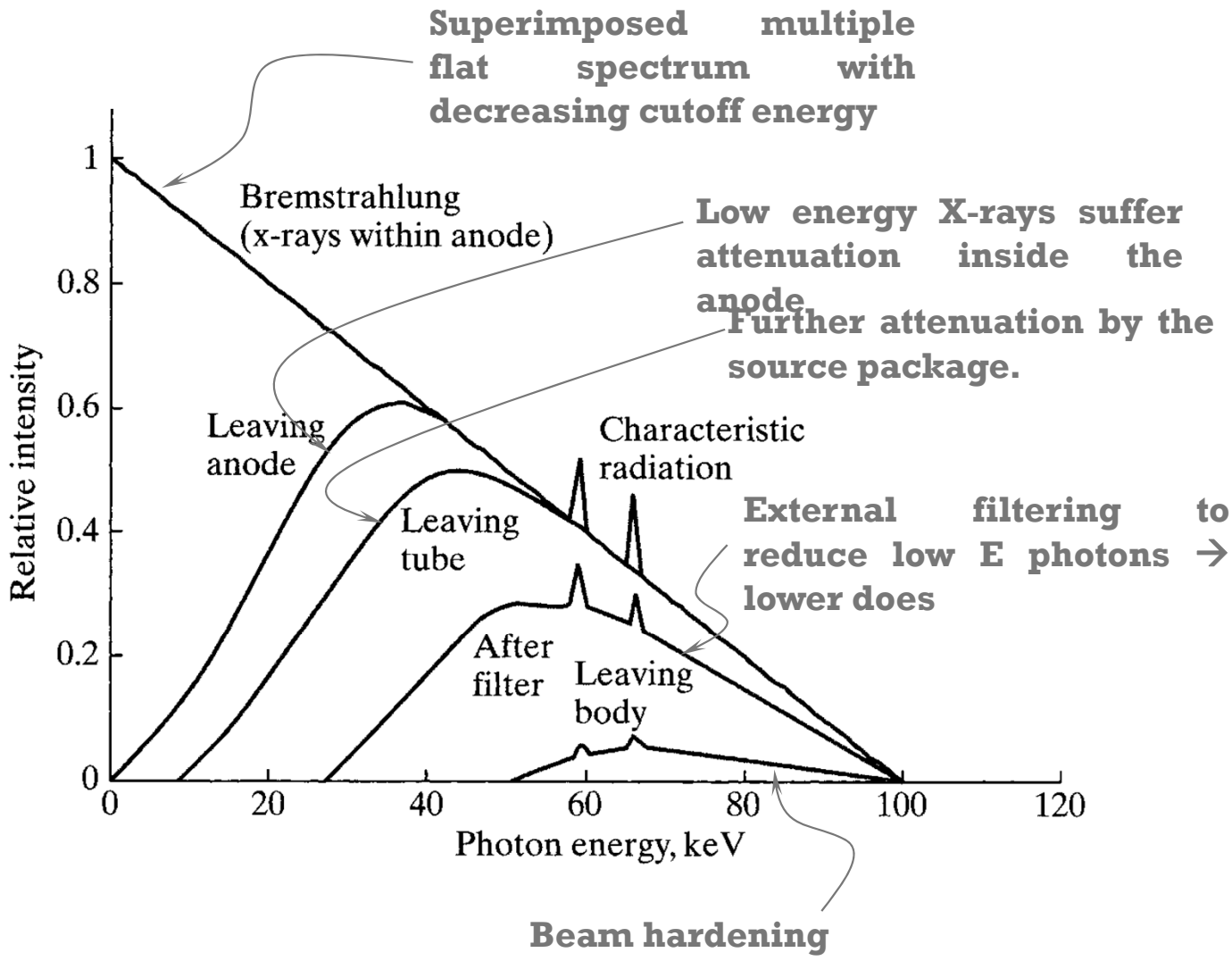

Figure 5.5
Relative intensity of x-ray photons. (Adapted from Webster, 1998. This material is used by permission of John Wiley & Sons, Inc.)

X-ray Generation – X-ray Tube

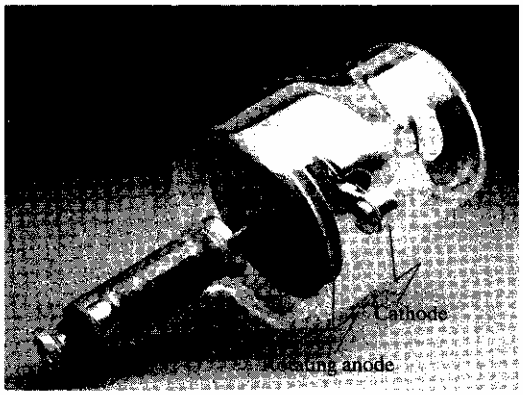

Figure 5.3
An x-ray tube.

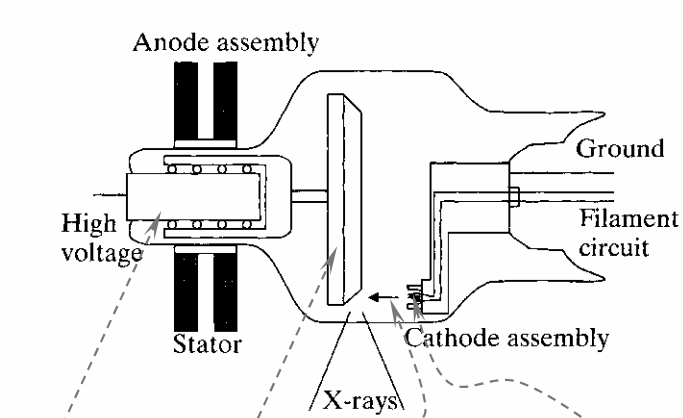

Figure 5.4
Schematic diagram of an x-ray tube.

Motor, Why?

Rotatin g target

Filament

Electron beam? How are electrons generated?

Compton Scattering

- ***Dominant interaction*** **of x-rays with** ***low-Z materials*** **in the diagnostic range and beyond (approx. 30 keV - 30MeV)**
- **Occurs** ***between the photon and a outer shell*** **e^-, which is considered free when E_g >> binding energy, E_b of the e^-.**
- **Encounter results in** ***ionization of the atom*** **and probabilistic distribution of the incident photon E to that of the scattered photon and the ejected e^-**
- **A probabilistic distribution determines the scattering angle.**

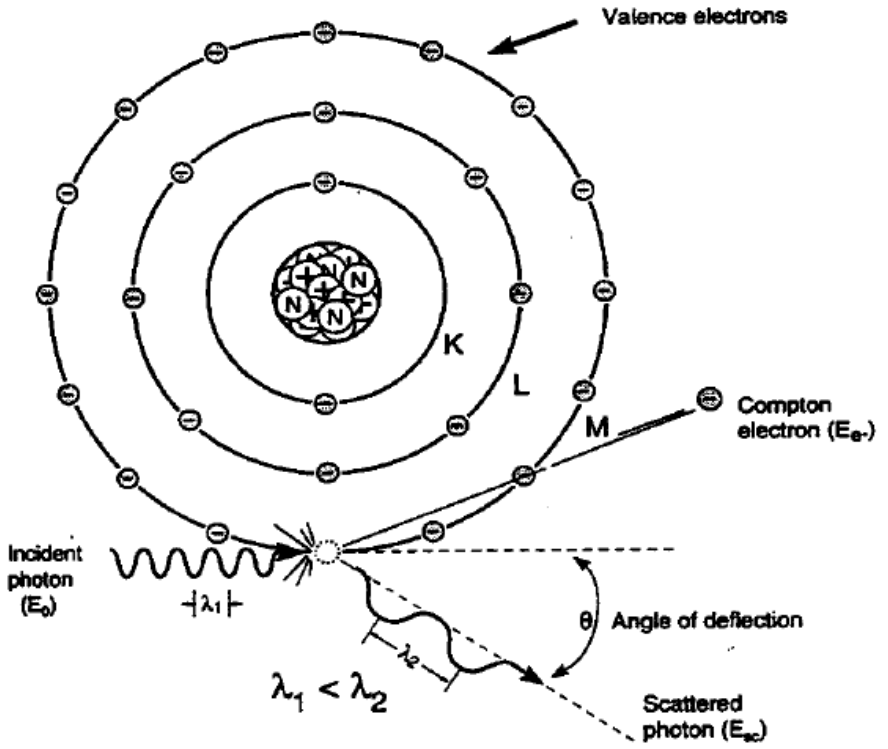

Compton Scattering

- **Compton interaction probability is dependent on *the total no. of e^- in the absorber vol.* ($e^-/cm^3 = e^-/gm \cdot$ density) or *electron density***
- **With the exception of ^1H, e^-/gm is fairly constant for organic materials ($Z/A \cong 0.5$), thus the probability of *Compton interaction proportional to material density (ρ)***
- ***Conservation of energy and momentum* yield the following equations:**

$$E_{h\nu'} = \frac{E_{h\nu}}{1 + \frac{E_{h\nu}}{m_e c^2}(1 - \cos\theta)},$$

where

$m_e c^2 = 511\text{keV}$

$E_{h\nu}$: energy of the incident photon

$E_{h\nu'}$: energy of the scattered photon

Photoelectric Effect

- **Interaction of incident photon with *inner shell* e^-, why?**
- **All E transferred to e^- (ejected *photoelectron*) as kinetic energy (E_e) less the binding energy: $E_e = E_0 - E_b$**
- ***Empty shell immediately filled with e^- from outer orbits* resulting in the emission of characteristic x-rays (E_γ = differences in E_b of orbitals), for example, Iodine: E_K = 34 keV, E_L = 5 keV, E_M = 0.6 keV**

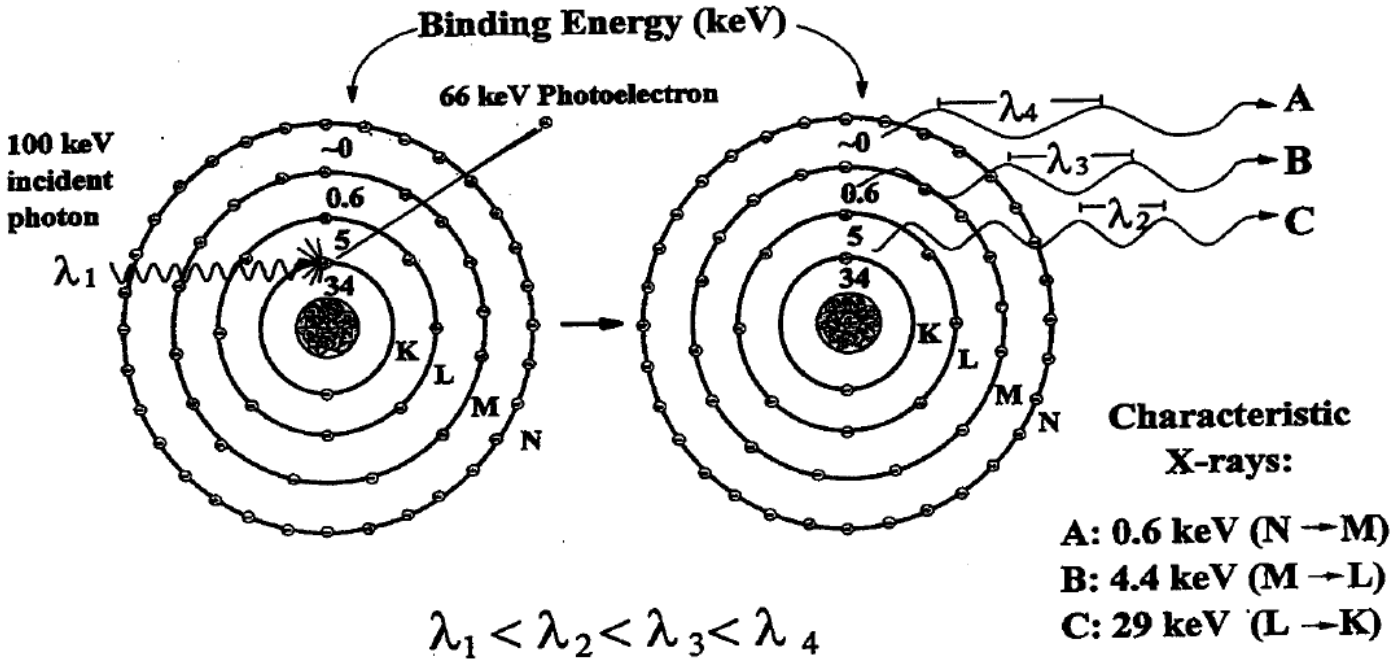

Photoelectric Effect

- **Photoe$^-$ absorption is the preferred interaction for X-ray imging.**
- **Rem.: $E_b \propto Z^2$; characteristic x-rays and/or Auger e^- → *preferred in high Z material*.**
- **Probability of photoe$^-$ absorption $\propto Z^3/E^3$ (Z = atomic no.) → *provide contrast according to different Z*.**
- **Due to the absorption of the incident x-ray without scatter, maximum subject contrast arises with a photoe$^-$ effect interaction → *No scattering contamination* → better contrast**
- **Explains why contrast ↓ as higher energy x-rays are used in the imaging process**
- **Increased probability of photoe$^-$ absorption just above the E_b of the inner shells cause discontinuities in the *attenuation profiles* (e.g., K-edge)**

Photoelectric Effect

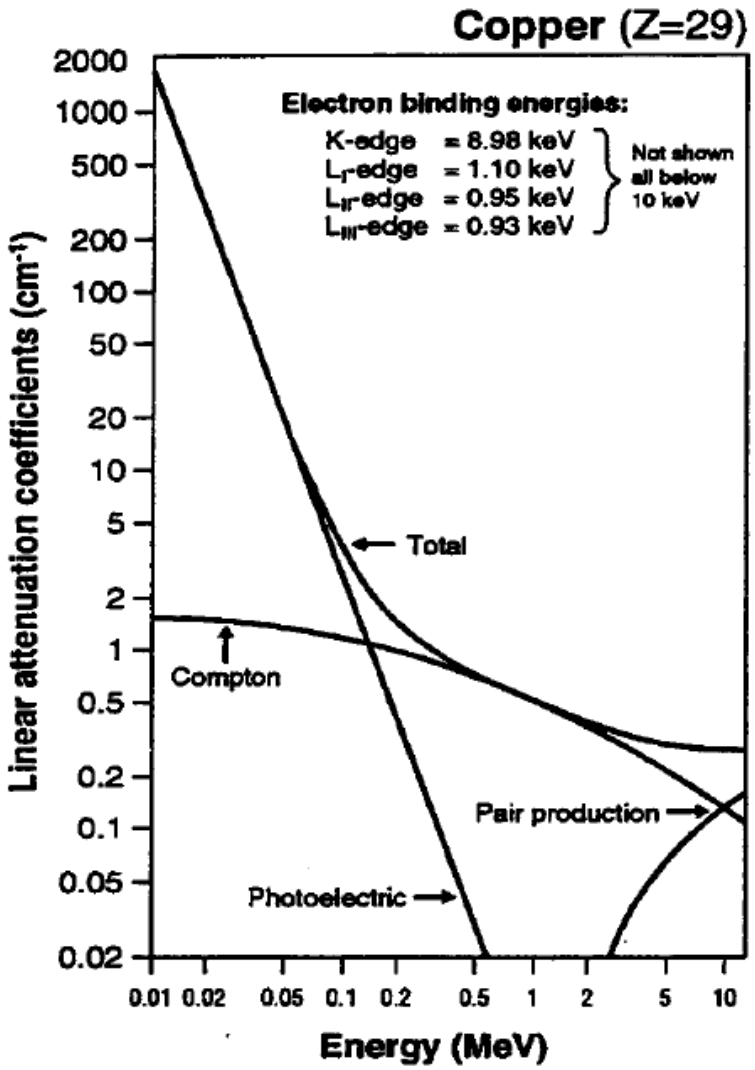

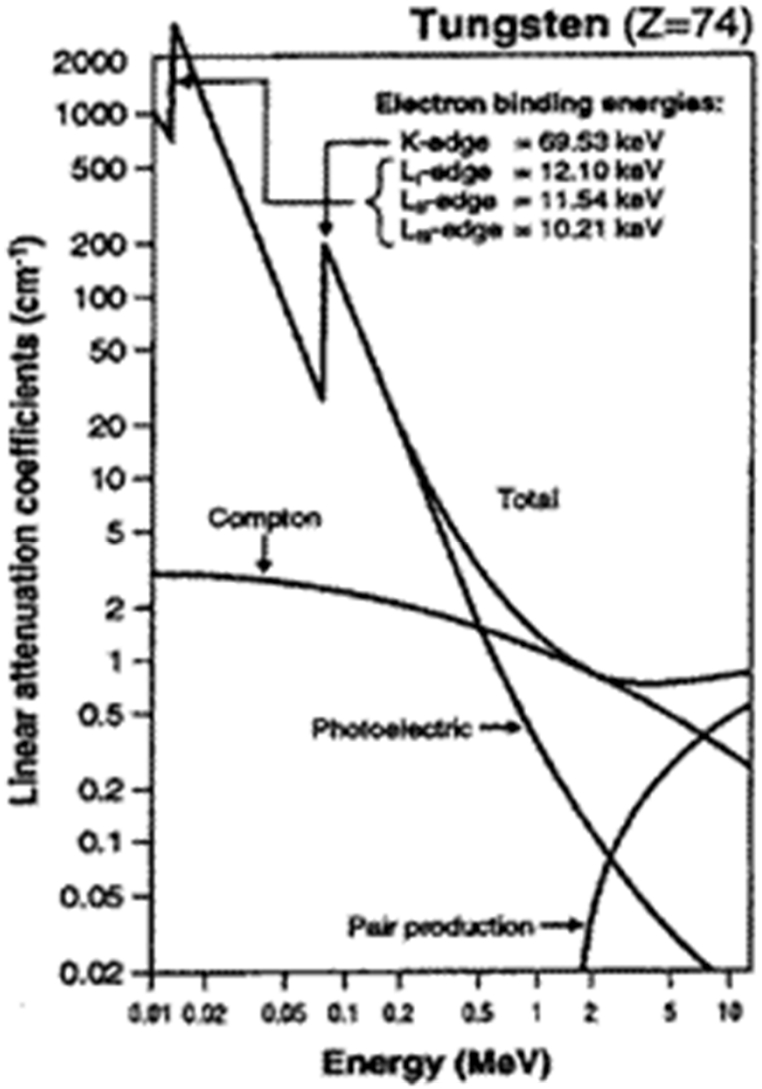

Attenuation Mechanism

- **Attenuation mechanisms as a function of energy**

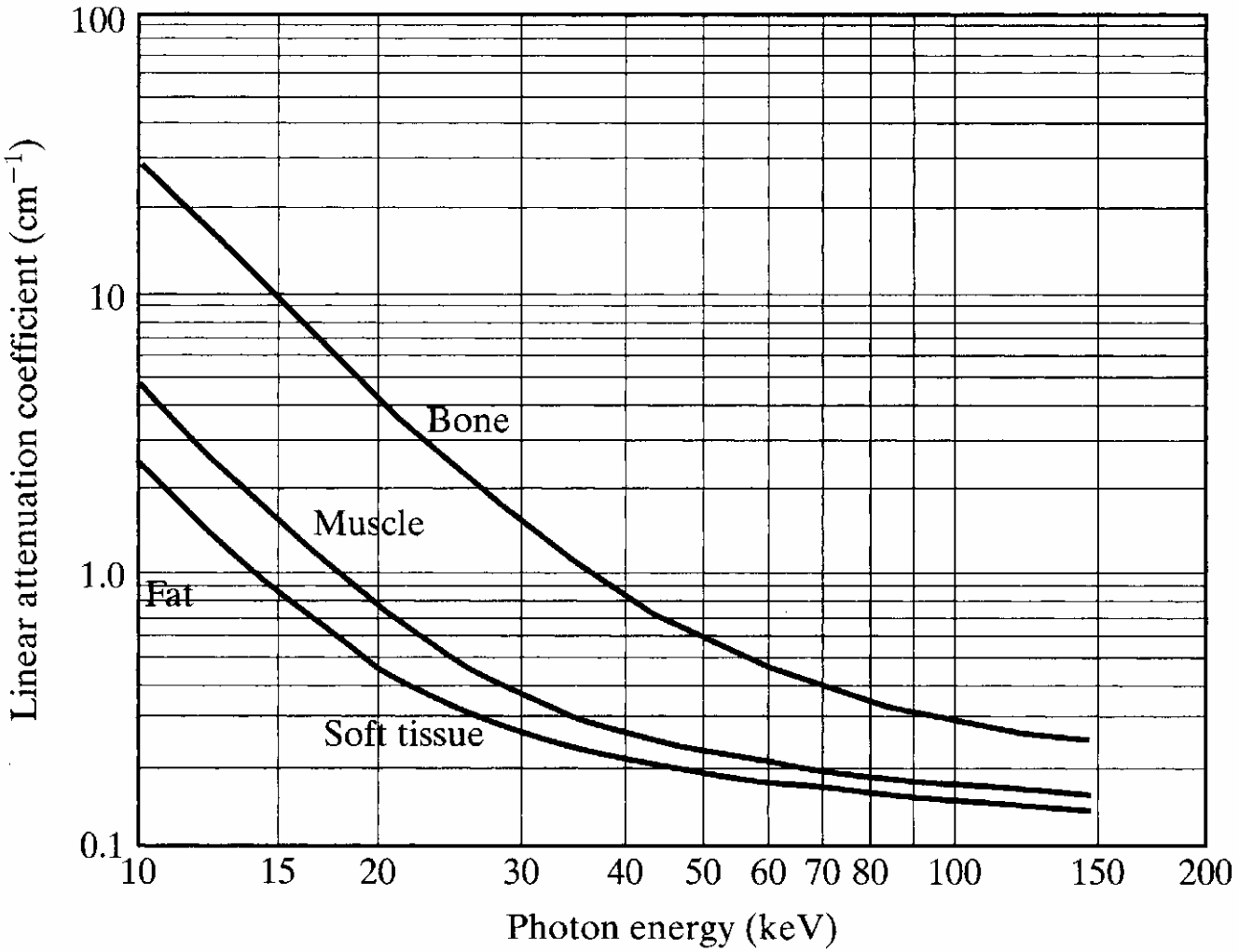

Figure 4.8
Linear attenuation coefficient for bone, muscle, and fat as a function of incident x-ray photon energy.

Photoelectric Effect

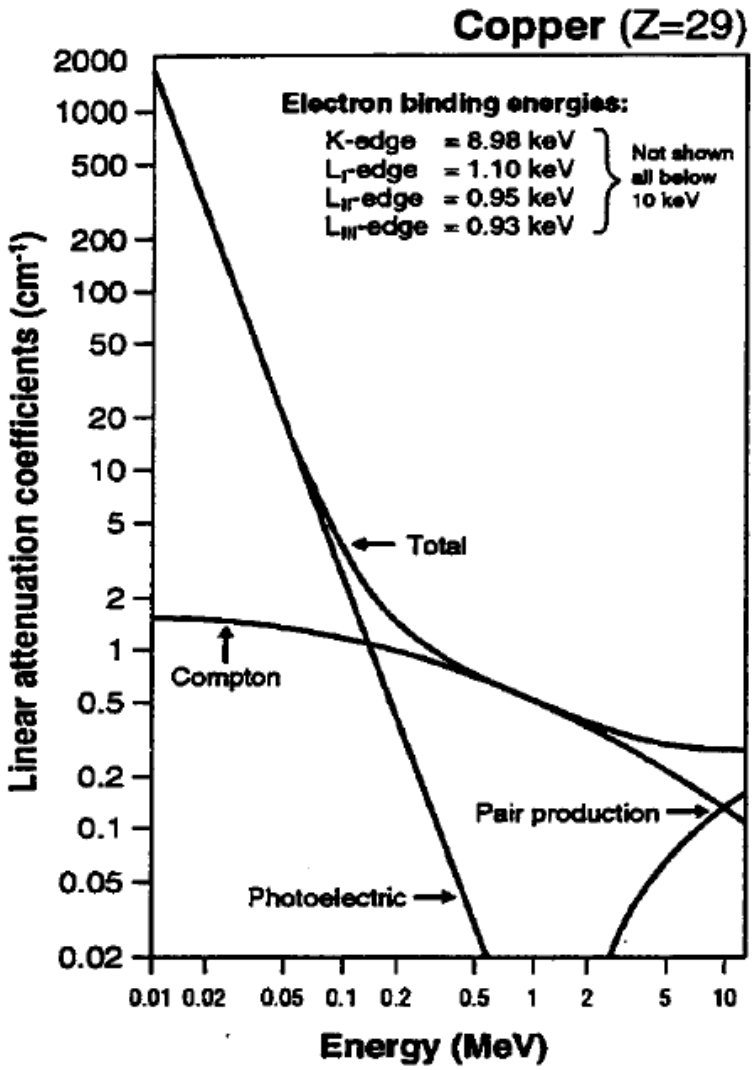

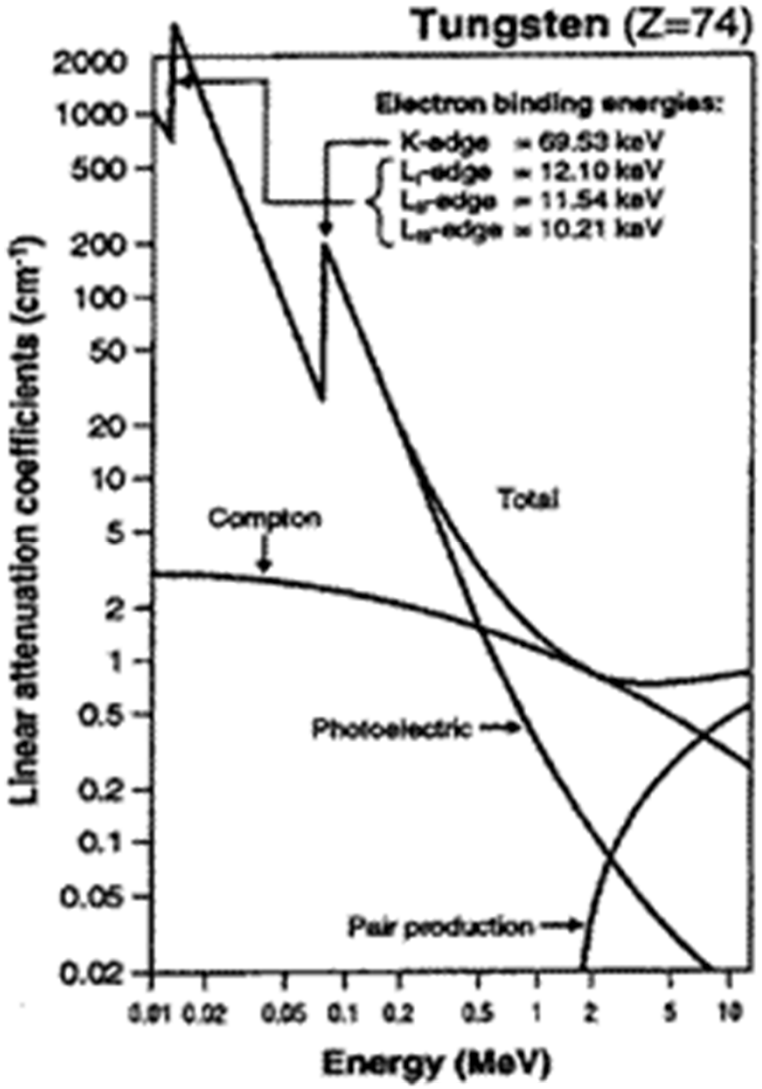

X-ray Generation – Filtration

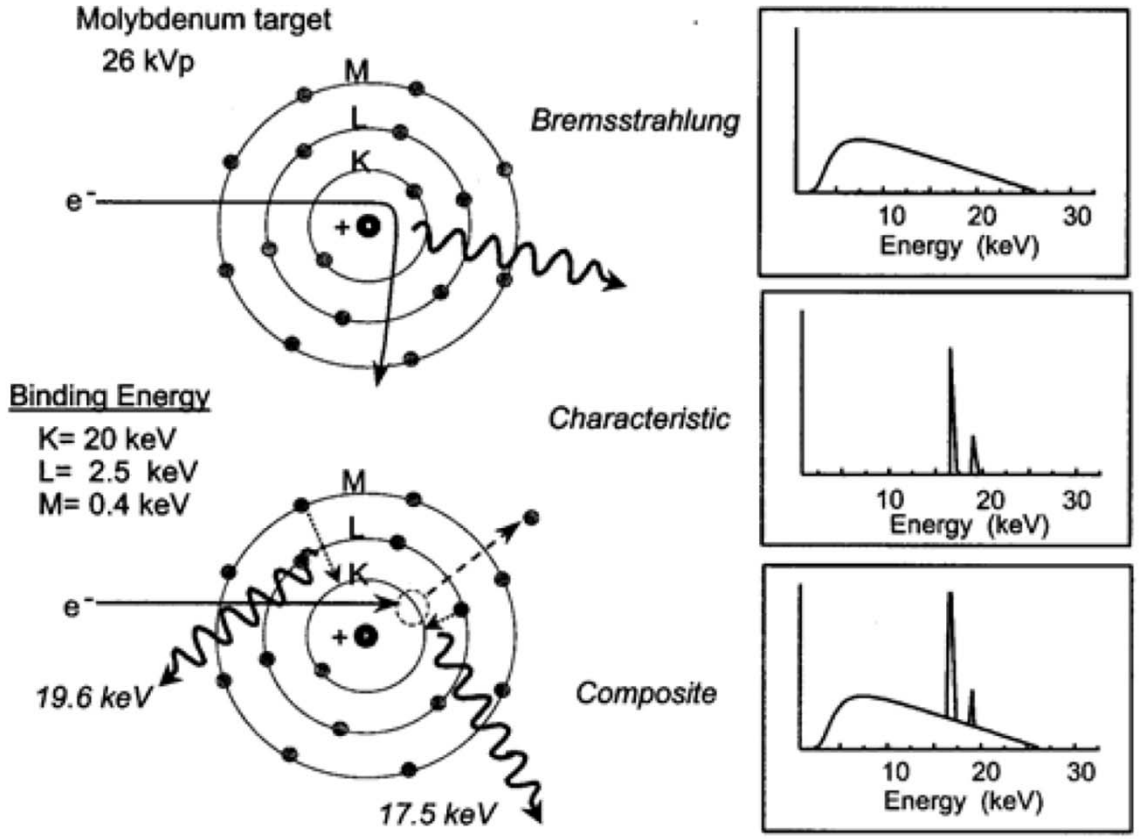

FIGURE 8-7. The output of a mammography x-ray system is composed of bremsstrahlung and characteristic radiation. The characteristic radiation energies of molybdenum (17.5 and 19.6 keV) are nearly optimal for detection of low-contrast lesions in breasts of 3- to 6-cm thickness.

Options:

Molybdenum (Mo)

Ruthenium (Ru)

Rhodium (Rh)

Palladium (Pd)

Silver (Ag)

Cadmium (Cd)

X-ray Generation – Filtration

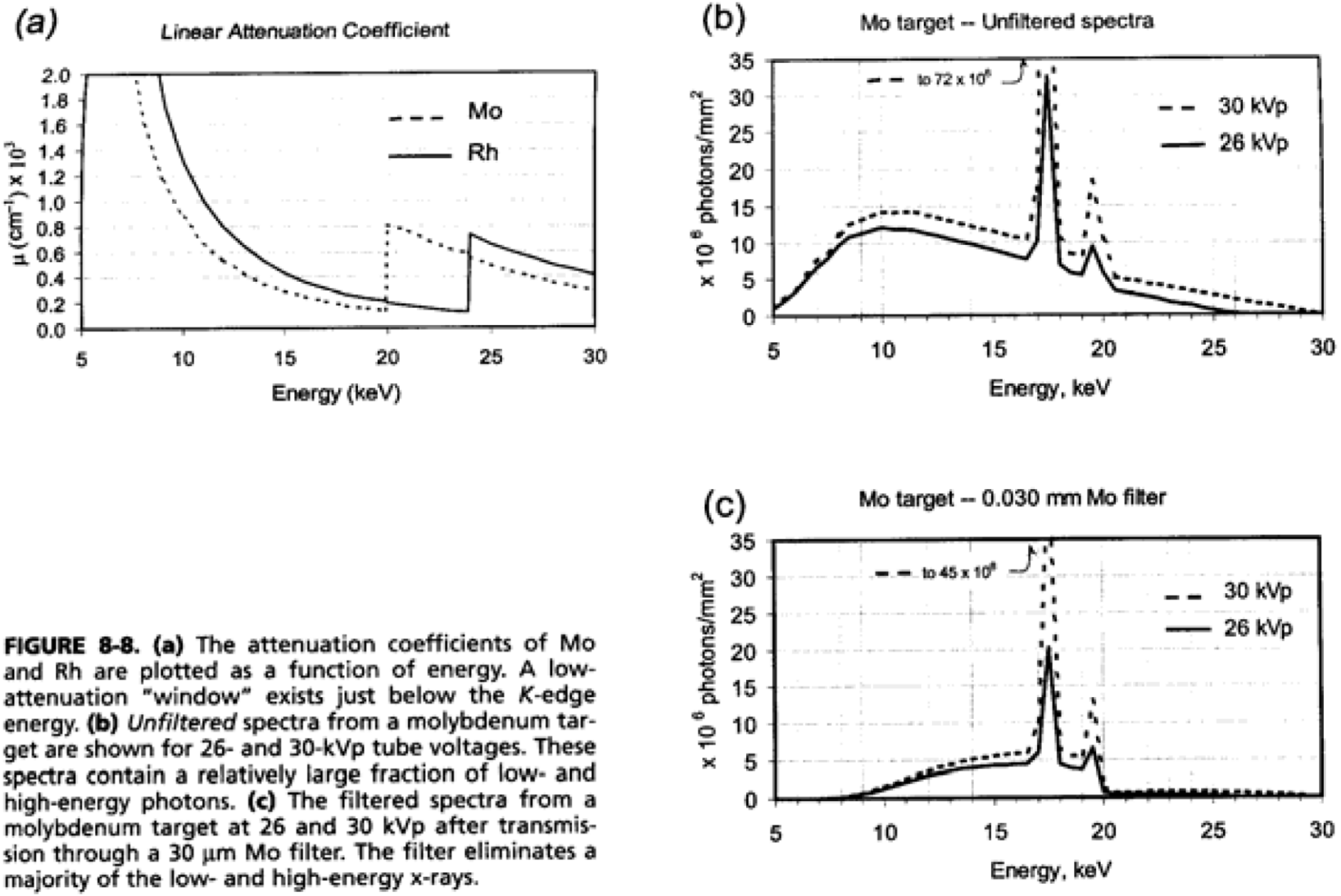

FIGURE 8-8. (a) The attenuation coefficients of Mo and Rh are plotted as a function of energy. A low-attenuation "window" exists just below the *K*-edge energy. **(b)** *Unfiltered* spectra from a molybdenum target are shown for 26- and 30-kVp tube voltages. These spectra contain a relatively large fraction of low- and high-energy photons. **(c)** The filtered spectra from a molybdenum target at 26 and 30 kVp after transmission through a 30 μm Mo filter. The filter eliminates a majority of the low- and high-energy x-rays.

Beam Hardening Effect

Mean Free Path and Beam Hardening

Mean free path (avg. path length of x-ray): = $1/\mu$ = HVL/0.693

Beam hardening:

- **The Bremsstrahlung process produces a wide spectrum of energies, resulting in a polyenergetic (polychromatic) x-ray beam**
- **As lower E photons have a greater attenuation coefficient, they are preferentially removed from the beam**
- **Thus the mean energy of the resulting beam is shifted to higher E**

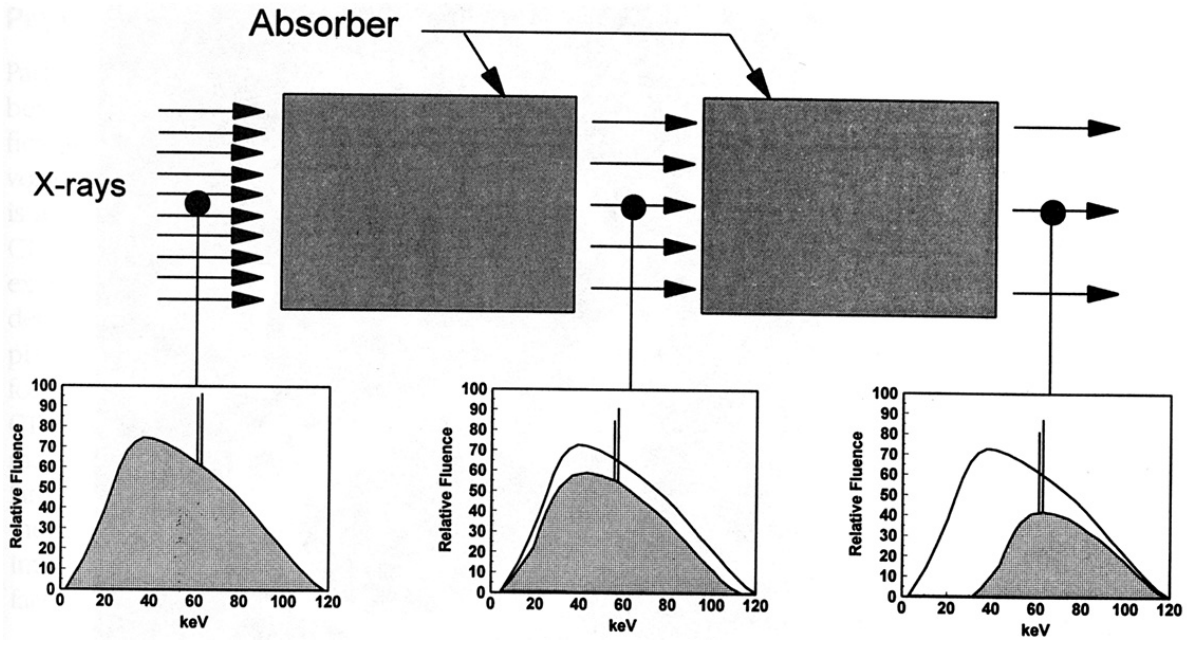

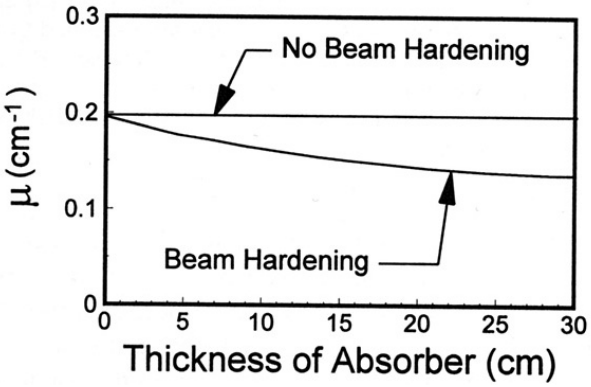

Mean Free Path and Beam Hardening

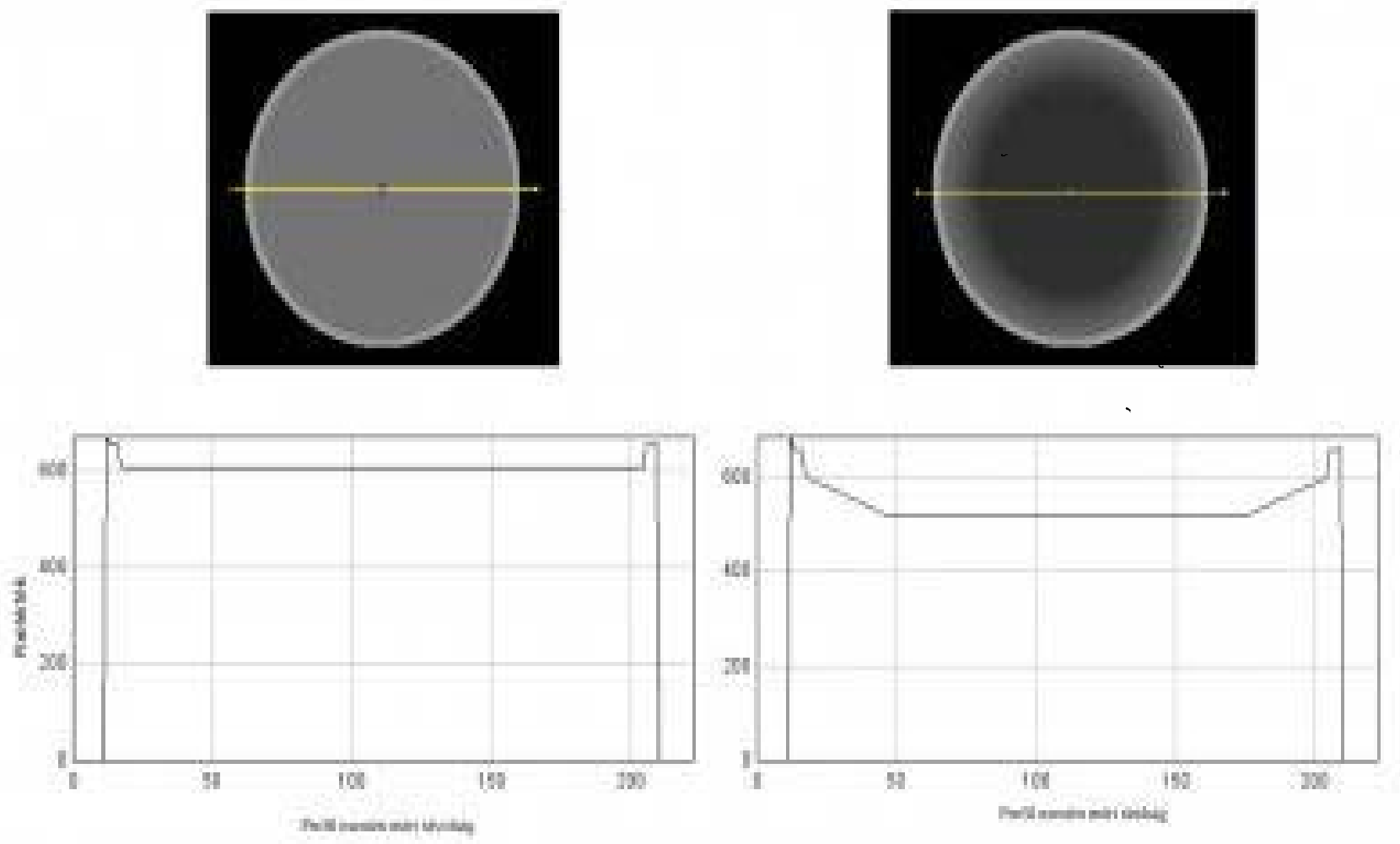

Beam-hardening effect and correction. The upper left picture shows a water-filled cylinder beam-hardening corrected homogeneous cross-sectional image, below the yellow line corresponding profile curve. The upper right is the image of the same cylinder without beam- hardening correction and the corresponding profile curve is shown below.

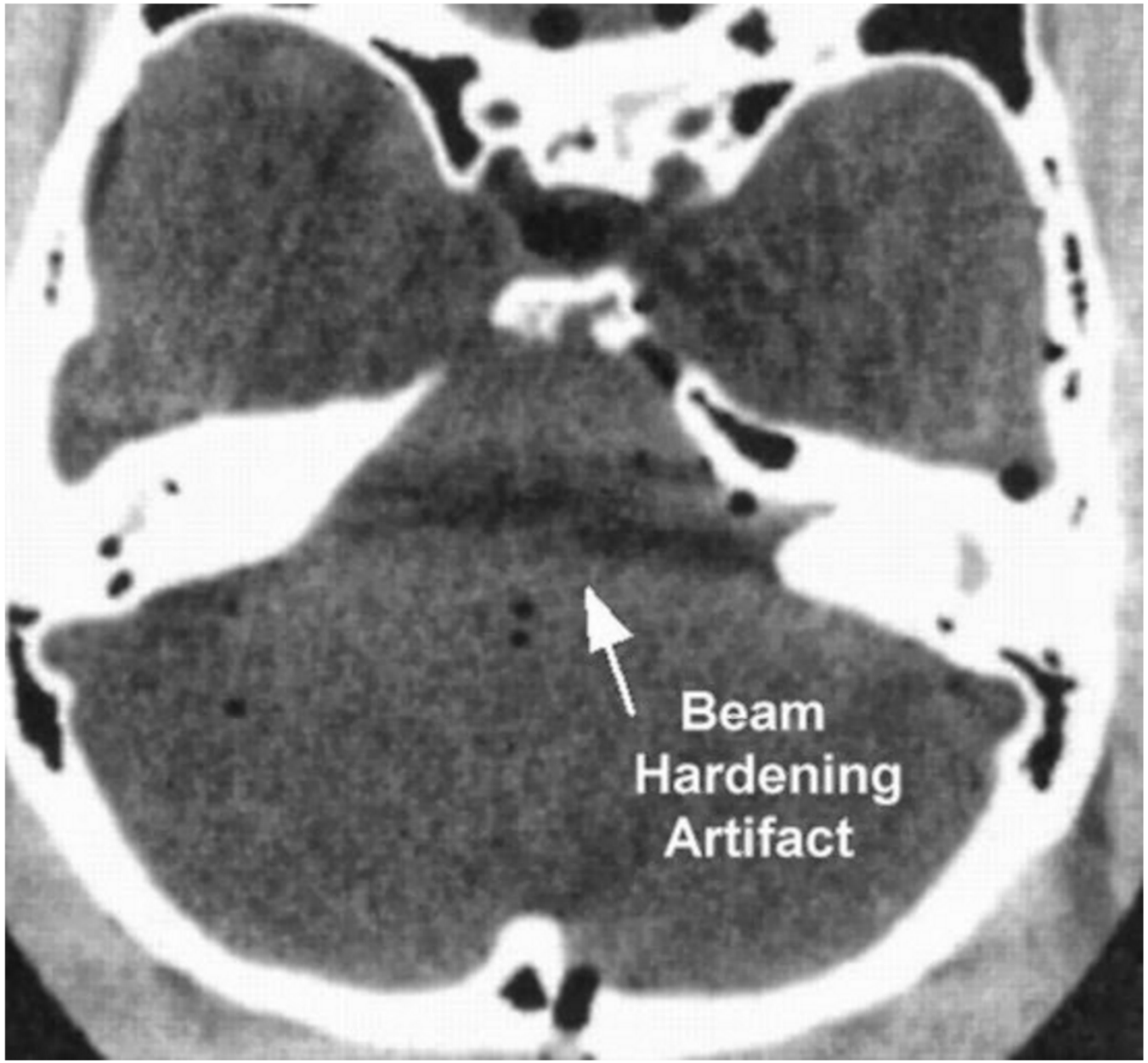

http://www.ctlab.geo.utexas.edu/about-ct/artifacts-and-partial-volume-effects/

X-ray Contrast Agents

Photoelectric Effect and Absorption Edge

- **Edges become significant factors for higher Z materials as the E_b are in the diagnostic energy range:**
- **Contrast agents – barium (Ba, Z=56) and iodine (I, Z=53)**
- **Rare earth materials used for intensifying screens – lanthanum (La, Z=57) and gadolinium (Gd, Z=64)**
- **Computed radiography (CR) and digital radiography (DR) acquisition – europium (Eu, Z=63) and cesium (Cs, Z=55)**
- **Increased absorption probabilities improve subject contrast and quantum detective efficiency**
- **At photon E << 50 keV, the photoelectric effect plays an important role in imaging soft tissue, amplifying small differences in tissues of slightly different Z, thus improving subject contrast (e.g., in mammography)**

Example of Contrast Agents

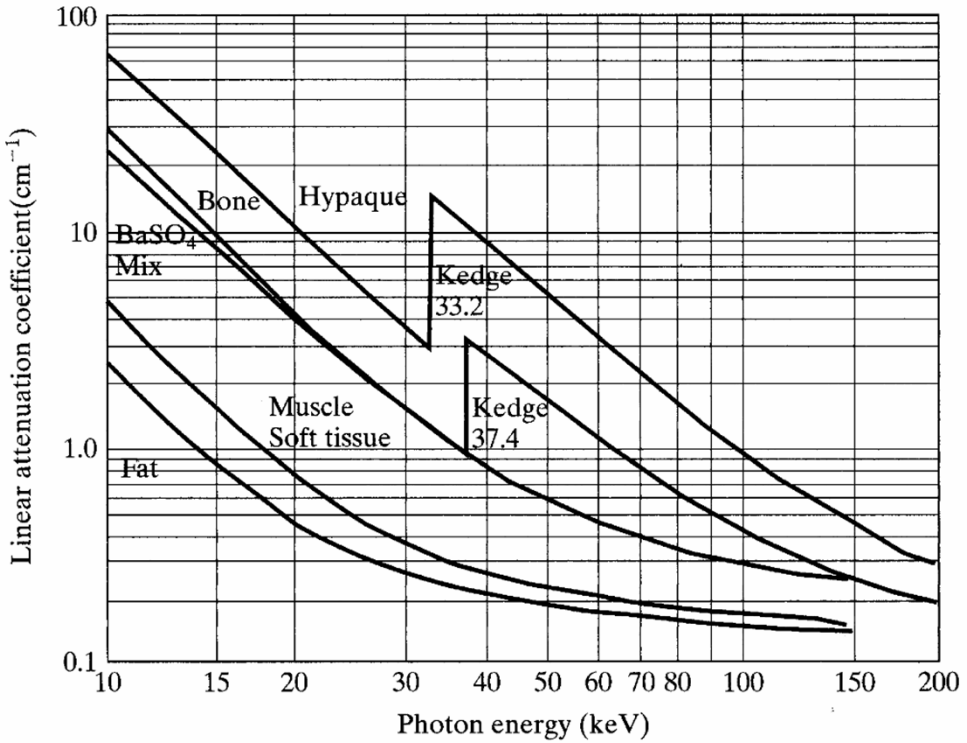

Figure 5.8
Linear attenuation coefficients of bone, muscle, fat, and two contrast agents. (From Johns and Cunningham, 1983.)

Bring out the difference between fat and soft tissues

X-ray Generation – Characteristic X-rays

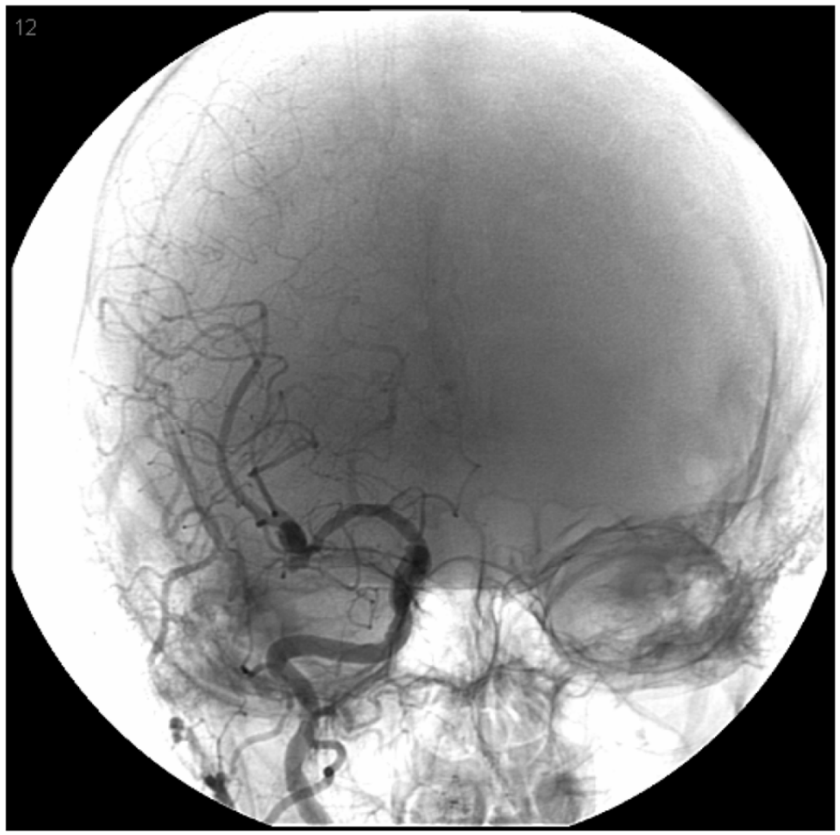

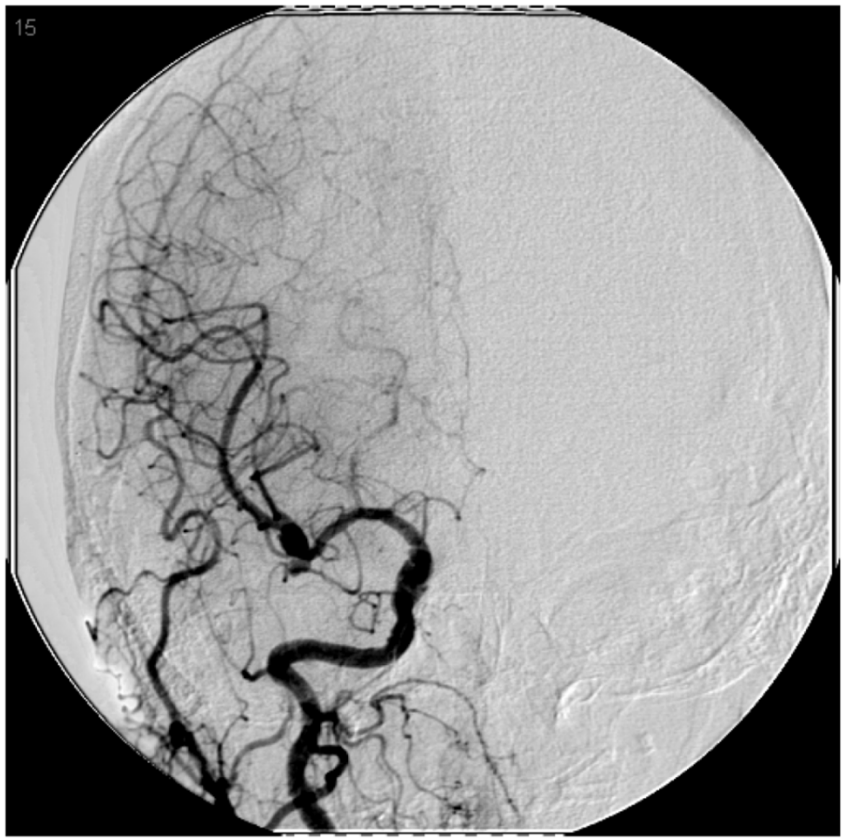

This is a mask image showing the background bone which obscures many of the smaller vessels.

Subtracted image with the background details removed.

Both images from Bushberg et al. 2003

Contrast Enhanced X-ray Imaging

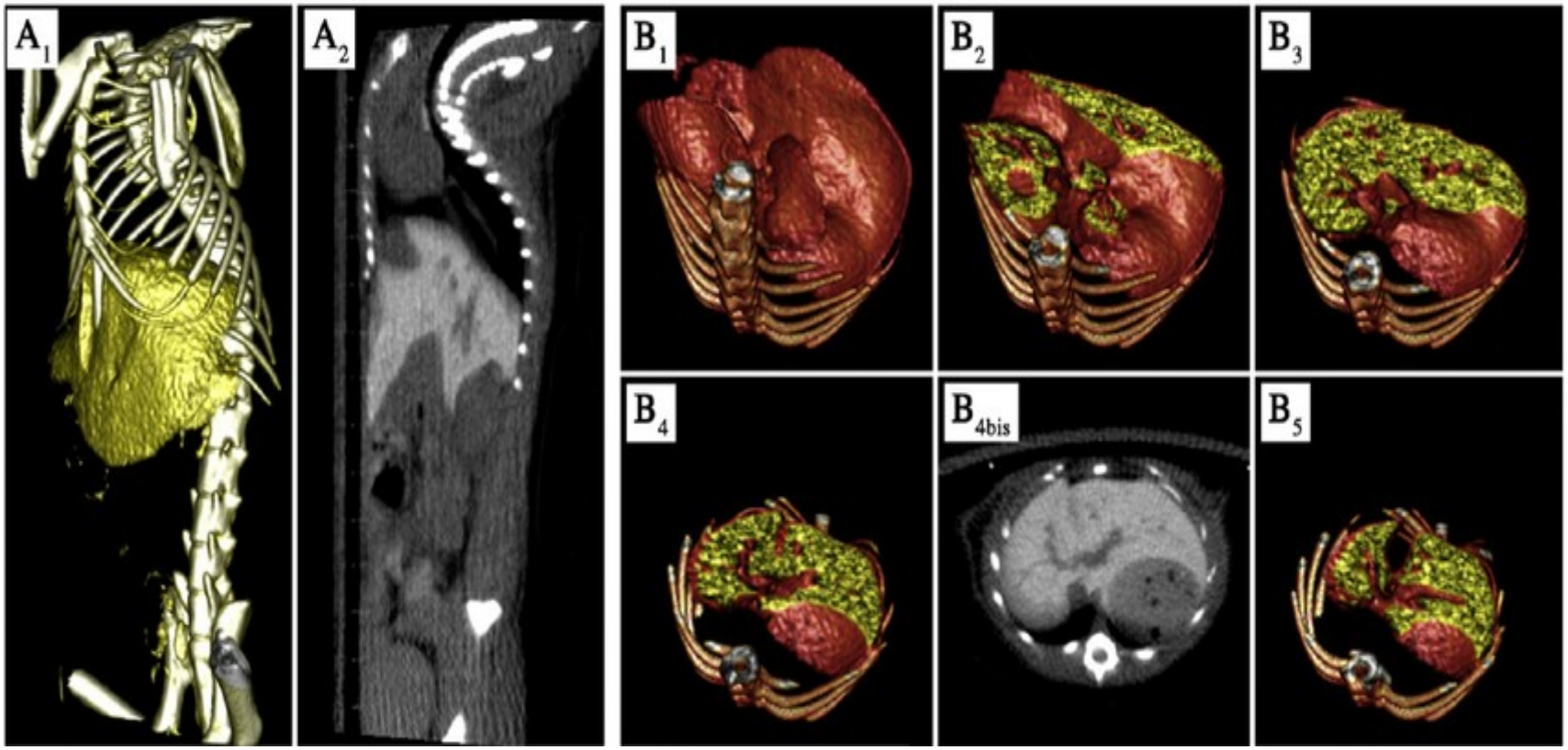

Fig. 5. Micro-CT liver imaging with hepatocyte-speci fi c contrast agent: vitamin E nano-emulsions, from [41]. (A 1) Left lateral view, 3D rendering, (A 1) sagittal view, maximal intensity projection. (B 1) to (B 5) show 3D rendering of liver sections, emphasizing the clear contrast different between the liver tissues and its vascularization. (B 4 bis) is the transverse view of maximal intensity projection corresponding to (B 4).

From "contrast agents for preclinical targeted X-ray imaging", 2014

X-Ray Detectors

X-Ray Detectors

- Film: sensitivity is very low, it would require too high a dose to the patient
- Film + screen: conventional radiography
- Image intensifier (I.I.): fluoroscopy
- Photosensitive phosphor (computed radiography)
- Flat panel detectors
- Direct digital radiography (semiconductor)

Roentgen's X-ray Setup (1895)

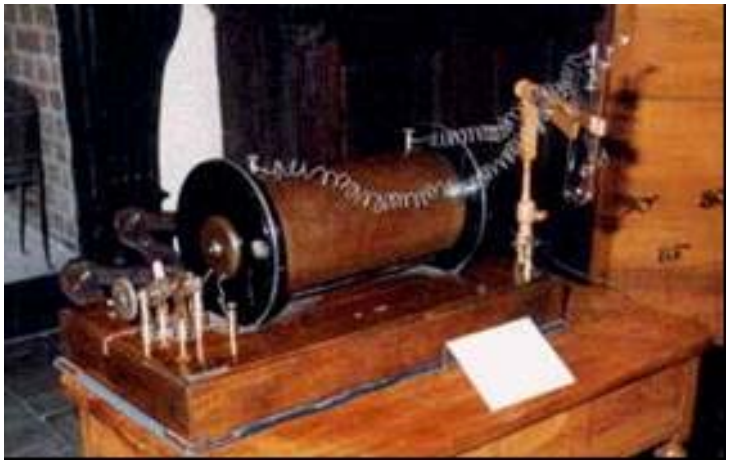

Roentgen's experimental apparatus (Crookes tube) that led to the discovery of the new radiation on 8 Nov. 1895 – he demonstrated that the radiation was not due to charged particles, but due to an as yet unknown source, hence "x" radiation or "x-rays"

Known as "the radiograph of Bera Roentgen's hand" taken 22 Dec. 1895

X-Ray Film-screen Detectors

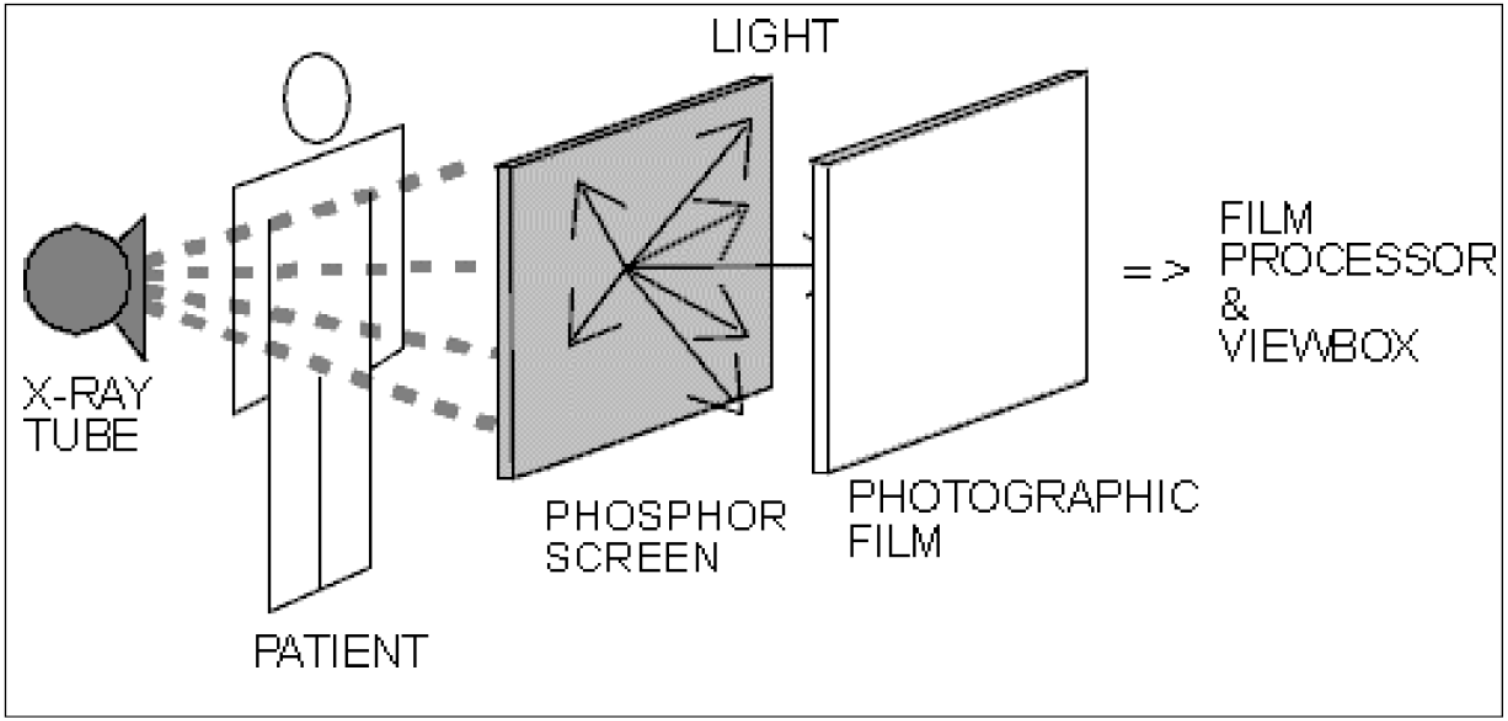

Film-Screen Radiography:

- Phosphor screen emits light in response to x-rays absorption.
- The resulting optical image is used to expose a photographic film

Currently most diagnostic radiographic systems (such as chest and breast imaging) are based on a phosphor screen.

X-Ray Film-screen Detectors

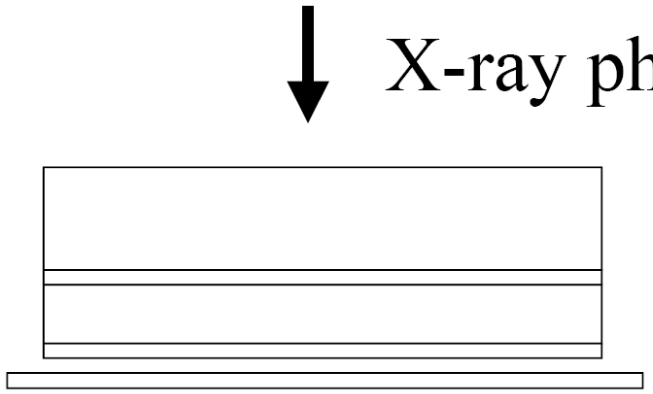

Screen Types: **$CaWO_4$, 430 nm blue**
Gd_2O_2S, 410 nm blue

Screen Sensitivity ~ thickness

Increased X-ray Absorption
=> more visible photons

Screen Resolution ~ $1/$thickness

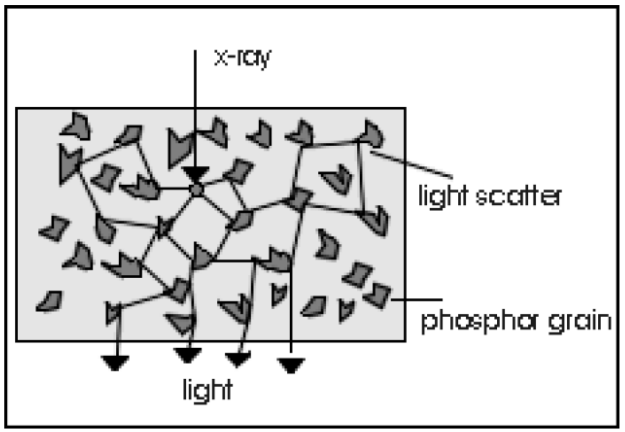

Flat panel detector: dynamical range

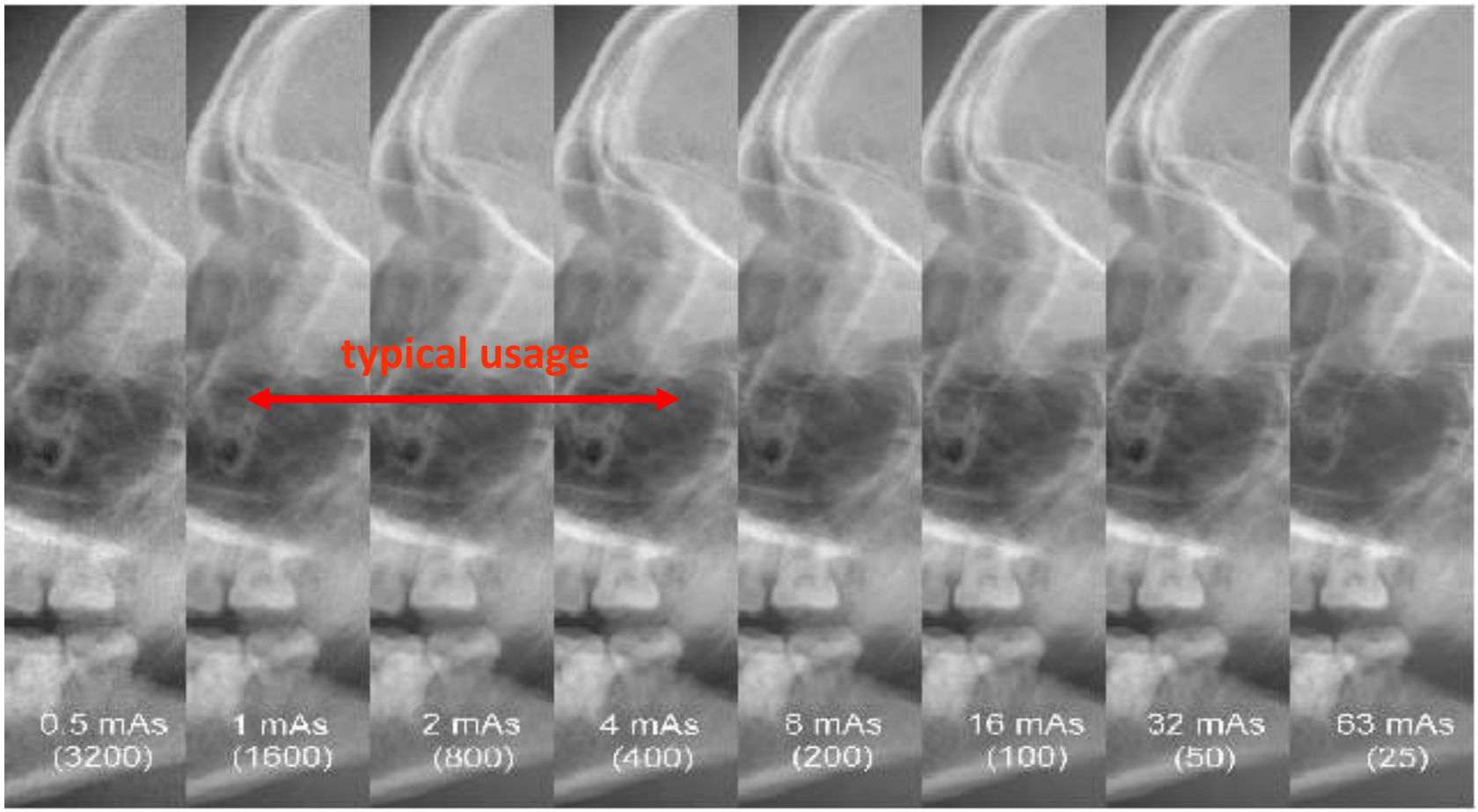

Digital Diagnost (PHILIPS) 43 cm x 43 cm, 143µm x 143 µm

M. Overdick (PHILIPS), 11/09/2002, IWORID 2002, Amsterdam

Image Plate based X-Ray Radiology

Digital X-ray image acquisition systems for projection radiography.

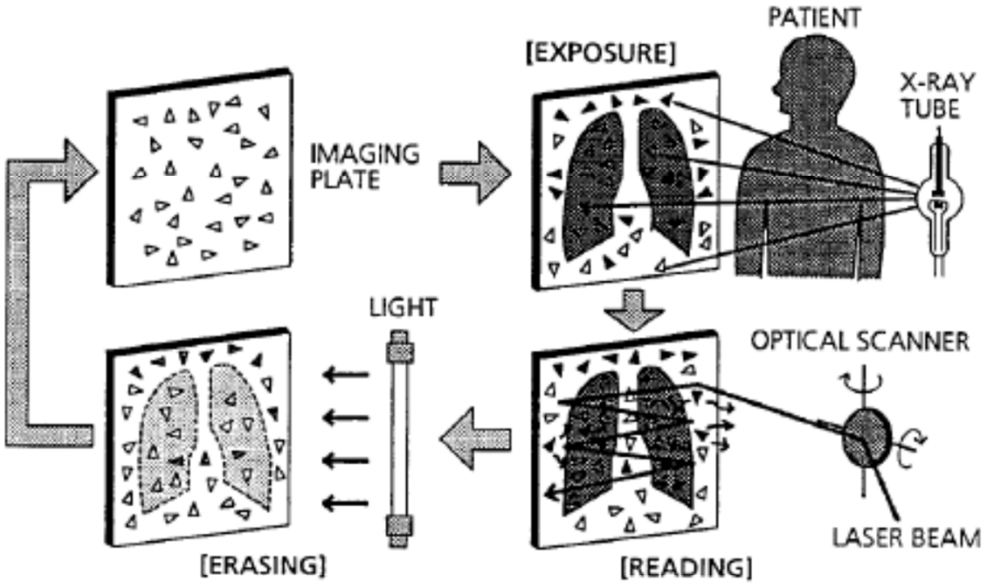

Stimulatable Phosphor System

- Imaging plate (stimulable phosphor) is exposed forming a latent image ("traps" in phosphor).
- latent image is read via laser scanning --> stored energy is released in form of "photostimulated luminescence light" proportional to the local X-ray exposure.
- The luminescence signal is converted to an electrical signal and is digitized.

Image Plate X-Ray Detector

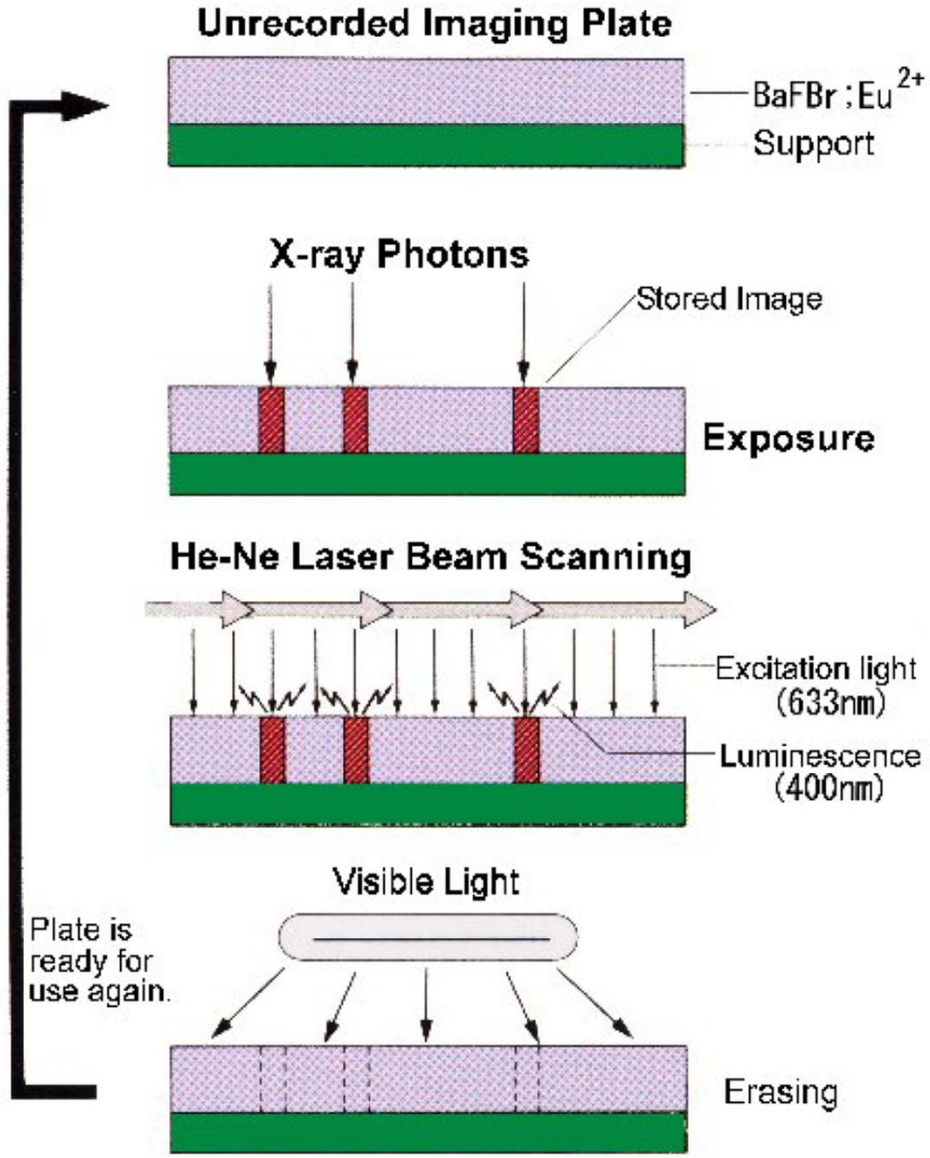

Image Plate X-Ray Detector

Success of CR:

– high dynamic range (> 104)
– digital nature
– easy to introduce
– relative low cost
– improvements for more than 25 years
– but not for image or dose performances !

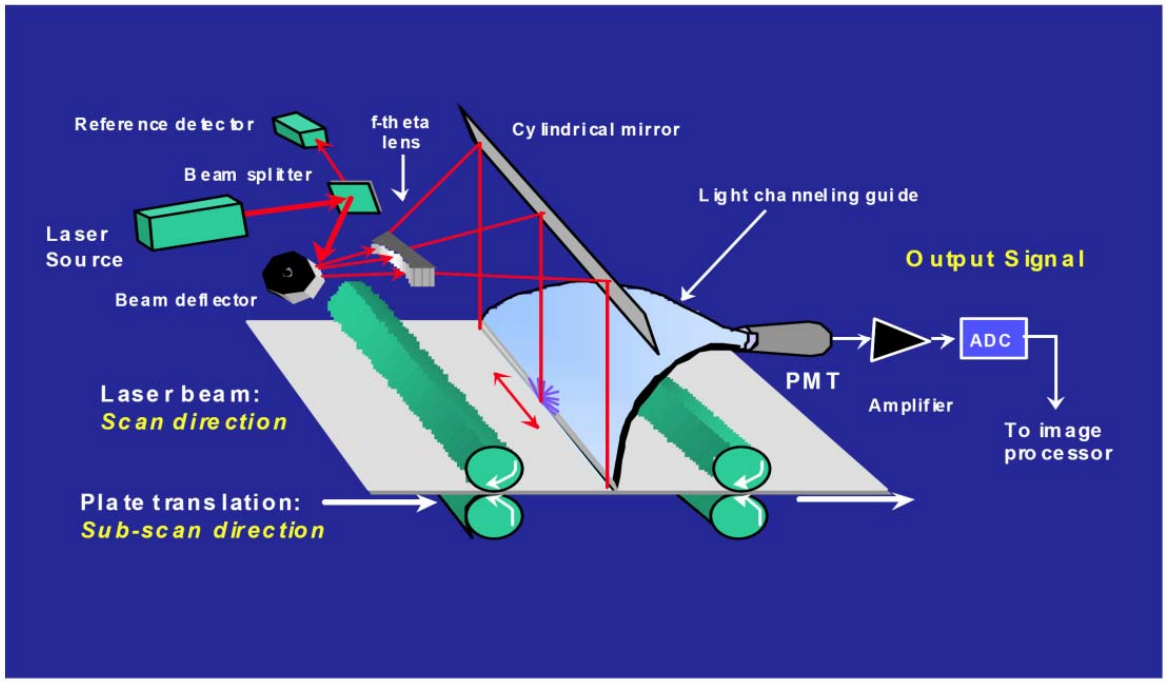

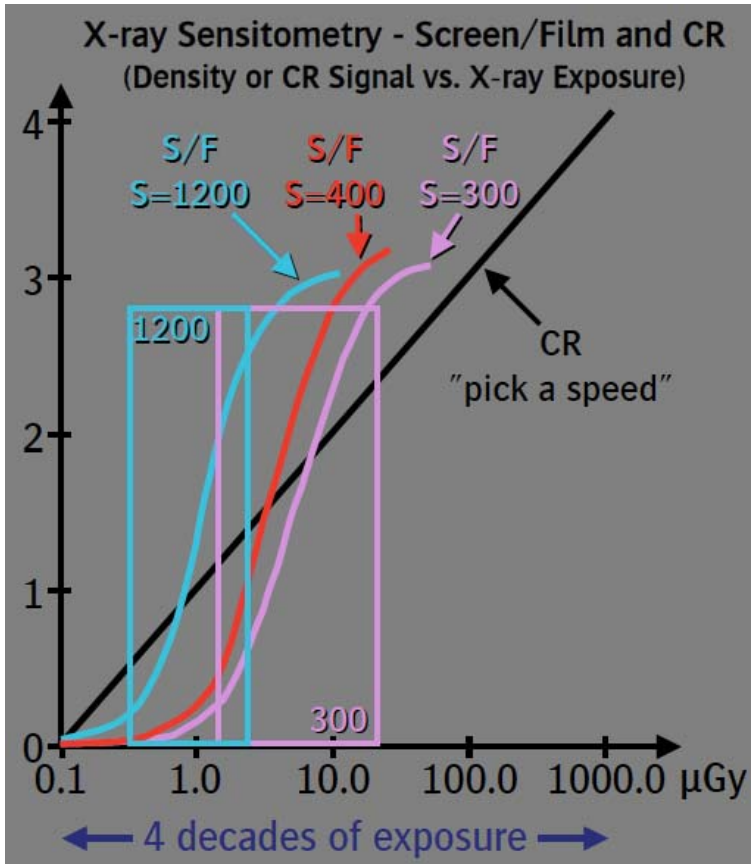

Limitation of Image Plate X-Ray Detector

Relatively small of "information carriers" created per x-ray photon.

— Low signal to noise ratio (SNR)

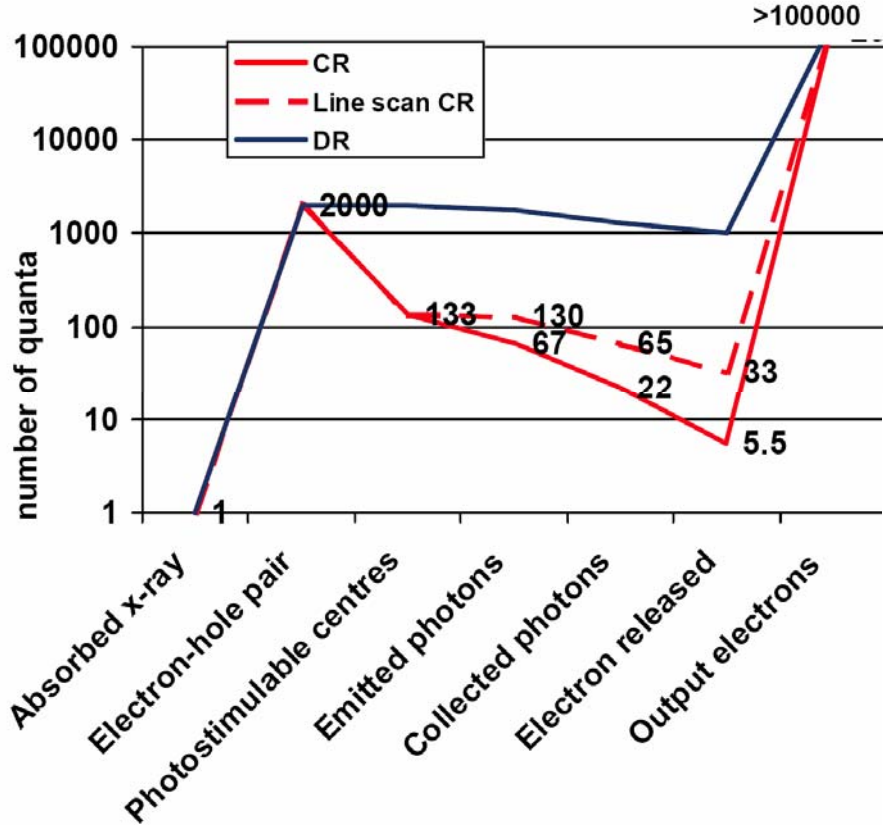

X-Ray Image Intensifier (X-ray II)

X-ray II is the standard detector for current projection radiography system

X-Ray Image Intensifier (X-ray II)

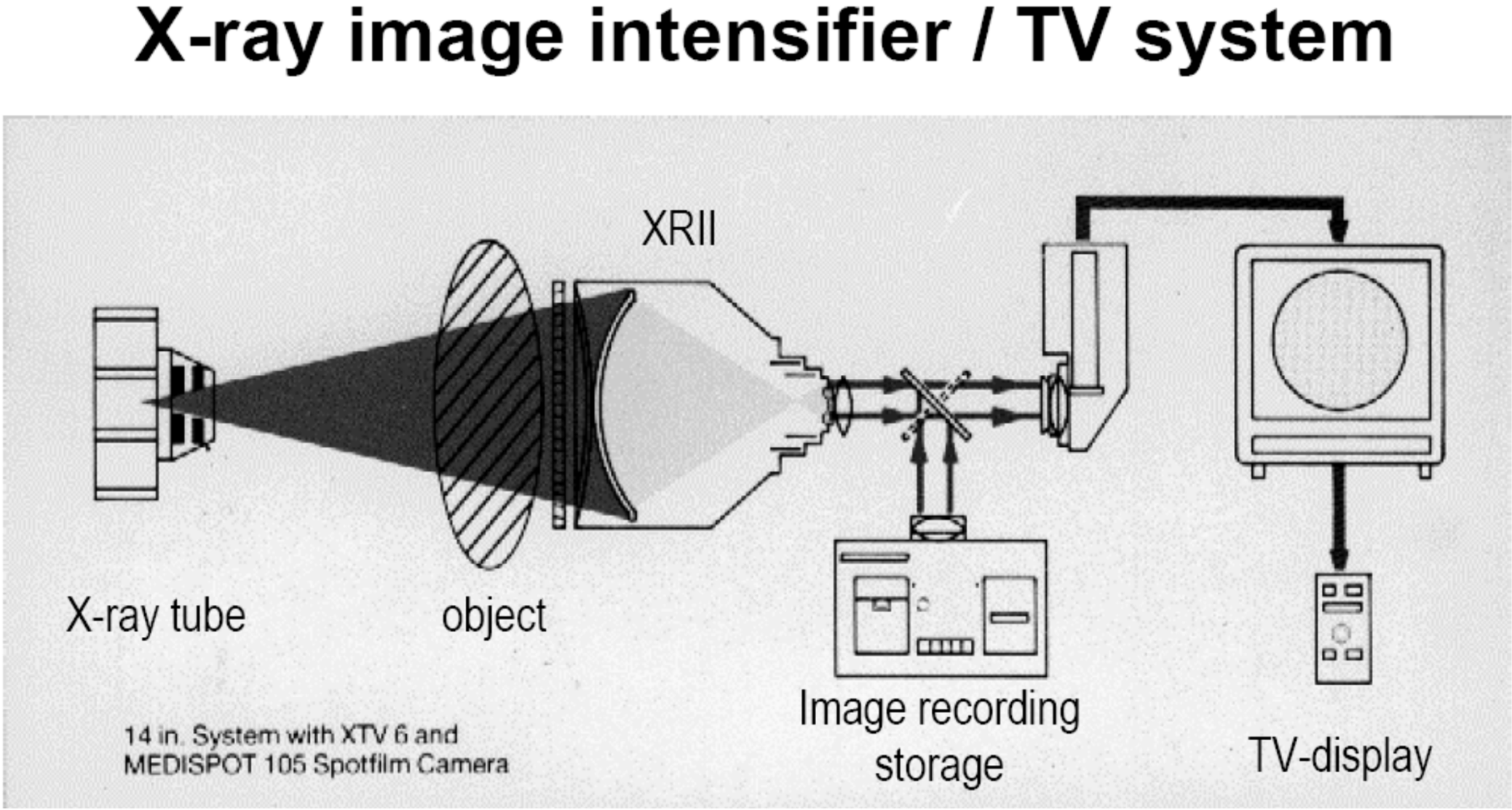

X-Ray Image Intensifier (X-ray II)

Principle Operation of XRII

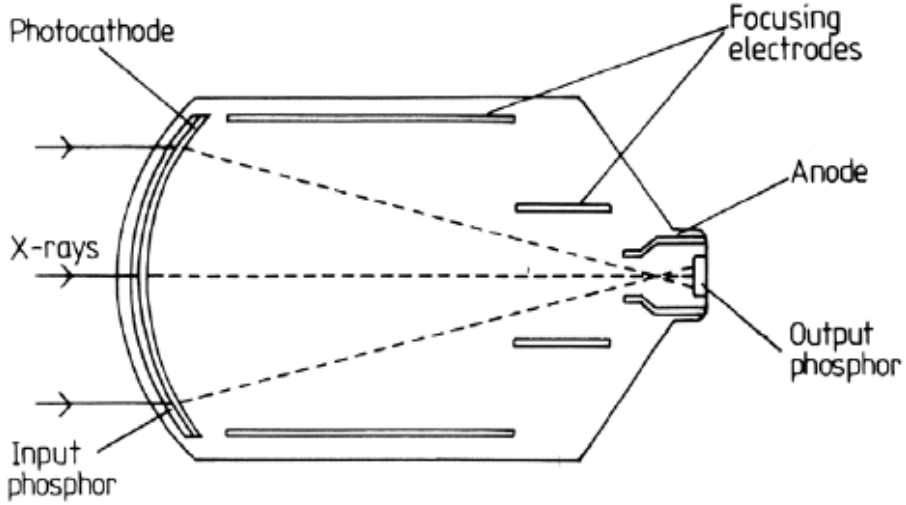

Construction of the image intensifier.

- X-rays are absorbed in CsI input phosphor.
- Emitted light is converted to electrons by photocathode.
- Electrons are focused and accelerated to output phosphor and converted to light..
- Bright light image at output window is imaged by TV-camera.

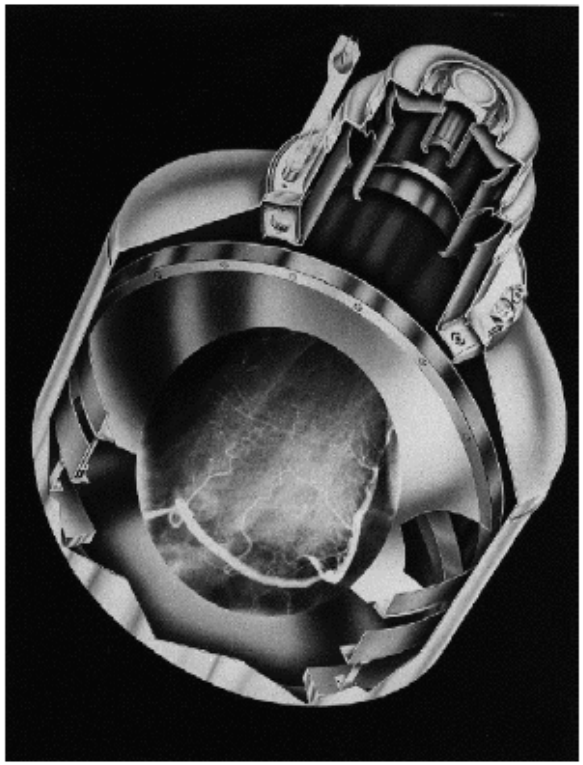

Flat Panel Detectors

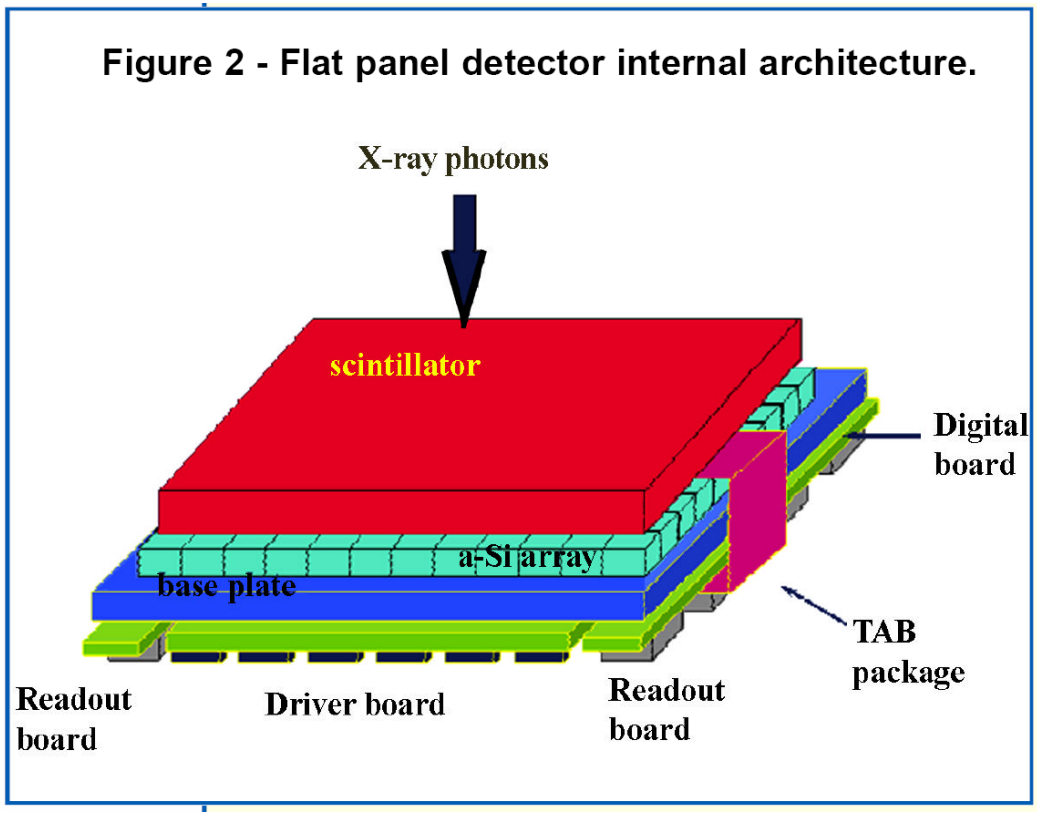

The construction of FPDs is similar in many ways to flat panel displays,
and uses many of the same technologies. Figure 2 shows the construction of a typical FPD. At the core is an amorphous-silicon TFT/photodiode array. Closely coupled to the array is the X-ray scintillator.

http://www.varian.com/xray/pdf/Flat%20Panel%20Xray%20Imaging%2017-11-04.pdf

Scintillation Material as Detection Media

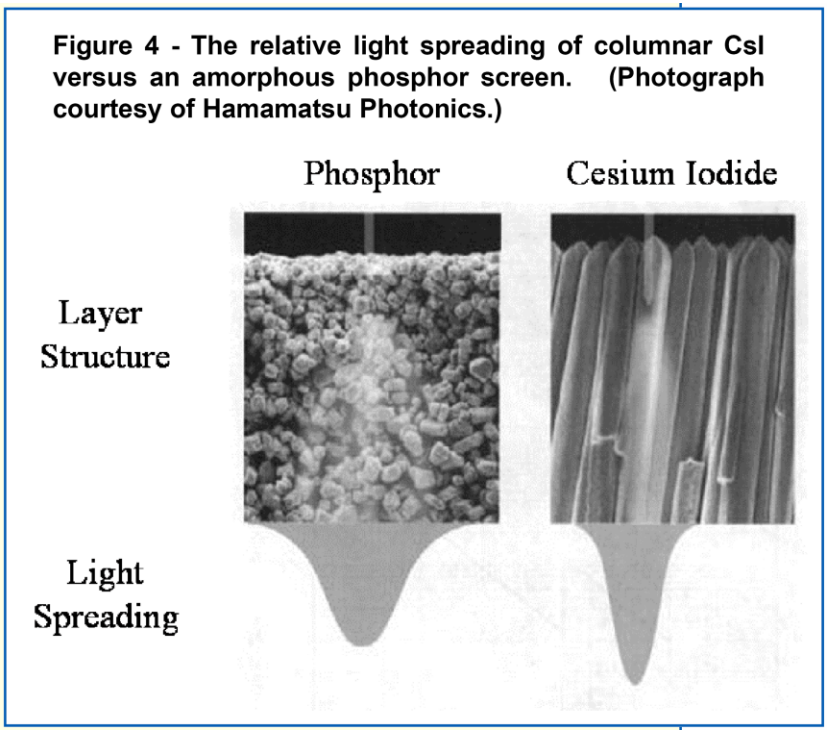

- **CsI(Tl) scintillator: density 4.6g/cm^3, emission peak ~550nm.**
- **Columnar structure of up to 3mm thick to provide an adequate stopping power and a reduced light spread.**

http://www.varian.com/xray/pdf/Flat%20Panel%20Xray%20Imaging%2017-11-04.pdf

Readout Electronics for Plat Panel Detectors

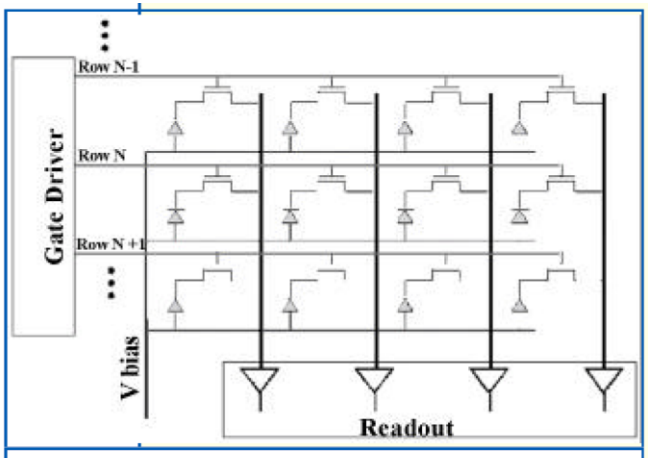

Figure 5 - TFT/Photodiode array schematic and view of a single 127μm pixel.

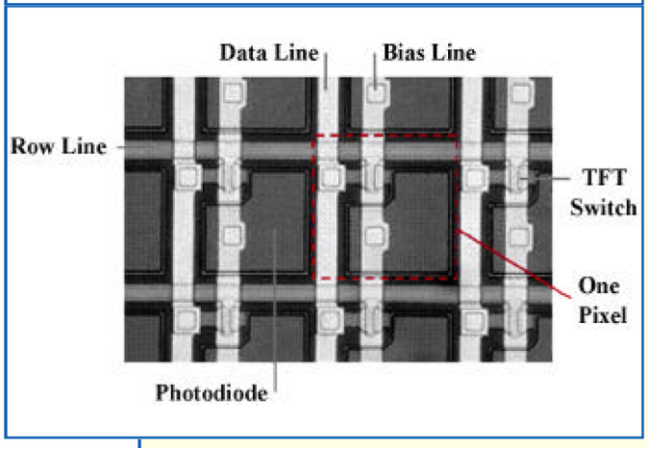

- scanned progressively, one line at a time from top to bottom. The TFTs are

essentially switches.

- When a large positive voltage is applied to one of the gate lines, the switches (TFTs) in the selected row are closed, causing them to conduct electricity.
- With the TFTs energized, each pixel in the selected row discharges the stored signal electrons onto the dataline. At the end of each dataline is a charge integrating amplifier which converts the charge packet to a voltage.
- a programmable gain stage and an Analog-to-Digital Converter (ADC), which converts the voltage to a digital number

http://www.varian.com/xray/pdf/Flat%20Panel%20Xray%20Imaging%2017-11-04.pdf

Direct Radiography (DR)

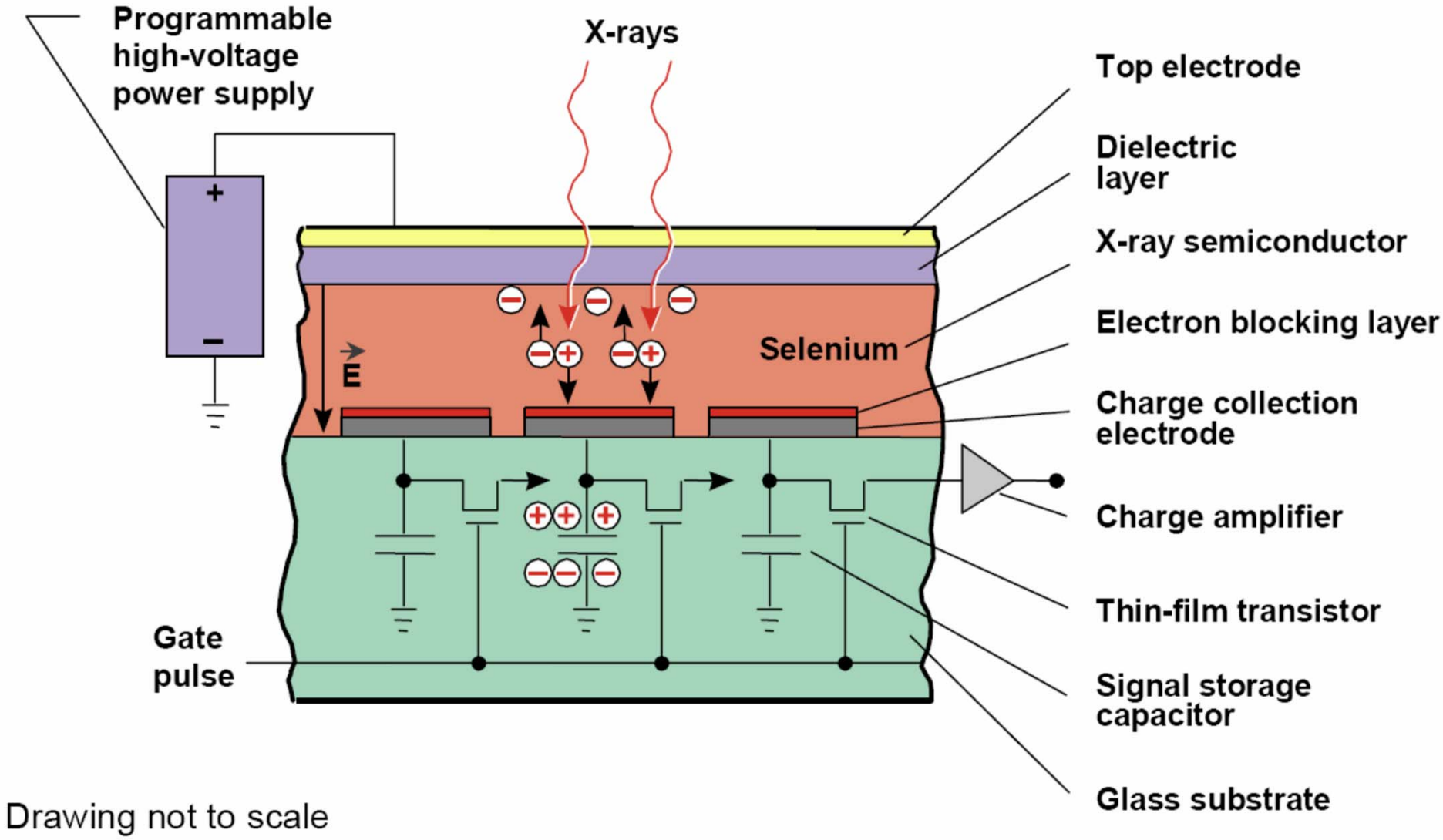

Fundamentals of Positron Emission Tomography (PET)

Attenuation of Internal Source

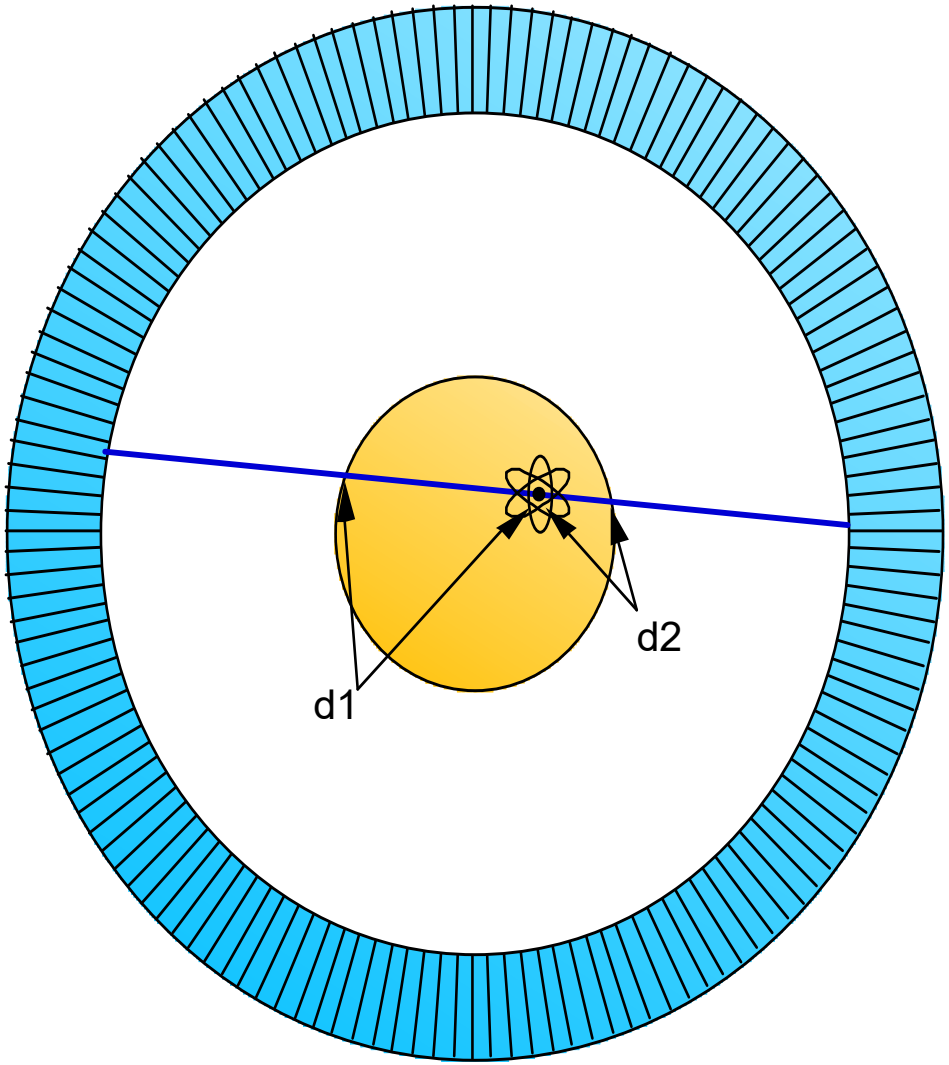

$$P_1 = e^{-\mu \cdot d1} \qquad P_2 = e^{-\mu \cdot d2}$$

$$P = e^{-\mu \cdot (d1+d2)}$$

Event detection probability is product of individual photon detection probabilities.

Detect Radioactive Decays

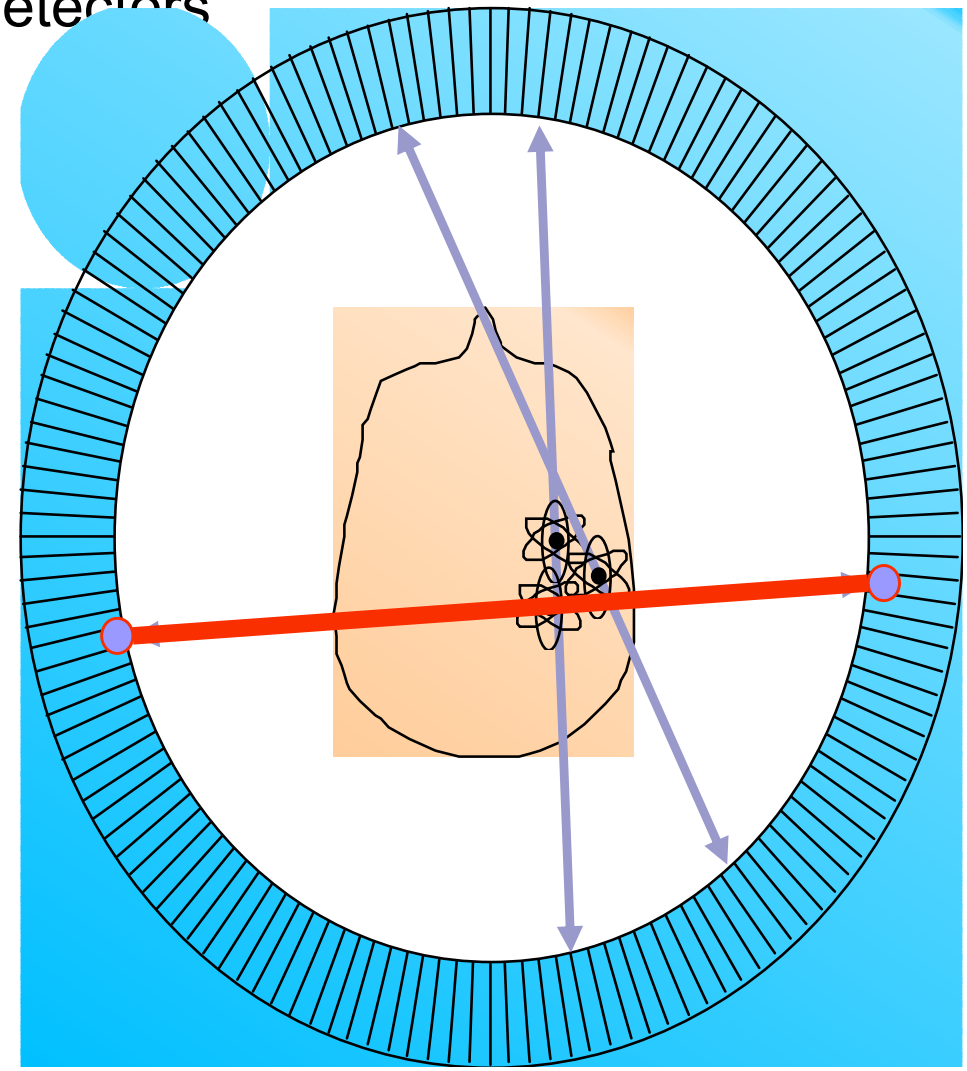

- **Radionuclide decays, emitting β^+.**
- **β^+ annihilates with e^- from tissue, forming back-to-back 511 keV photon pair.**
- **511 keV photon pairs detected via time coincidence.**
- **Positron lies on line defined by detector pair (known as a *chord* or a *line of response* or a *LOR*).**

Detect Pair of Back-to Back 511 keV Photons

Multi-Layer PET Cameras

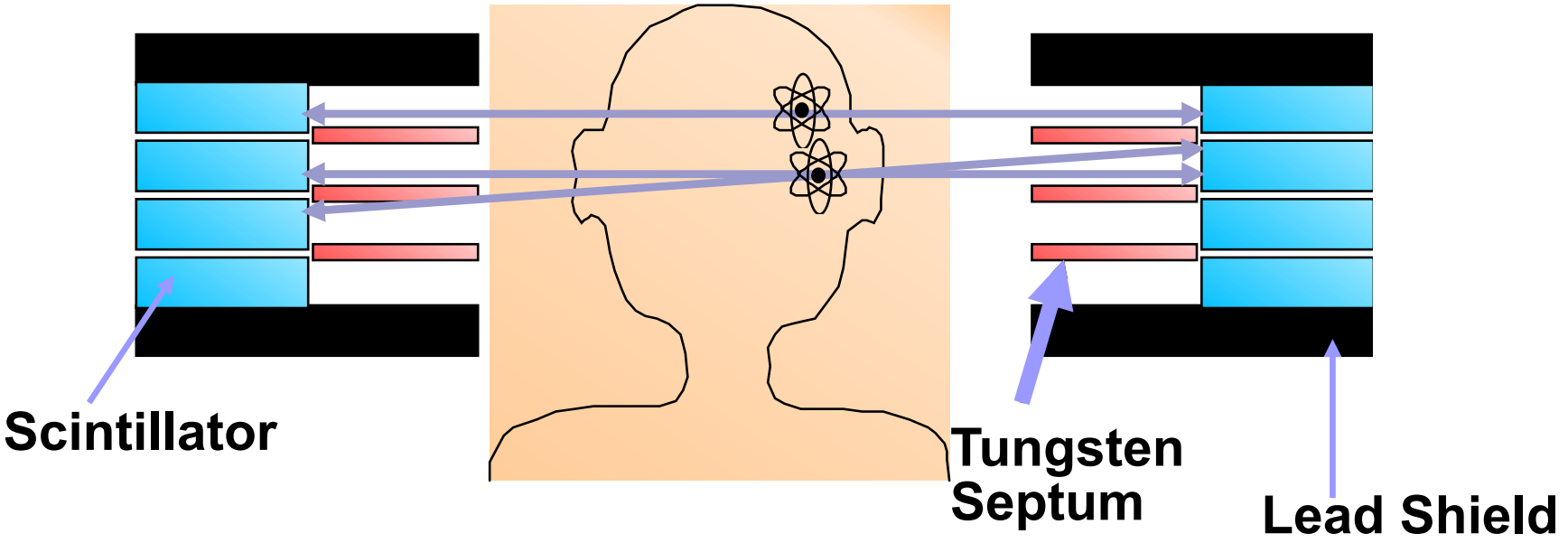

- Can image several slices simultaneously.
- Can image cross-plane slices.
- Can remove septa to increase efficiency ("3-D PET")

Planar Images "Stacked" to Form 3-D Image

Principle of Computed Tomography

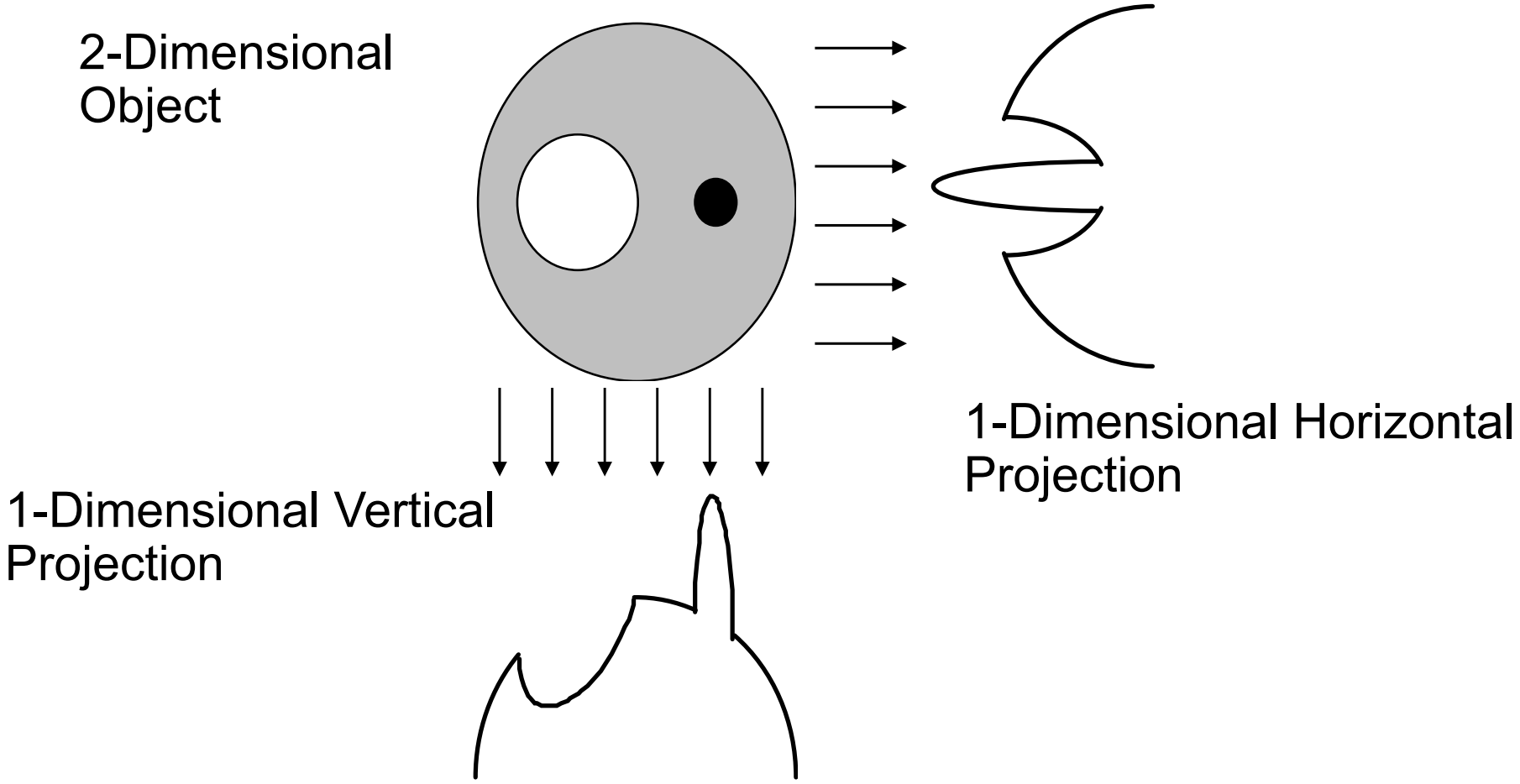

By measuring all 1-dimensional projections of a 2-dimensional object, you can reconstruct the object

PET data acquisition

- Organization of data
  - True counts in LORs are accumulated
  - In some cases, groups of nearby LORs are grouped into one average LOR (“mashing”)
  - LORs are organized into projections

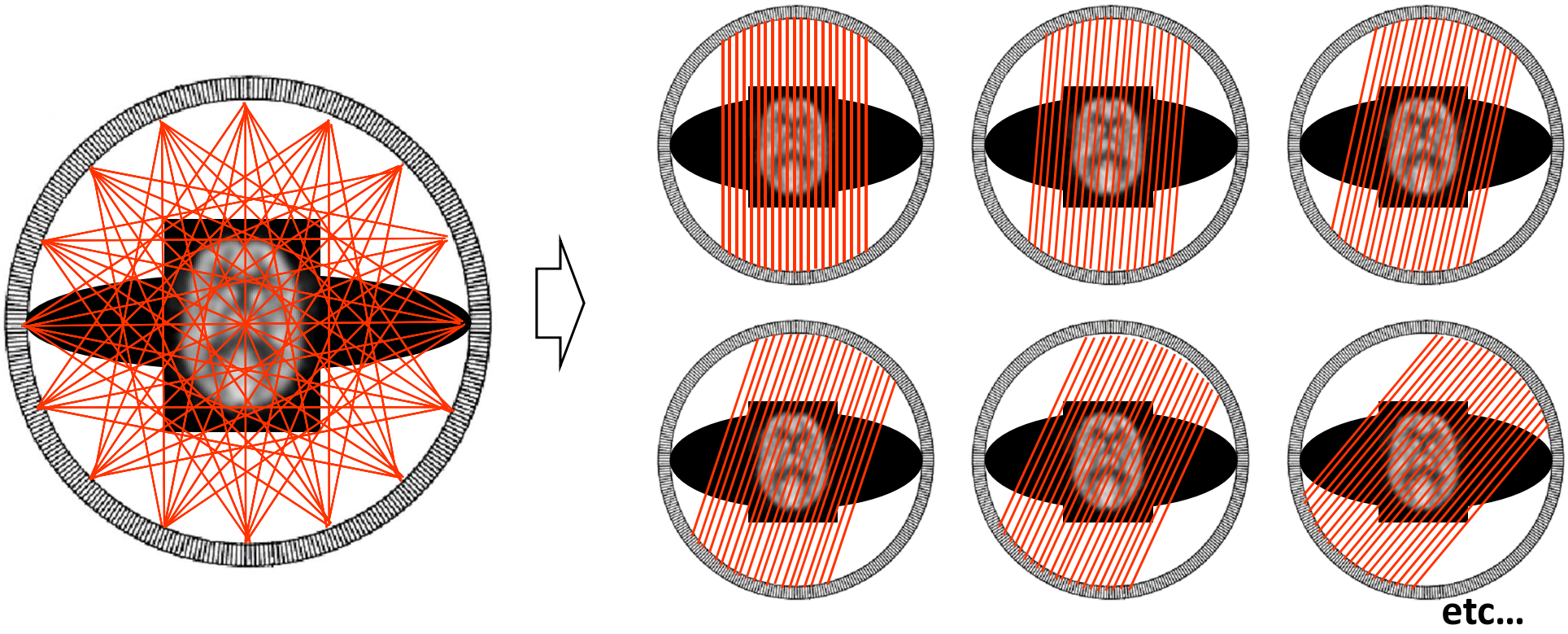

PET data acquisition

- 2D and 3D acquisition modes

2D mode
(= with septa)

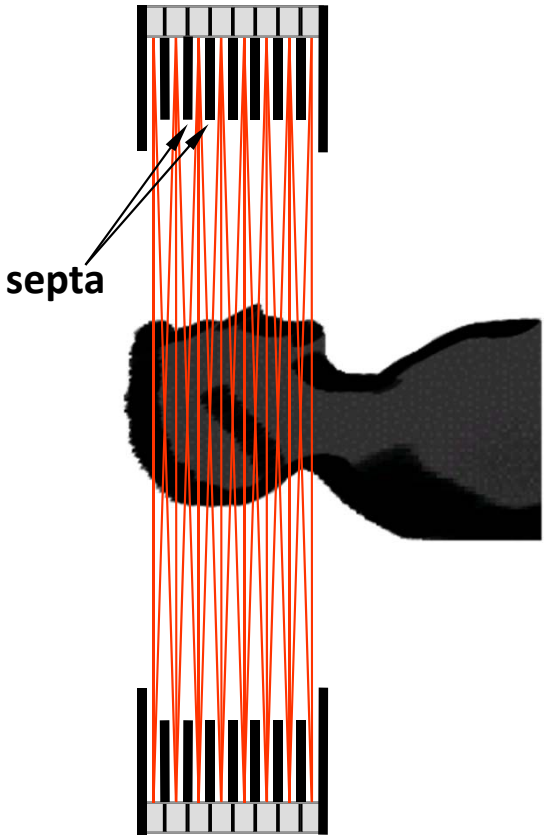

3D mode
(= no septa)

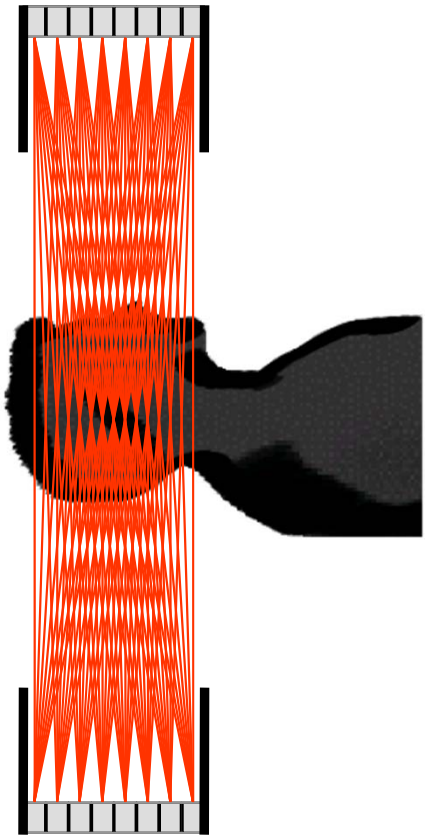

In the 3D mode there are no septa: photons from a larger number of incident angles are accepted, increasing the sensitivity.

Note that despite the name, the 2D mode provides three-dimensional reconstructed images (a collection of transaxial, sagittal and transaxial slices), just like the 3D mode!

PET image reconstruction

- 2D Reconstruction
  - Each parallel slice is reconstructed independently (a 2D sinogram originates a 2D slice)
  - Slices are stacked to form a 3D volume ***f(x,y,z)***

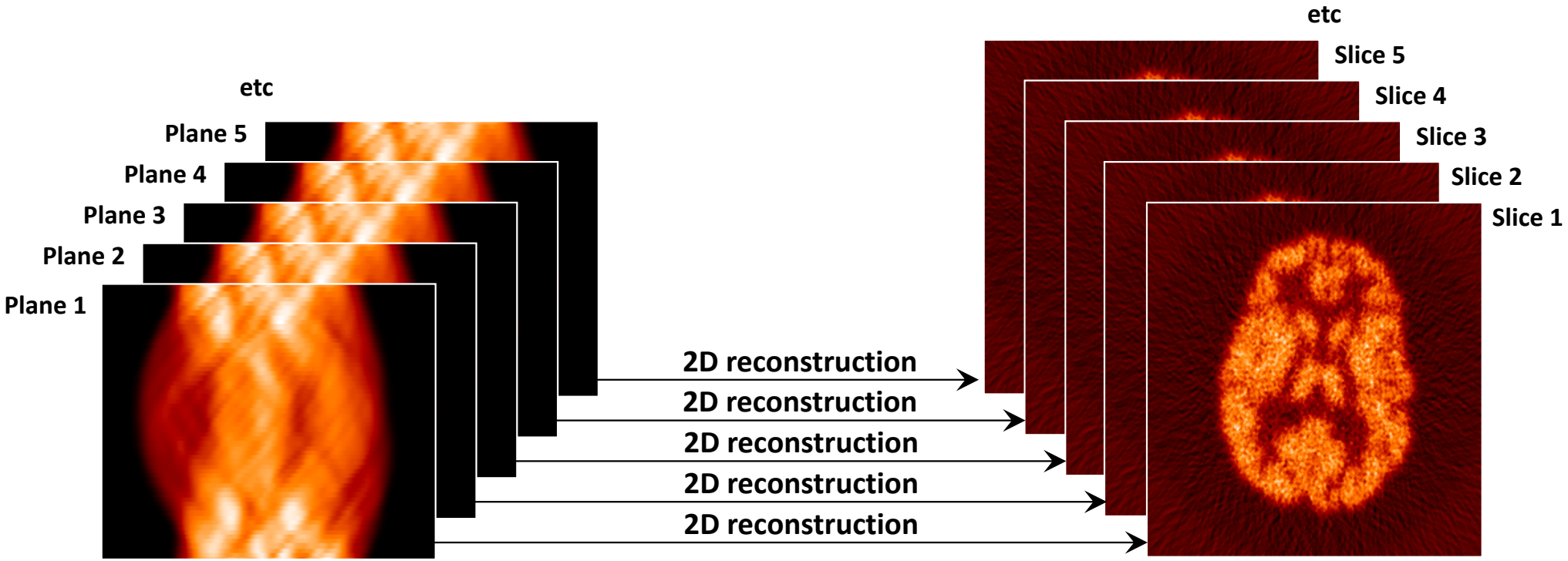

PET data acquisition

- 2D mode vs. 3D mode

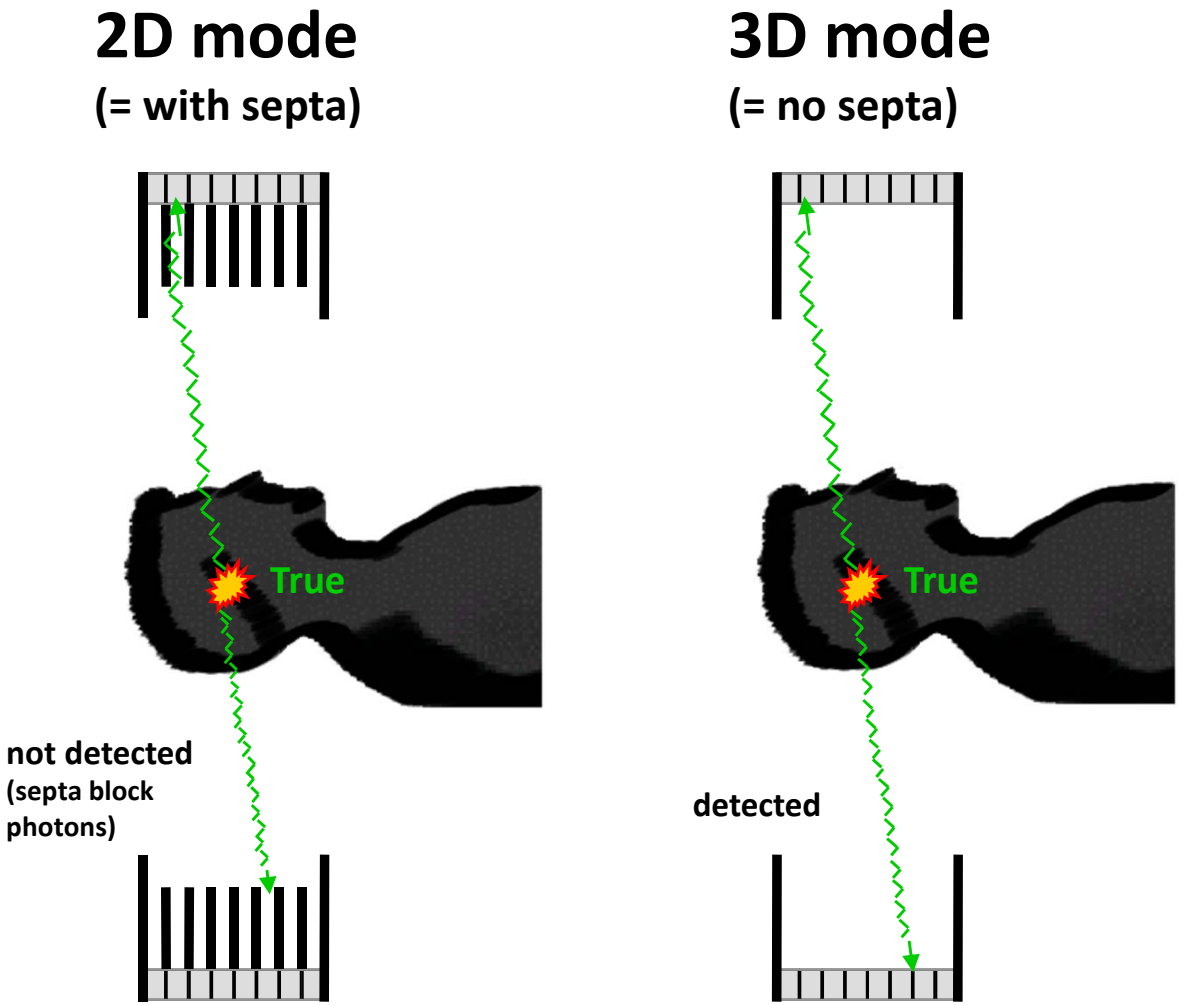

PET data acquisition

- Organization of data
  - In 3D, there are extra LORs relative to 2D

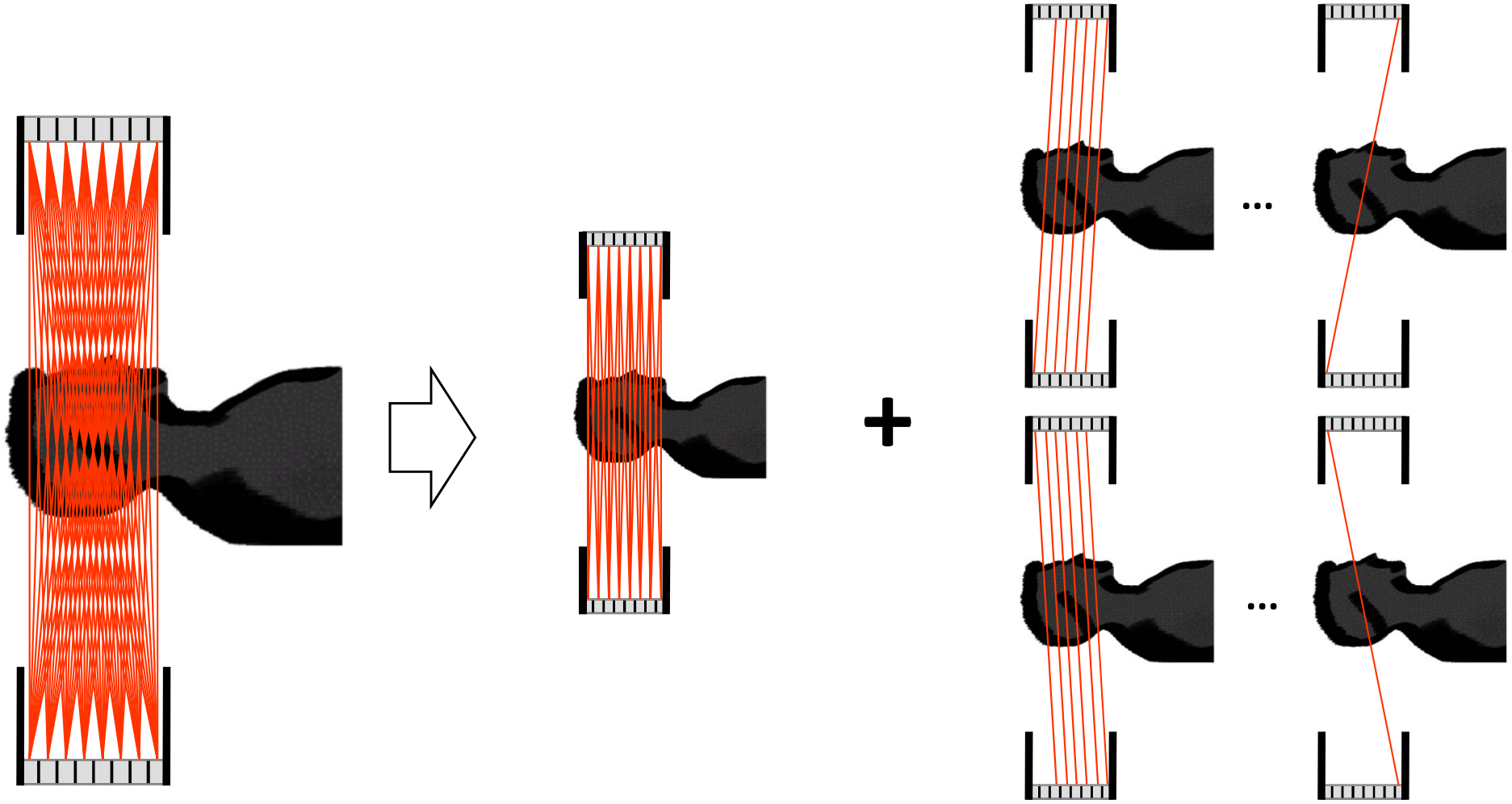

3D mode **same planes as 2D** **+** **oblique planes**

Positron Emission

- A **positron** is the anti-particle of electrons, which carries the same mass as an electron but is positively charged.
- Positrons are normally generated by those nuclides having a **relatively low neutron-to-proton ratio**.
- An typical example of positron emitter is

$$^{22}_{11}Na \rightarrow {}^{22}_{10}Ne + {}^{0}_{1}\beta + \upsilon$$

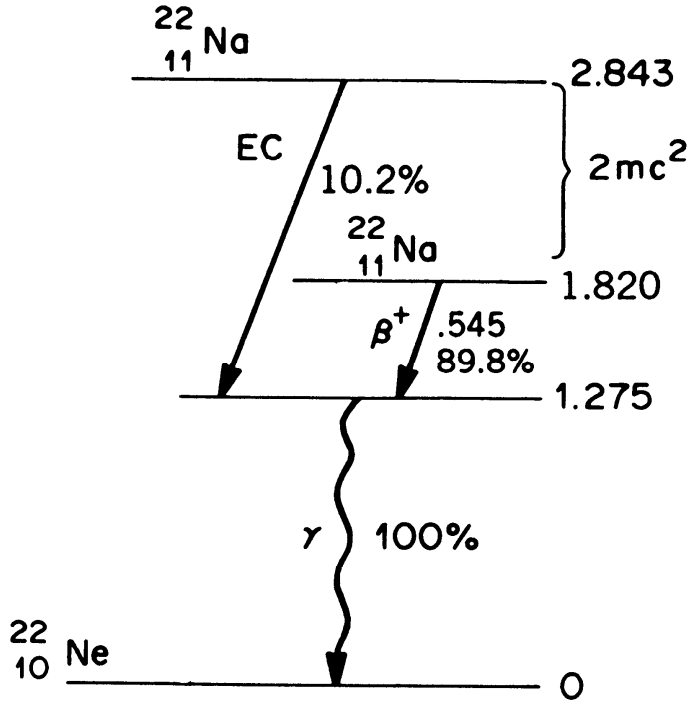

(c)

FIGURE 3.11. Decay scheme of $^{22}_{11}$Na.

Annihilation Radiation following Positron Emission

Beta - plus decay or positron decay :

$$ {}^{A}_{Z}X \rightarrow {}^{A}_{Z-1}Y + {}^{0}_{1}\beta + \upsilon $$

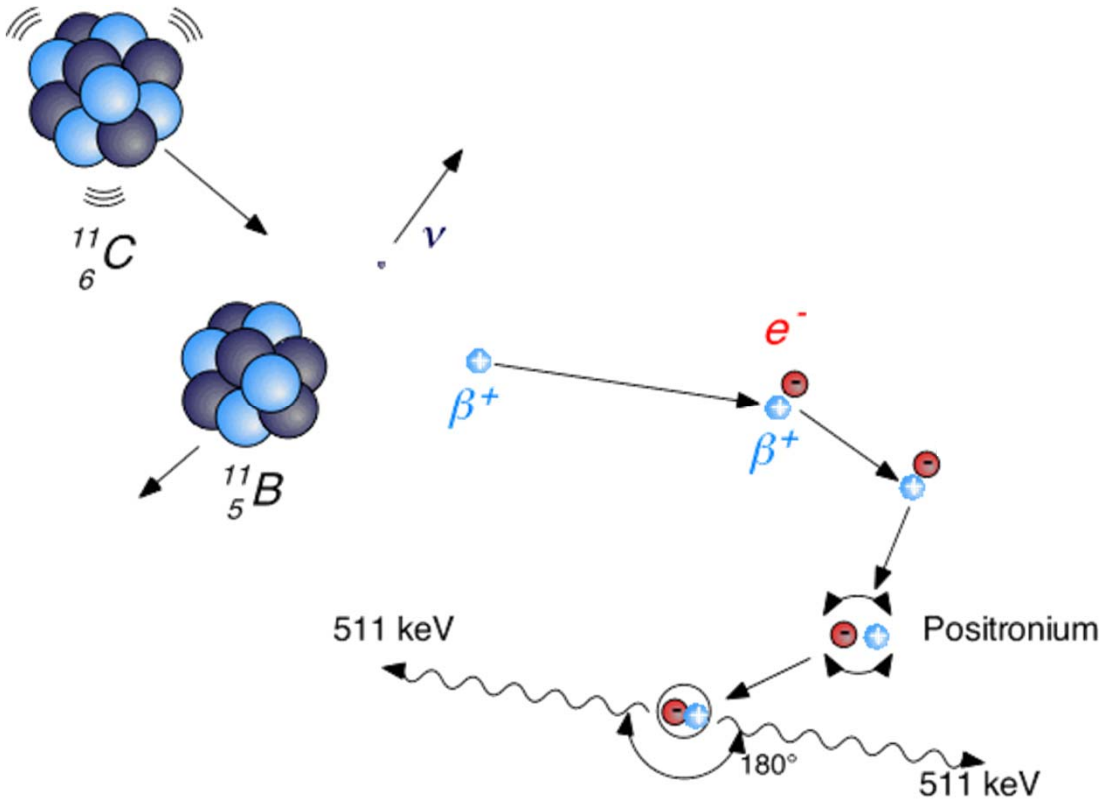

Commonly Used PET Isotopes

Isotope	half-life (min)	Maximum positron energy (MeV)	Positron range in water (FWHM in mm)	Production method
^{11}C	20.3	0.96	1.1	cyclotron
^{13}N	9.97	1.19	1.4	cyclotron
^{15}O	2.03	1.70	1.5	cyclotron
^{18}F	109.8	0.64	1.0	cyclotron
^{68}Ga	67.8	1.89	1.7	generator
^{82}Rb	1.26	3.15	1.7	generator

Table 2. Properties of commonly used positron emitting radio-isotopes

The Tracer Principle Again

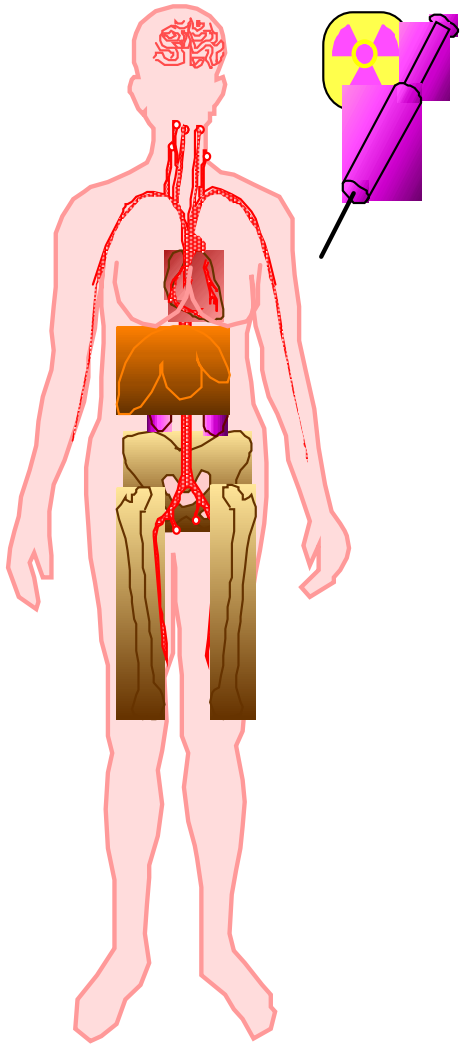

- Drug is labeled with positron (β^+, anti-particle of an electron) emitting radionuclide.
- Drug localizes in patient according to metabolic properties of that drug.
- Trace (pico-molar) quantities of drug are sufficient.
- Radiation dose fairly small (<1 rem).

Why PET

- Interesting Chemistry

  Easily incorporated into biologically active drugs.

- 1 Hour Half-Life

  Maximum study duration is 2 hours.

  Gives enough time to do the chemistry.

- Easily produced

  Short half life $\Rightarrow$ local production.

^{18}F	2 hour half-life
^{15}O, ^{11}C, ^{13}N	2–20 minute half-life

Ideal Tracer Isotope

- Tracers contain elements of life – perfect for providing the functional information such as metabolism rate.
- Electronic collimation – high sensitivity.
- Easier attenuation correction.

^{18}F	2 hour half-life
^{15}O, ^{11}C, ^{13}N	2–20 minute half-life

Photon Attenuation

- Attenuation length of 511 keV photons in water (*i.e.* tissue) is 10 cm.
- Brain is 20 cm diameter.

$\Rightarrow$ up to e^{-2} = 86% of the events are lost.

- Loss fraction depends on position in patient.

$\Rightarrow$ Need to correct for attenuation.

Attenuation of Internal Source

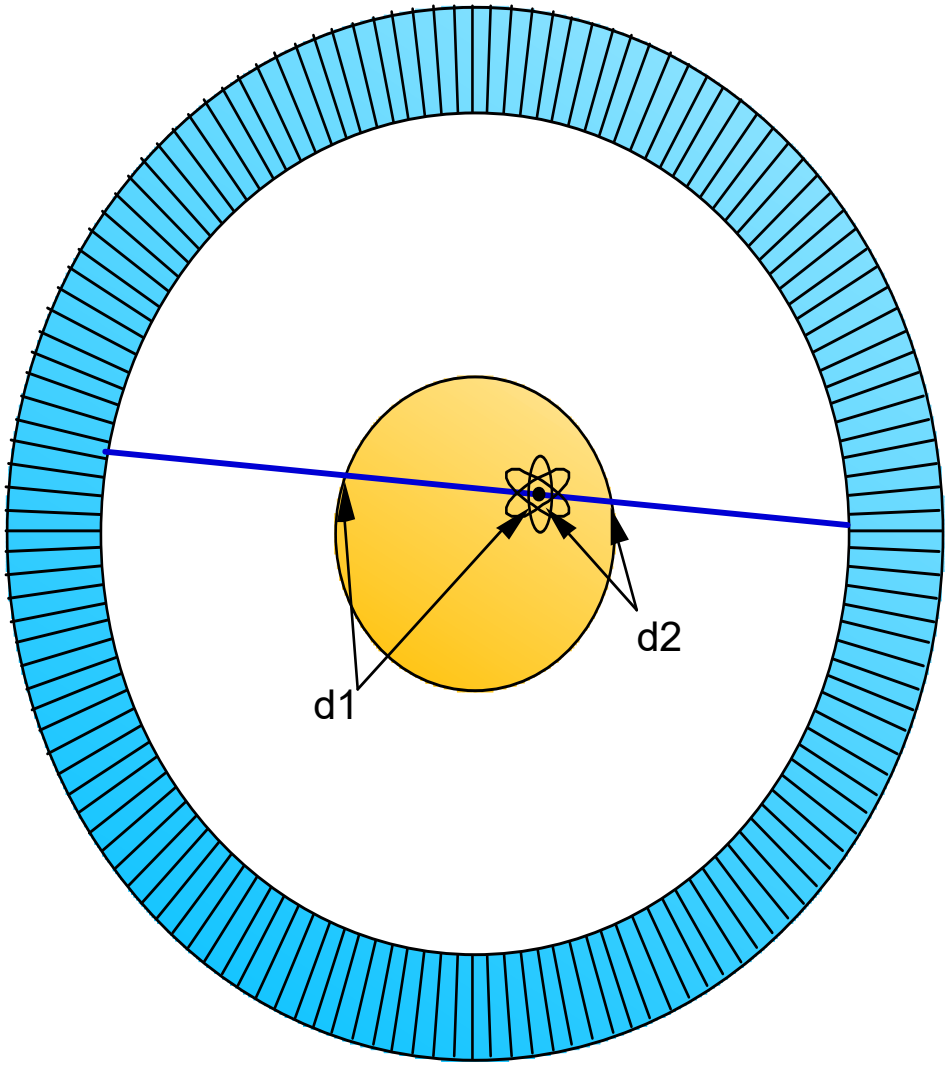

$$P_1 = e^{-\mu \cdot d1} \qquad P_2 = e^{-\mu \cdot d2}$$

$$P = e^{-\mu \cdot (d1+d2)}$$

Event detection probability is product of individual photon detection probabilities.

Transmission Scan Using an Isotopic Source

XBB 887-6863

- **Can reconstruct an image of the attenuation.**
- **Essentially a 511 keV x-ray CT image.**

Attenuation Correction w/ X-Ray CT

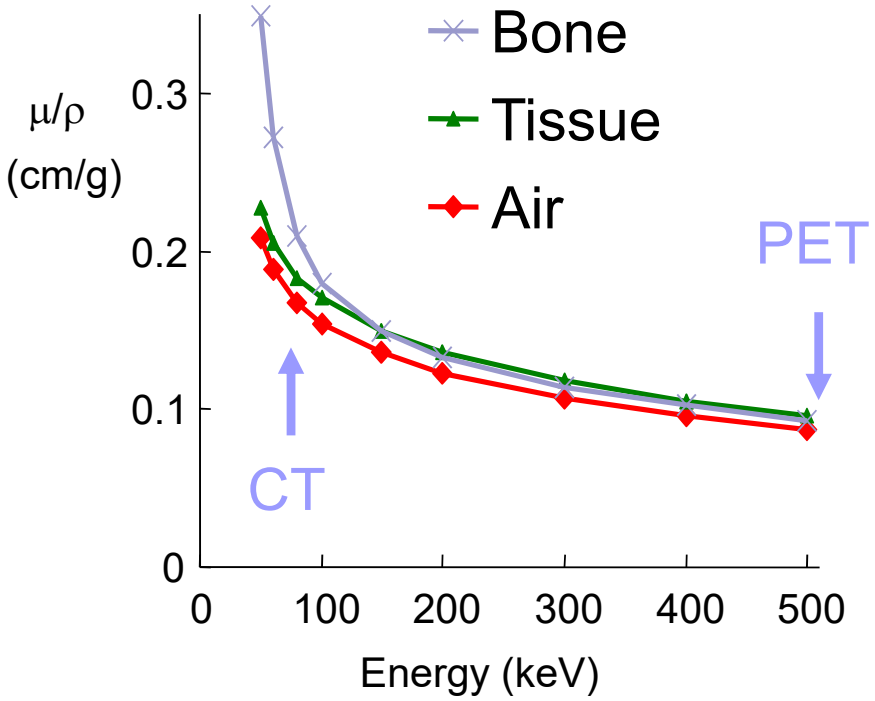

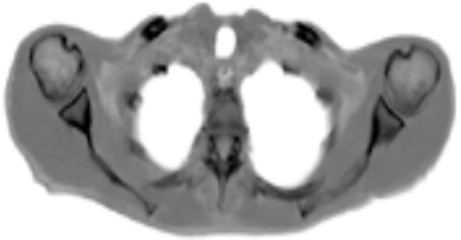

CT:
70 keV

Scaled:
511 keV

- Can use x-ray CT data to obtain attenuation data
- Attenuation coefficients μ are energy dependent

$\Rightarrow$ μ at 70 keV (x-ray CT energy) not equal to μ at 511 keV

- "Scale" data — use CT to classify voxels as either air, tissue, or bone, then multiply by known ratio of μ_{511}/μ_{70} to do correction

*Data courtesy of David Townsend, U. Tenn.

Random Coincidences

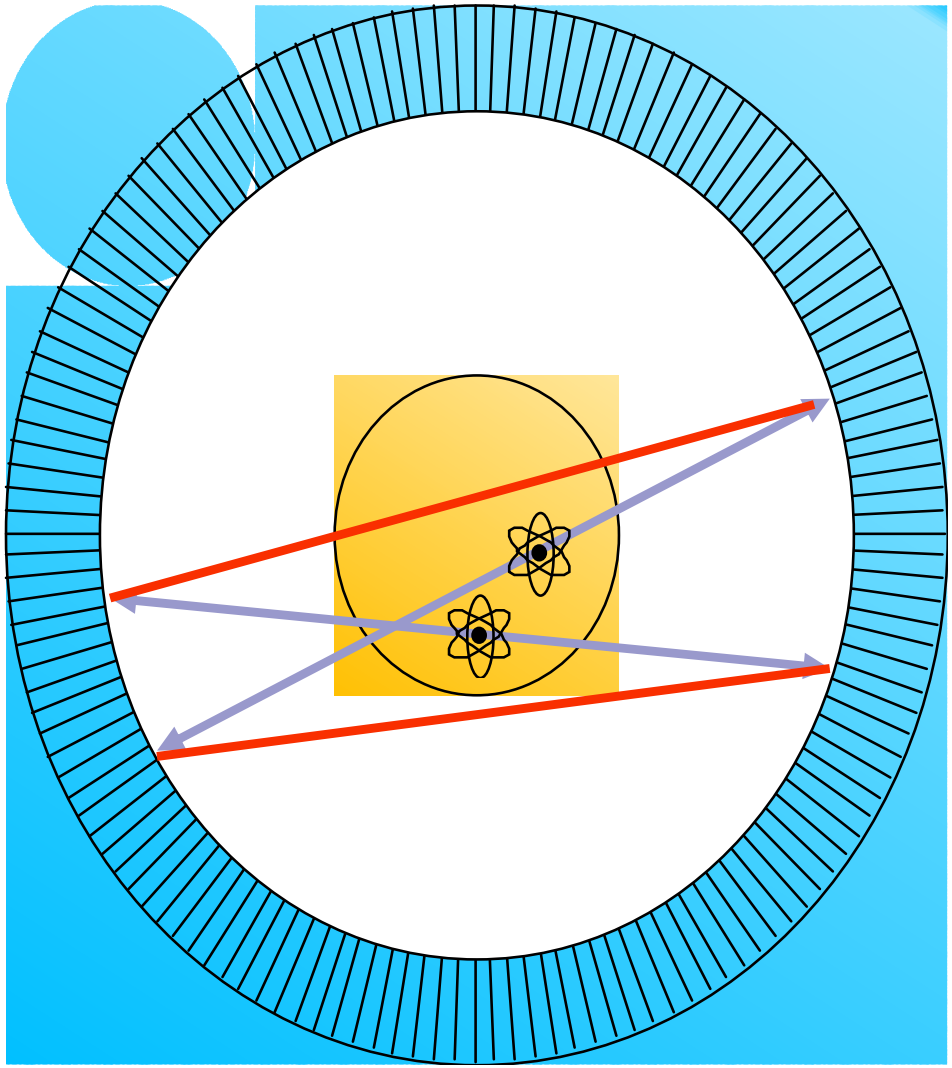

- Simultaneous decays can cause erroneous coincident events called Randoms.
- For 3-D PET, randoms can be as high as 50% of image.
- Random Rate is $Rate_1 \times Rate_2 \times 2\,\Delta t$
- Randoms reduced by narrow coincidence window Δt.
- Time of flight across tomograph ring requires $\Delta t > 4$ ns.

Random Rate $\propto$ (Activity Density)^2

PET Detectors

Early PET Detector Module

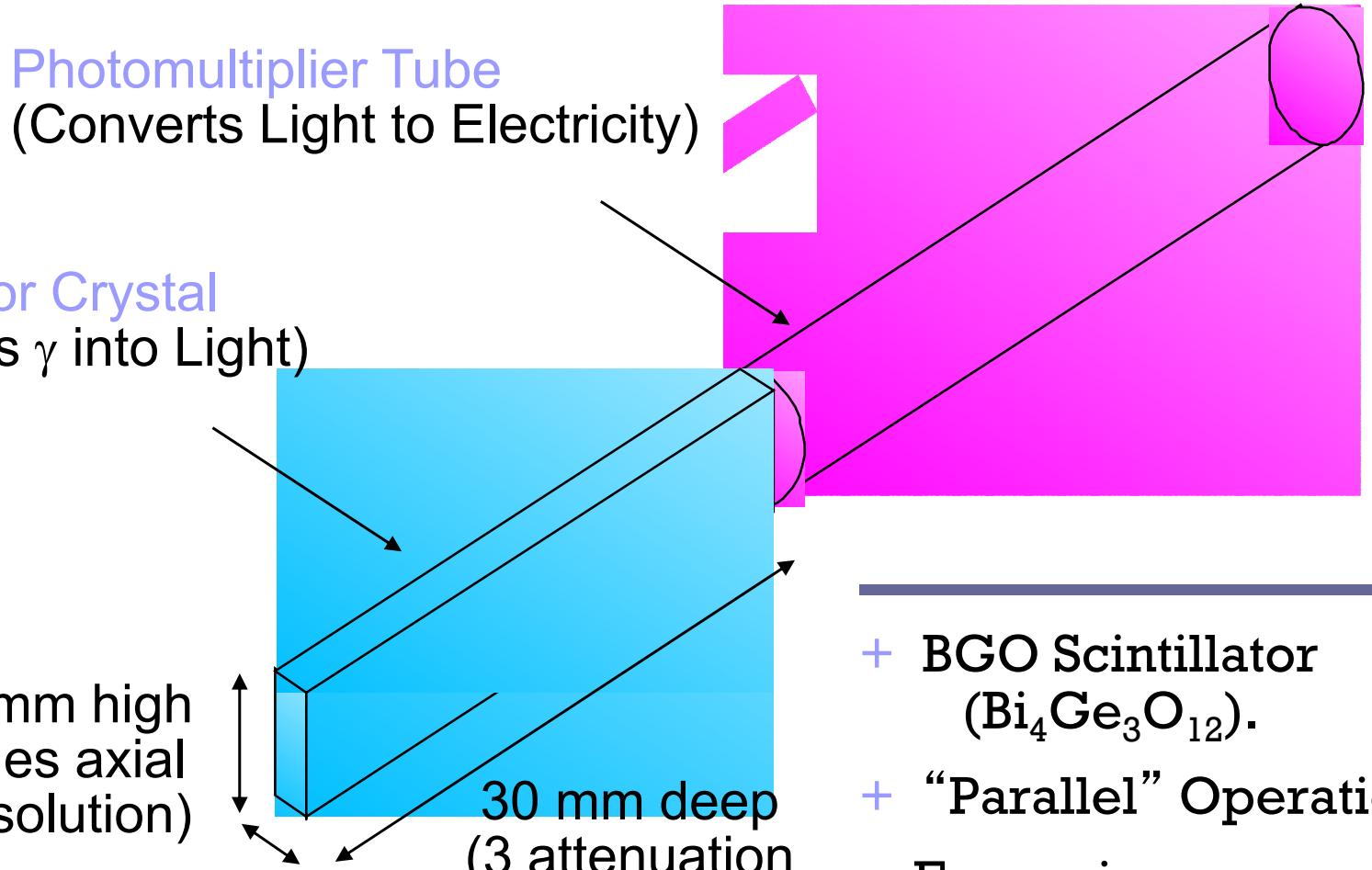

+ BGO Scintillator ($Bi_4Ge_3O_{12}$).
+ "Parallel" Operation.
– Expensive.
– Difficult to Pack.

Block Design Using Anger Logic

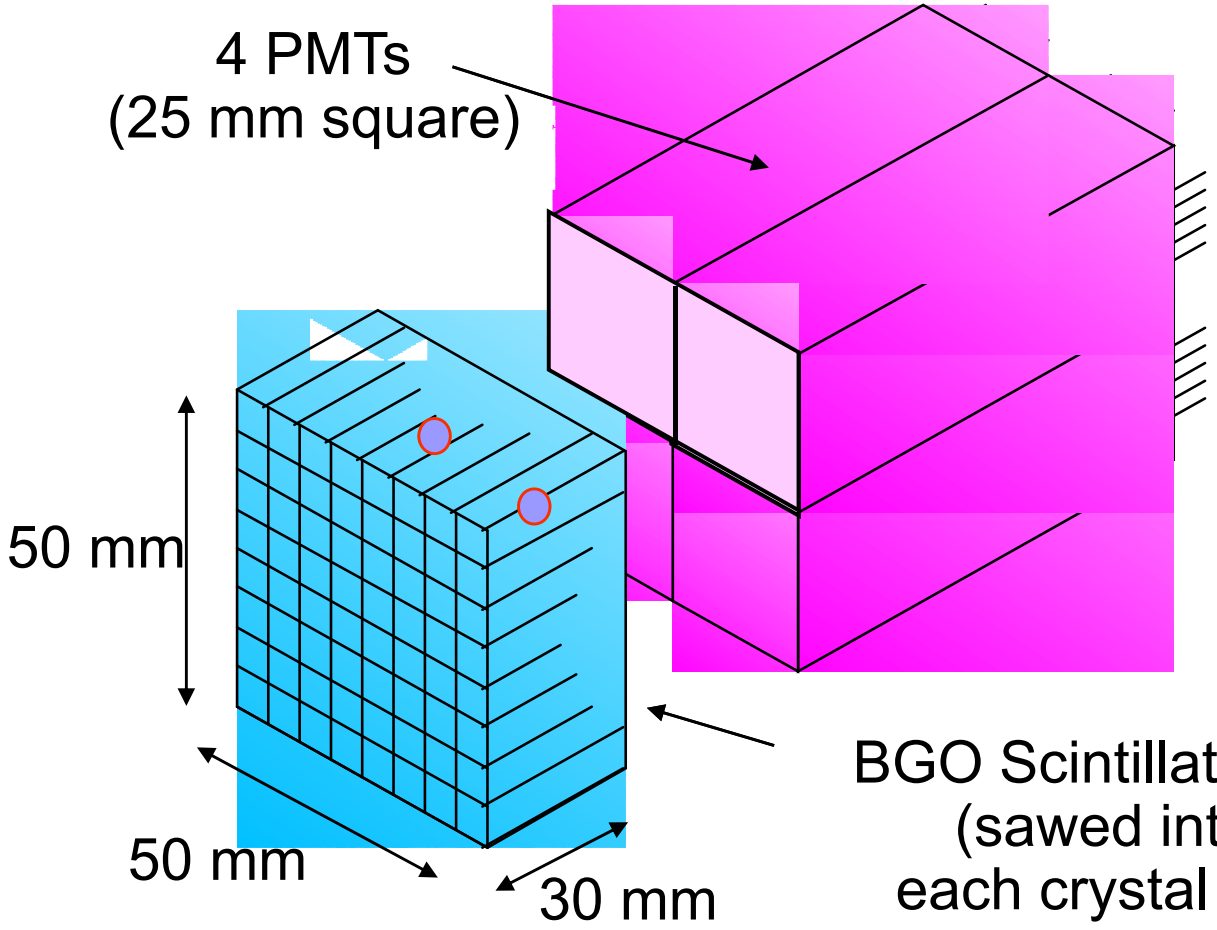

- Saw cuts direct light toward PMTs.
- Depth of cut determines light spread at PMTs.
- Crystal of interaction found with Anger logic (i.e. PMT light ratio).

Good Performance, Less Expensive, Easy to Pack

Crystal Identification with Anger Logic

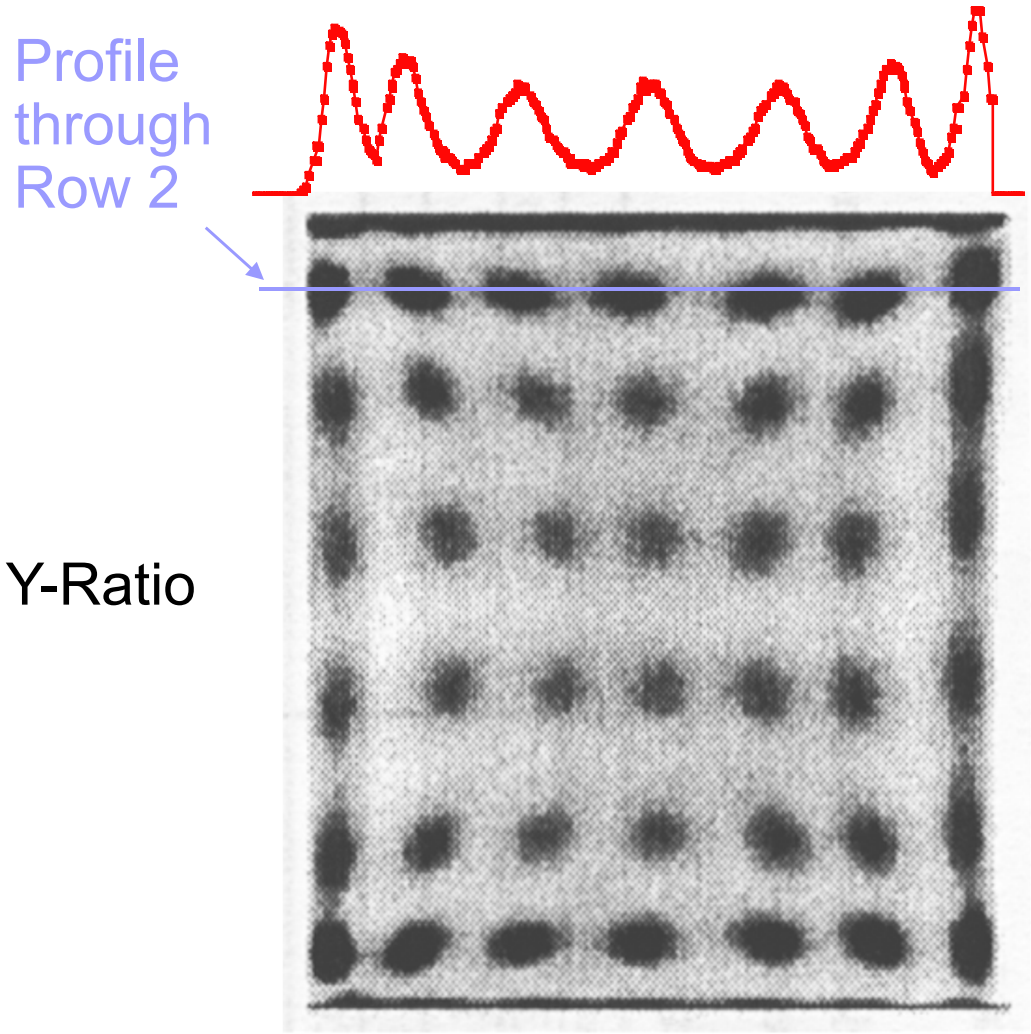

- Uniformly illuminate block.
- For each event, compute X-Ratio and Y-Ratio, then plot 2-D position.
- Individual crystals show up as dark regions.
- Profile shows overlap (i.e. identification not perfect).

Can Decode Up To 64 Crystals with BGO

Event Rates

Singles Events:

~3 ns timing accuracy

10^6 events / sec / module (25 cm^2)

200 modules $\Rightarrow$ $2x10^8$ events / sec / camera

Coincidence Events:

Time window ~10 ns

Lots of chords
(~280,000,000 in 48 layer camera with septa removed).

$5x10^6$ coincidence events / sec

Parallel Electronics is Necessary

Detector Requirements

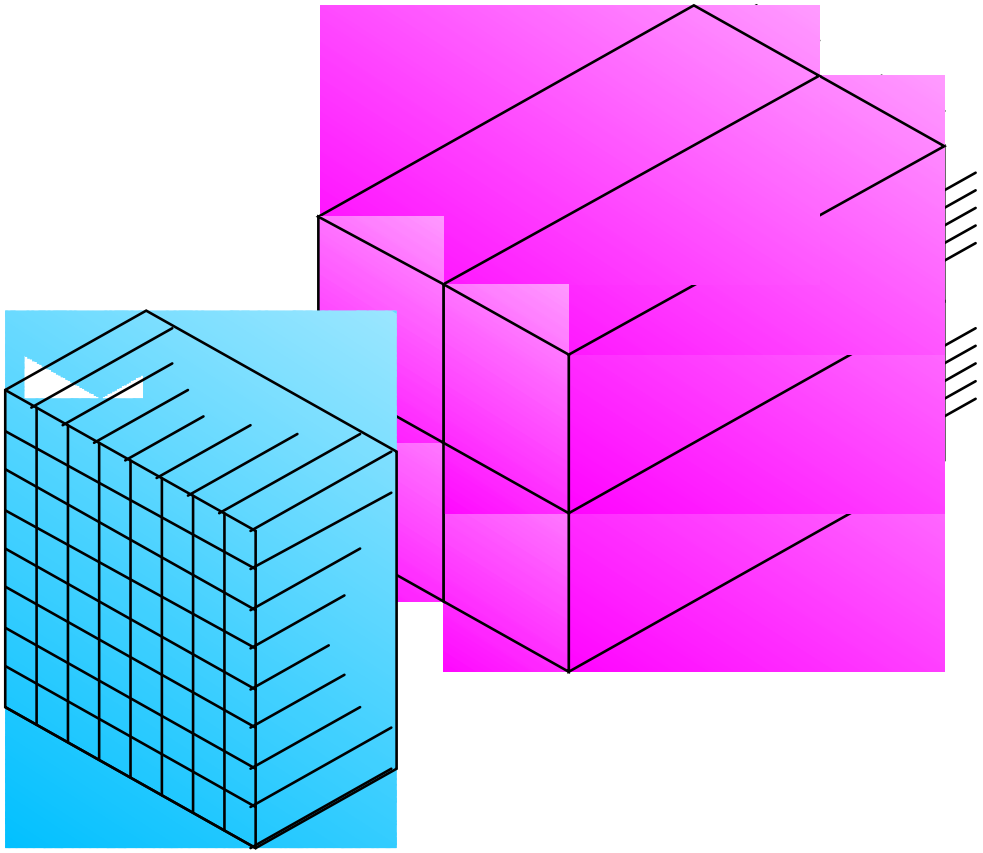

Detect 511 keV Photons With (in order of importance):

- >85% efficiency
- <5 mm spatial resolution
- "low" cost (<$100 / cm^2)
- "low" dead time (<1 µs cm^2)
- <5 ns fwhm timing resolution
- <100 keV energy resolution

Based on Current PET Detector Modules

Scintillation Crystal Properties

TABLE 1 Properties of Common Scintillation Crystals Used in Small-FOV Imager Designs

Scintillator	Effective Z	Density (g/cc)	Radiation Length (mm)[a]	Relative Light Yield	Refractive Index	Decay Time (ns)	Peak Emission Wavelength (nm)	Hygroscopic?	Rugged?
NaI(Tl)	51	3.67	3.4	100	1.85	230	410	Yes	No
CsI(Tl)	54	4.51	2.2	135	1.79	1000	530	No	Yes
CsI(Na)	54	4.51	2.2	75	1.79	650	420	No	Yes
BGO	74.2	7.13	10.5	15	2.15	300	480	No	Yes
LSO(Ce)	65.5	7.4	11.6	75	1.82	40	420	No	Yes
$CaF_2(Eu)$[b]	16.9	3.17	N/A	50	1.43	940	435	No	Yes

[a]Radiation lengths for NaI(Tl), CsI(Tl) and CsI(Na) are for 140-keV photons; Values for BGO and LSO are at 511 keV.
[b]$CaF_2(Eu)$ is used in beta imaging.

Lutetium Orthosilicate (LSO) Scintillator

Compared to BGO, LSO has:

Same Attenuation Length:

⇒ Good Spatial Resolution

Higher Light Output:

⇒ Decode More Crystals per Block

⇒ Better SNR for "Enhanced" Readout
(*e.g.* Depth of Interaction)

Shorter Decay Time:

⇒ Less Dead Time
(Allows Larger Block Areas)

⇒ Better Timing Resolution

Reduce Cost OR Increase Performance

Improvements In Scintillators Needed

Image courtesy of Paul Lecoq, *CERN*

Combine Best Properties of:

- $LaBr_3$:30% Ce
  - Timing resolution <100 ps
  - Energy resolution <4%
- LuI_3:Ce
  - Light output >100,000 ph/MeV
- $PbWO_4$
  - Density >8 g/cc
  - High atomic number
  - Inexpensive

PET Performance Determined by Scintillator

Animal PET Camera

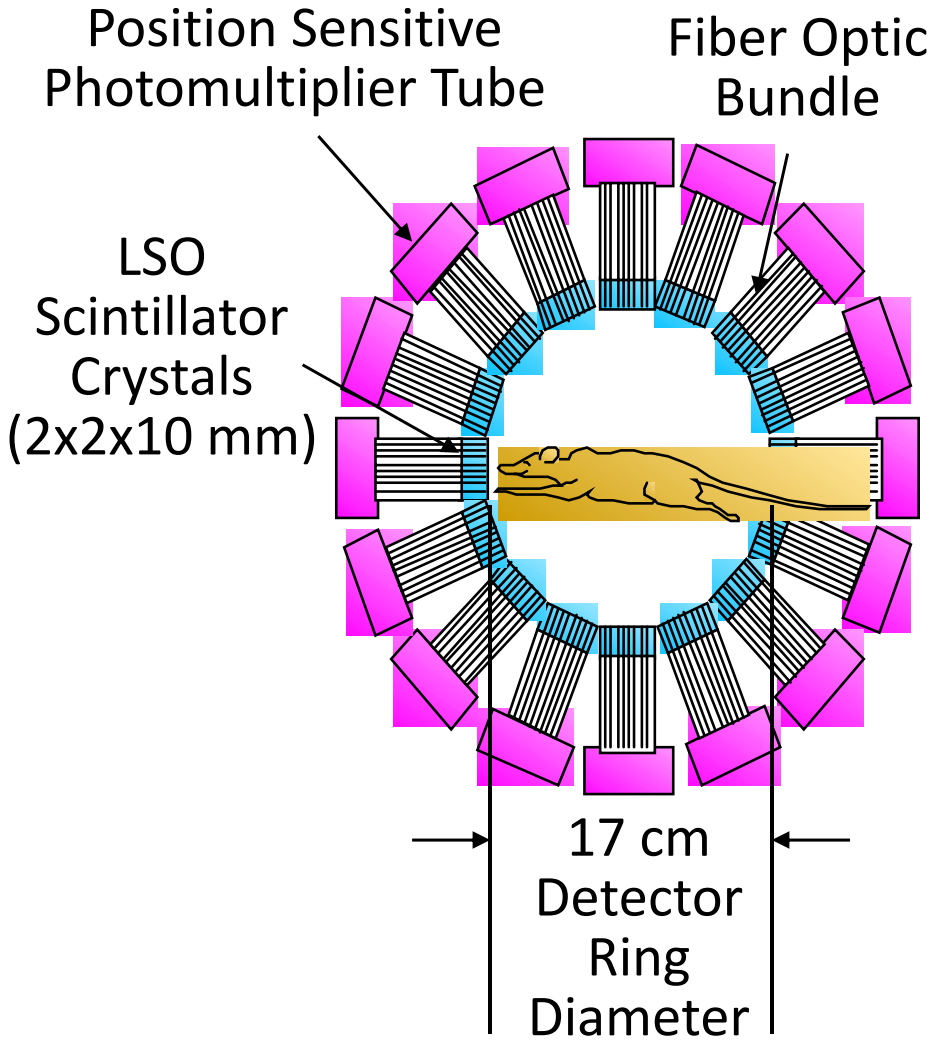

*Image courtesy of Simon Cherry, UC Davis

Miniature Version of “Standard” PET Camera

Electromagnetic Interferences Between Nuclear and MR Data Acquisition Systems

Photomultiplier Tube (PMT)

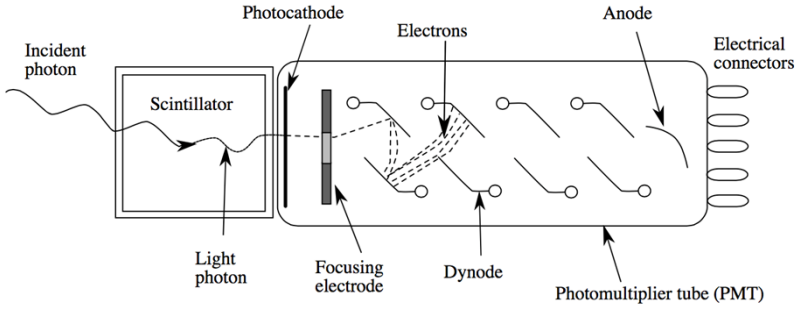

http://nl.wikipedia.org/wiki/Fotomultiplicator

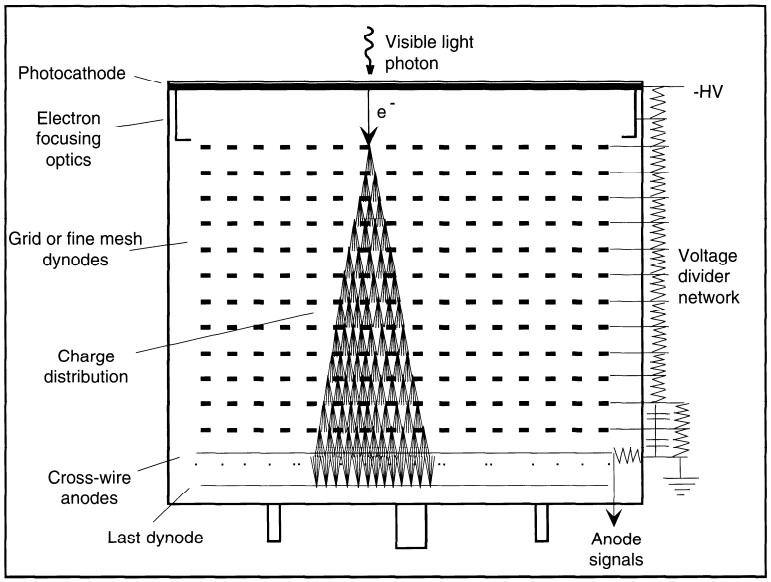

FIGURE 11 Depiction of the cross-wire anode PSPMT and its signal formation process. For simplicity, the charge avalanche created from only a single photoelectron is shown. A 10^5 photoelectron amplification factor is typical. Setting the cathode at ground and biasing the anode at +HV through a coupling capacitor is also possible.

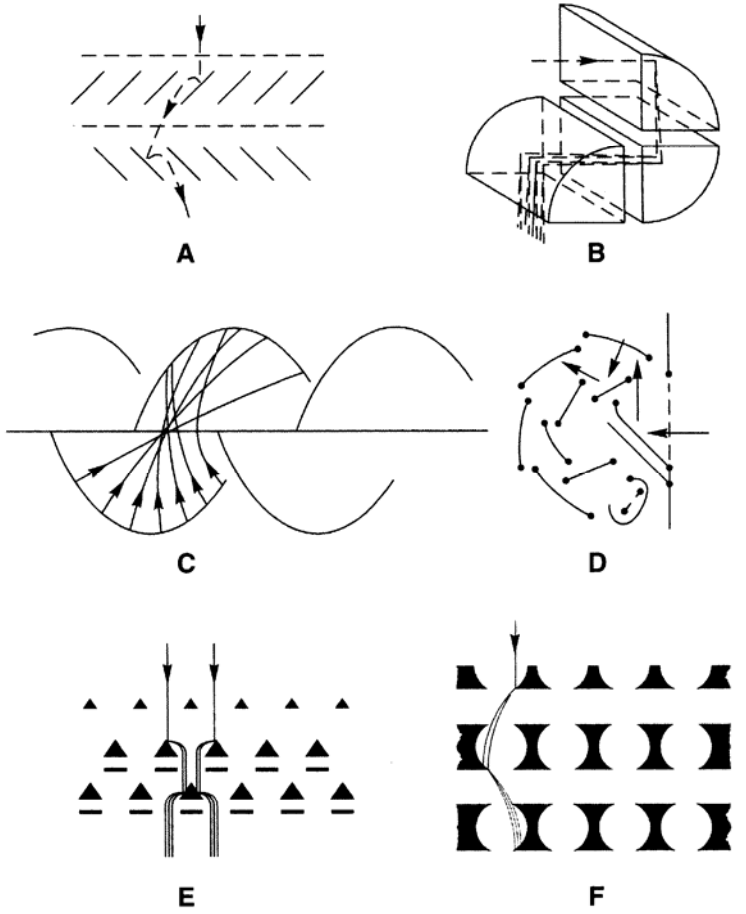

FIGURE 2 Scheme of dynode configurations: (a) venetian blind dynodes, (b) box dynode structure, (c) linear focusing dynodes, (d) circular cage dynodes, (e) mesh dynodes, and (f) foil dynodes. (From Photonis, 1994, *Photomultiplier Tubes: Principles and Applications*.)

K F Knoll, Radiation Detection and Measurements, Third Edition, Wiley.

(Gas) Multiplication Process in Solid-State Photon Sensors??

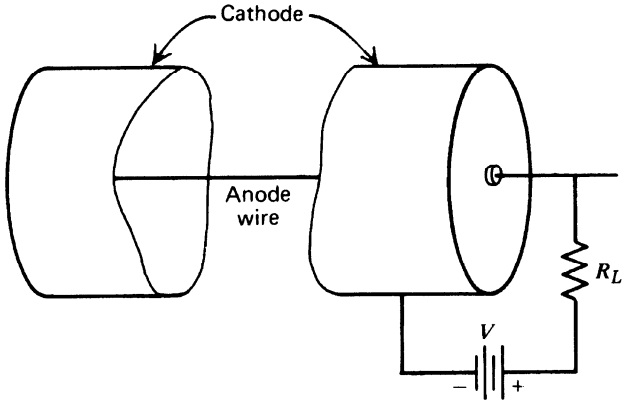

Figure 6.3 Basic elements of a proportional counter. The outer cathode must also provide a vacuum-tight enclosure for the fill gas. The output pulse is developed across the load resistance R_L.

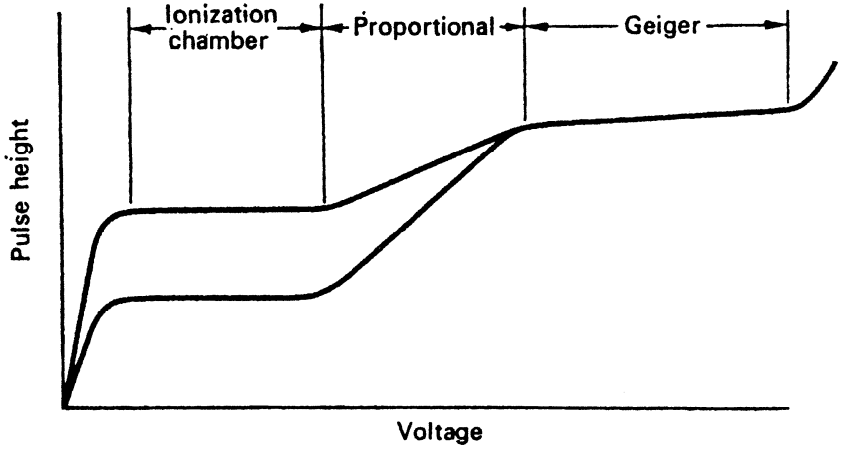

FIGURE 9.3. Curve of pulse height versus voltage across a gas-filled pulse counter, illustrating the ionization chamber, proportional, and Geiger regions.

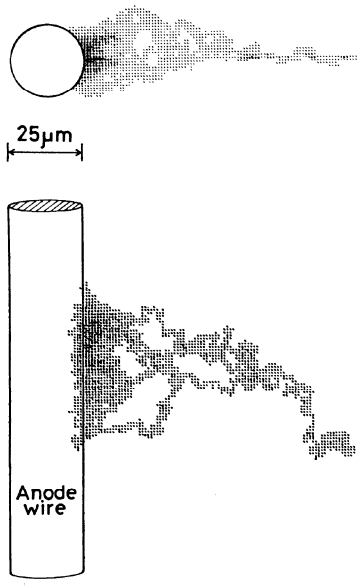

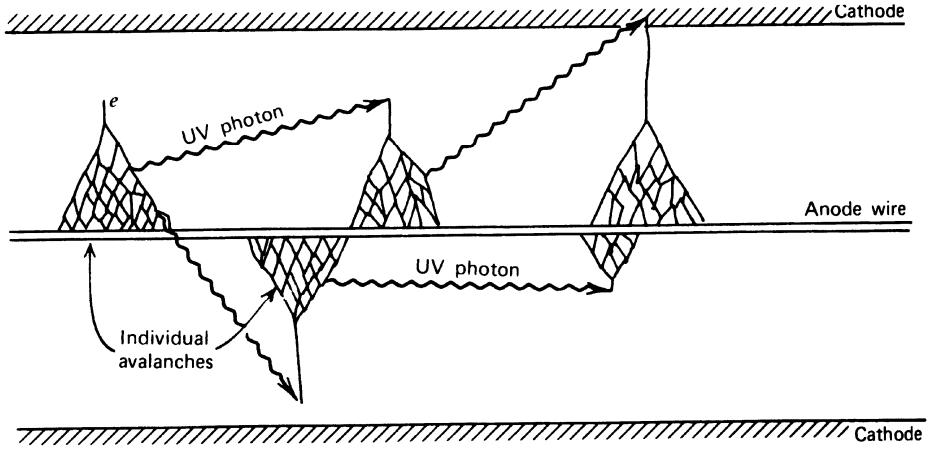

Figure 7.1 The mechanism by which additional avalanches are triggered in a Geiger discharge.

Figures from K F Knoll, Radiation Detection and Measurements, Third Edition, Wiley.

Photodiode Detectors

Figure 1-1 Photodiode cross section

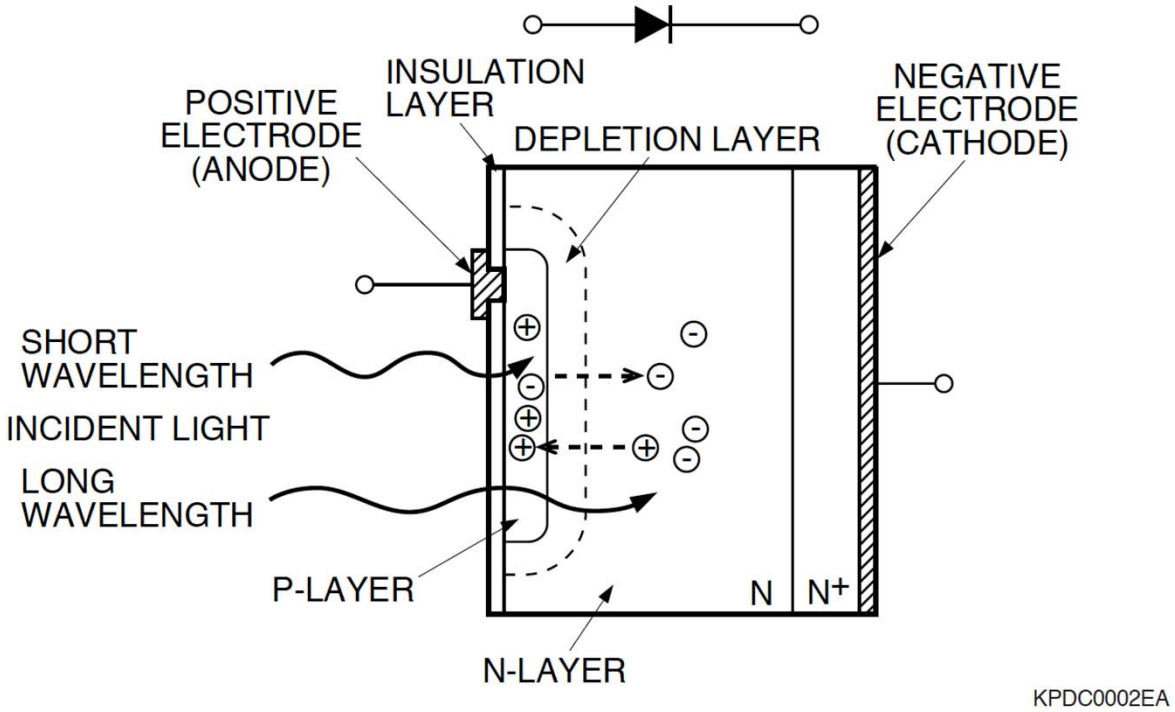

Typical reversed-biased photodiode detectors

- **No internal gain**
- **Very high QE for red light (up to 90%)**
- **Limited timing resolution**

Hamamatsu photodiode technical information

Avalanche Photodiode (APD)

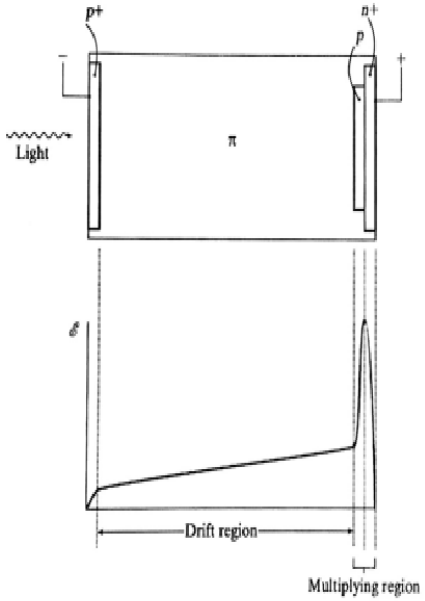

From K F Knoll, Radiation Detection and Measurements, Third Edition, Wiley.

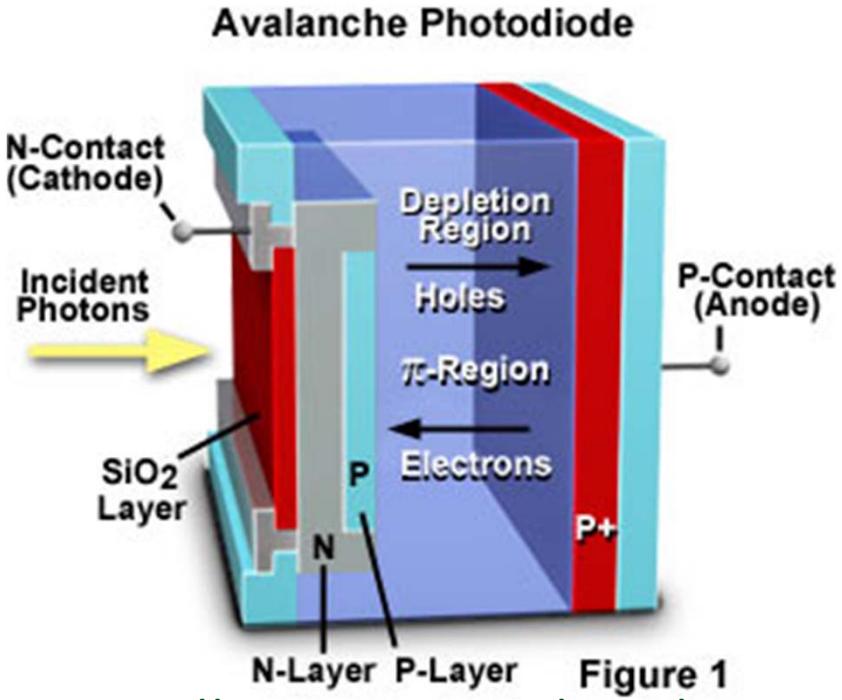

Figure 1

http://learn.hamamatsu.com/articles/avalanche.html

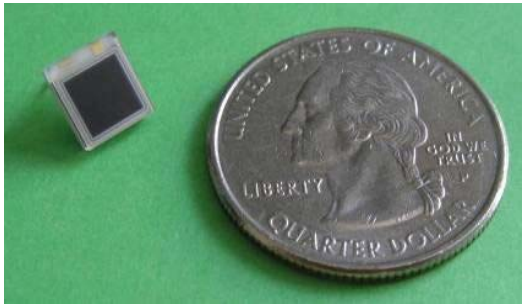

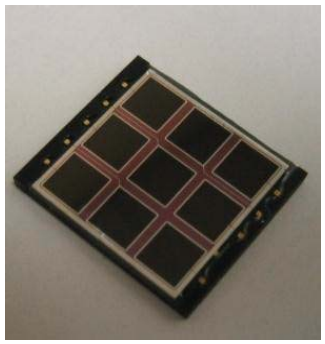

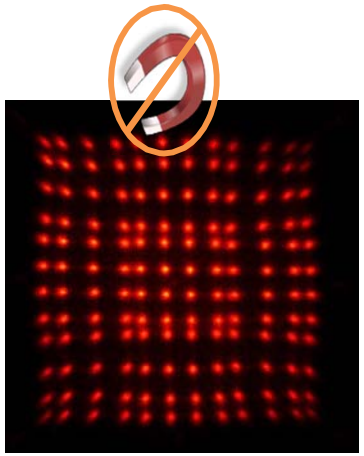

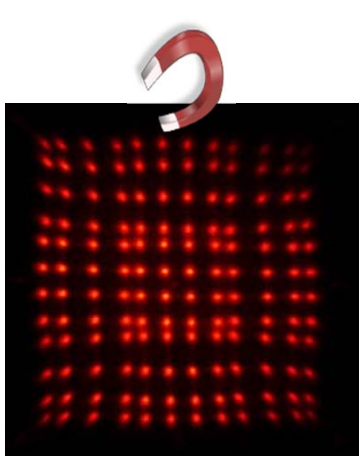

Avalanche Photo Diodes (APD), proof to be suitable detectors for PET/MRI

- Could be operated inside strong magnetic field
- Added internal gain
- Fast timing property
- Gain critically depends on bias voltage
- Temperature stability could be an issue

Silicon Photomultipliers

Silicon Photo Multipliers (SiPM, Geigermode-APD)
a novel MR compatible PET detector

G-APD 6.5 x 7 mm² **3 x 3 mm², 60x60 cells** **Each cell 50 x 50 µm²**

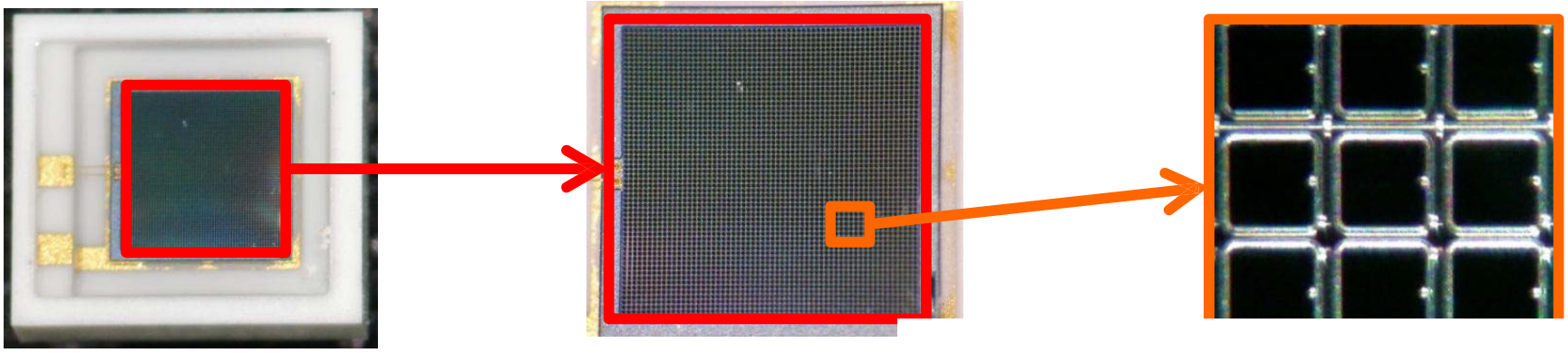

- Each cell is operated above breakdown
- Output signal is sum of all cells
- Each cell provides maximum-gain signal on photon interaction

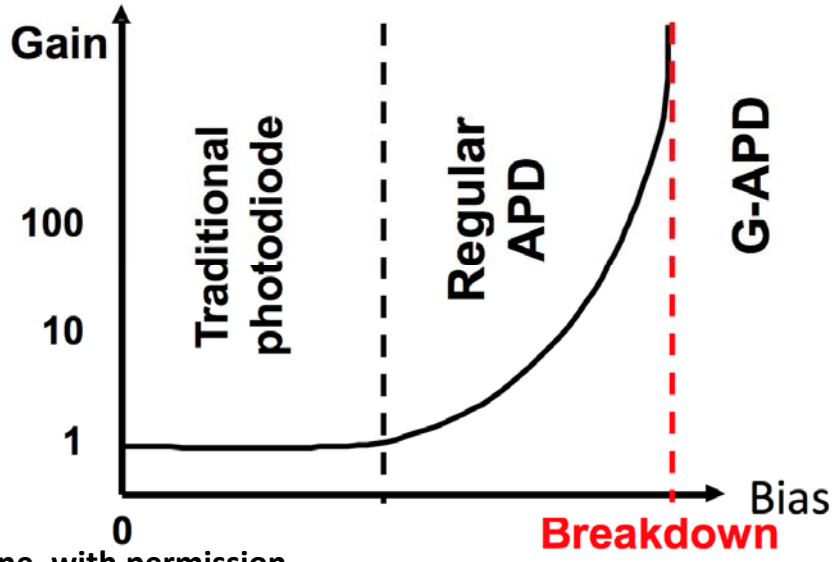

This slide was derived from Martin S. Judenhofer, Seminars in Nuclear Medicine, with permission.

Silicon Multiplier (SiPM) Detectors

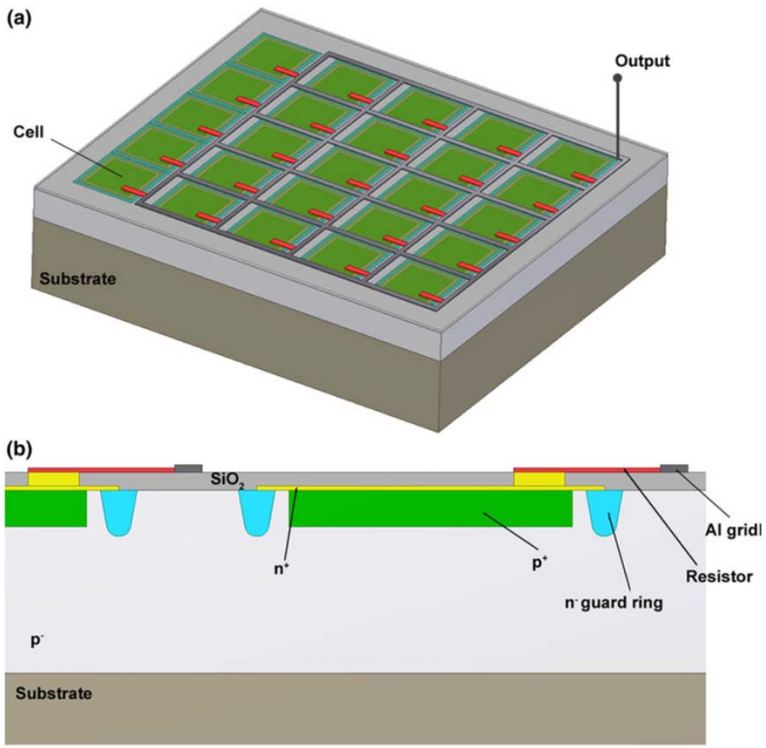

FIGURE 1. (a) Simplified structure of a SiPM composed of G-APD cells. The G-APDs are joined together on a common substrate and are electrically decoupled. The outputs of the cells are connected to an Al grid used for the readout of the output signals. Each cell has a quenching resistor in series. (b) Each cell (G-APD) is a p–n junction with a very thin depletion layer between p+ and n+ layers.15 Drawings courtesy of Julien Bec, UC Davis.

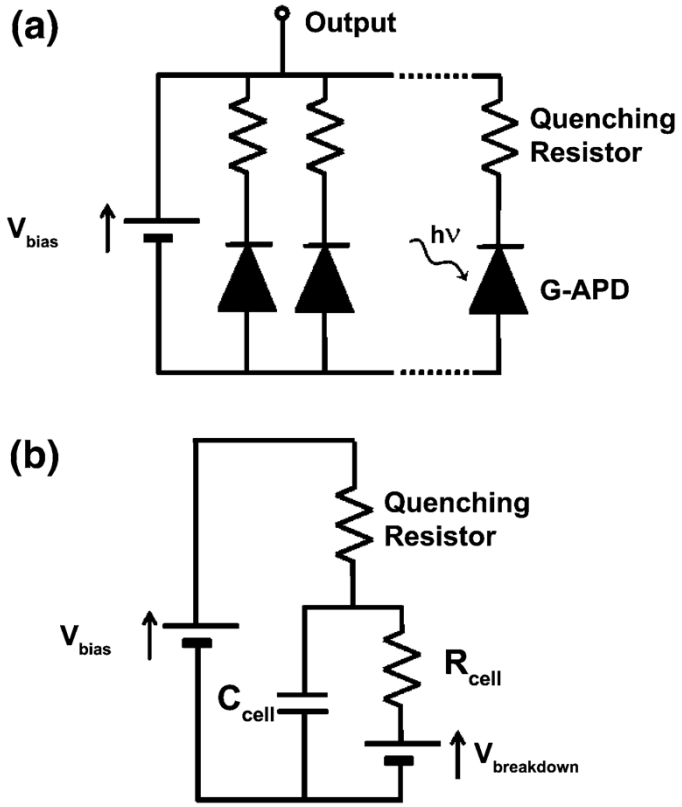

FIGURE 2. (a) Simplified electric structure of a SiPM com- posed of several G-APDs in series with a quenching resistor. (b) Equivalent circuit of a single cell when the device is on (a bias voltage Vbias is applied) and is detecting photons. The capacitor Ccell initially charged at Vbias discharges through Rcell dropping the bias voltage to Vbreakdown. The avalanche process is quenched via the quenching resistor and then the device is recharged.

EMILIE RONCALI and SIMON R. CHERRY, Application of Silicon Photomultipliers to Positron Emission Tomography, **Annals of Biomedical Engineering, Vol. 39, No. 4, April 2011 (2011) pp. 1358–1377**

Silicon Multiplier (SiPM) Detectors

"Digital" Silicon Photo Multiplier

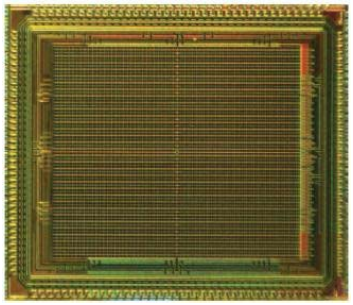

SiPM Microphotograph
~8100 cells

- Each cell's bias voltage and output signal can be controlled
- A trigger network and embedded time to digital (TDC) converter provide fast timing
- Energy is estimated by counting the pulses of fired cells
  - Cells with bad performance can be deactivated online

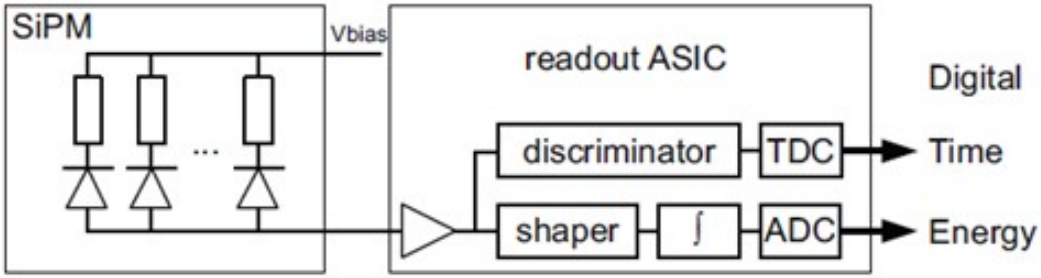

Conventional readout of SiPM for PET

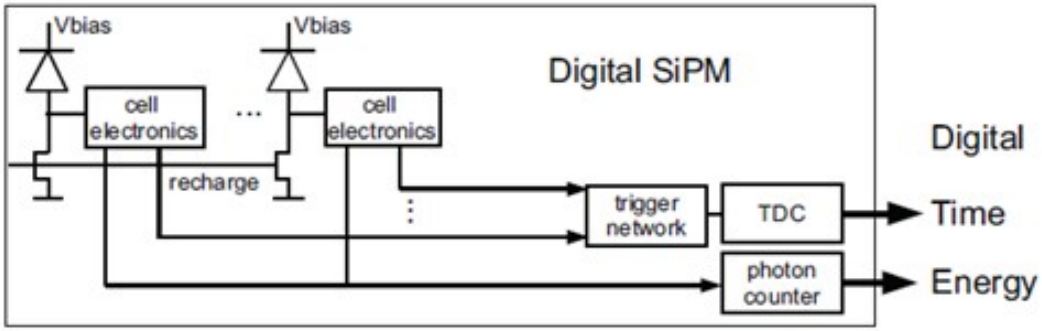

Readout of "digital" SiPM for PET

This slide was derived from Martin S. Judenhofer, Seminars in Nuclear Medicine, with permission.